UNIVERSIDADE DE LISBOA
FACULDADE DE CIÊNCIAS

Nearshore sedimentary dynamics in a wave-dominated coast

Doutoramento em Geologia
Especialidade Geodinâmica Externa

Ivana Bosnic Coelho

Tese orientada por:
Professor Doutor Rui Pires de Matos Taborda
Anabela Tavares Campos Oliveira

Documento especialmente elaborado para a obtenção do grau de doutor

2017

UNIVERSIDADE DE LISBOA

FACULDADE DE CIÊNCIAS

Nearshore sedimentary dynamics in a wave-dominated coast

Doutoramento em Geologia

Especialidade Geodinâmica Externa

Ivana Bosnic Coelho

Tese orientada por:

Professor Doutor Rui Pires de Matos Taborda

Doutora Anabela Tavares Campos Oliveira

Júri:

Presidente:

- Doutora Maria da Conceição Pombo de Freitas, Professora Catedrática da Faculdade de Ciências da Universidade de Lisboa

Vogais:

- Doutor Paulo Manuel da Cruz Alves da Silva, Professor Auxiliar
  Departamento de Física da Universidade de Aveiro;
- Doutor João Manuel Alveirinho Dias, Professor Associado Aposentado
  Faculdade de Ciências e Tecnologia da Universidade do Algarve;
- Doutor José Paulo dos Santos Ferreira Pinto, Técnico Superior
  Instituto Hidrográfico na qualidade de individualidade de reconhecida competência na área científica;
- Doutor Rui Pires de Matos Taborda, Professor Auxiliar
  Faculdade de Ciências da Universidade de Lisboa (orientador);
- Doutor João Pedro Veiga Ribeiro Cascalho, Professor Auxiliar convidado
  Faculdade de Ciências da Universidade de Lisboa.

Documento especialmente elaborado para a obtenção do grau de doutor

Fundação para a Ciência e Tecnologia no âmbito da Bolsa de Doutoramento SFRH/BD/77224/2011

2017

Ao Zoki

This thesis should be cited as: Bosnic, I. 2017. Nearshore sedimentary dynamics in a wave-dominated coast. PhD thesis. University of Lisbon, Portugal, 196 pp.

Agradecimentos|Acknowledgements

O percurso é longo e certamente só chega ao fim graças à existência, ao apoio e ajuda de muitos.

Aos meus orientadores Rui e Anabela, por acreditarem na minha capacidade como investigadora, quando por muitas vezes eu própria duvidei. A confiança por vocês depositada foi, sem dúvidas, o grande motor deste trabalho. Ao Rui um agradecimento especial por partilhar do seu entusiasmo contagiante pela dinâmica costeira. Este, sem dúvidas, contribuiu para uma motivação ascendente ao longo do percurso deste trabalho.

À FCT (Fundação para a Ciência e Tecnologia) pelo financiamento deste trabalho através da concessão de uma bolsa de doutoramento (SFRH/BD/77224/2011).

Às minhas instituições de acolhimento IH e IDL, e ao Departamento de Geologia da Fcul, pelo espaço e disponibilização das condições necessárias para a concretização deste trabalho.

À toda equipa do projeto SHORE, em especial à Teresa e ao Marco, incansáveis e fundamentais para a realização deste trabalho.

À toda a equipa do IH envolvida no projeto SURGE, em particular ao Nuno Lapa pela disponibilidade constante em ajudar.

Ao José Paulo Pinto e ao Sérgio Larangeiro, pelas conversas esclarecedoras a cerca do mundo da modelação numérica.

Ao Richard Soulsby, não sei o que seria da minha tese sem o *Dynamics of Marine Sands: A manual for practical applications*.

Ao Leslie Lamport, a quem devo toda a poupança de tempo que tive na formatação deste trabalho. Obrigada por desenvolver o LateX!

Ao Murilo (Gun) Dantas e toda a equipE KLS, vocês foram muito importantes nesta reta final.

A todos que participaram da jornada de workshops levada a cabo no Departamento de Geologia da Fcul. A dinâmica incorporada na equipe e a troca de conhecimento na altura foi sem igual.

Aos meus colegas da costeira, por todo apoio e incentivo e sobretudo pela disponibilidade constante de todos em ajudar. Vocês são espetaculares! Ana Bastos, Ana Maria, Cris e Pedro, tenho um orgulho enorme em poder partilhar da vossa amizade. Peço licença para agradecer

em particular à safra 2016-2017 de doutoras em Geologia , foi maravilhoso e muito mais fácil percorrer este caminho ao vosso lado. Mafalda, Mónica e Tanya: *we made it*!

Ao João Pedro, que esteve sempre muito presente na elaboração deste trabalho. Obrigada pela partilha de conhecimentos e pelas conversas descontraídas e sempre bem-vindas ao longo desta jornada.

À minha colega e amiga Cris, pelo apoio e incentivo constante. Obrigada pelas conversas, desabafos e risadas, momentos estes fundamentais para manter a sanidade mental em muitas das alturas do percurso como doutoranda.

À minha irmã na ciência Mónica (sim, copiei da tua Tese :D), que desde o saudoso Beach Sand Code, transformou-se de uma companheira de trabalho espetacular numa amiga sem igual. Obrigada pela revisão da "dita", pelas sugestões dadas, pelos mimos em forma de bolos e gelados e sobretudo pela amizade.

À minha parceira de reta final, Tanya, que encheu o nosso gabinete de sorrisos nos dias bons e nos menos bons. Obrigada pelas sugestões, revisões, críticas, ideias, por estar sempre disponível e sobretudo por tornar esta jornada muito mais leve!

À minha tia-sogra, a quem devo todo o meu percurso académico percorrido em Portugal, entre muitas outras coisas. *Gracias a la vida que me ha dado tanto*!

Aos meus pais, eternos incentivadores das minhas escolhas. À minha Cherry um agradecimento especial por todo o apoio dado como mãe, avó e amiga. Obrigada por nunca faltar.

Aos meus meninos, por simplesmente existirem. E à minha malandra, por ter existido.

Abstract

Coastal management issues are mainly associated to imbalances in the coastal sediment budget and concerns regarding this topic have significantly increased in recent years. One of the main consequences of these imbalances is reflected in coastal erosion, that in medium to long-term compromises the stability of the coastline. Thus, understanding the movement of sediments in and out of the beach system is a key to understand how the coast evolves and how it responds to coastal engineering interventions. However, the existence of the depth of closure (DoC) concept casts some doubts regarding the importance of the sedimentary exchanges between the beach and the continental shelf. The lack of information concerning the nature and magnitude of sediment transport across the whole nearshore environment, especially seaward of the DoC, is likely to be the main cause of the uncertainties associated to the sedimentary activity on this environment.

This work aims to advance the understanding of the nearshore sedimentary dynamics and to recognize its relationship with forcing mechanisms, especially seaward of the depth of closure. To reach the objective of this work, a pluridisciplinary approach was carried out involving sediment transport, oceanographic, sedimentological and morphological data across two distinct nearshore environments at the Portuguese continental shelf.

Nearshore sediment transport was estimated through in situ measurements and numerical modelling. Local measurements were performed at the mid shelf through a sand tracer experiment by injecting 400 kg of fluorescent tracer and monitoring its displacement during one year. The modelling approach was conducted by the application of a wave-current bottom boundary layer (bbl) model developed in the scope of this work and validated by the in situ measurements.

Oceanographic data was based on in situ measurements of waves and currents complemented by wave propagation modelling, and also served as input to the bbl model. In situ data included upward-looking ADCP measurements and wave buoy data, and was taken as representative of typical annual conditions. The sedimentological dataset was based on both in situ measurements as well as pre-existing textural distribution maps. Bottom morphology relied essentially on field data from single beam and multibeam surveys, and to a lesser extent on pre-existing morphodynamic studies.

The multiproxy approach was replicated at two energetically contrasting nearshore environments (except for the tracer experiment that was only held in one study area). The first case study is representative of a moderate-energy environment in southern Portugal, offshore Tavira barrier island. The second one is representative of a high-energy environment in the Portuguese west coast, offshore Almagreira beach, Peniche. Modal wave conditions are characterized by offshore significant wave heights of 0.92 and 2.2 m, and peak periods of 8.2 and 10.4 s, for the moderate and high-energy environments, respectively.

Despite the energetically distinct character of the nearshore zones addressed in this work, the integrated analysis of multidisciplinary data put in evidence common features between them. These similarities, mainly represented by sediment texture and related dynamics, led to the definition of depth limits that define domains with characteristic dynamics, being them: upper and lower inner shelf, mid shelf and outer shelf. Also, the integrated analysis of the multidisciplinary data allowed the development of a conceptual sediment dynamic model for a wave-dominated nearshore zone with low sediment supply. In this model the sedimentary dynamics within each nearshore domain is described and supported mainly by results from this work, complemented with external data.

In the present conceptual model, the inner shelf domain is characterized by littoral deposits with a seaward fining trend - maintained by reworking and redistribution processes induced by the present hydrodynamic regime. Overall, the bedload mode of transport is considered the mechanism driving coarser sands onshore, while the seaward transport of finer sands is made essentially as suspended load. This domain can be segmented in two sections: 1) the upper inner shelf; and 2) the lower inner shelf. The first is marked by intense remobilization and frequent sediment exchange with subaerial beach, translating into measurable morphological changes and limited offshore by the morphological depth of closure. The lower inner shelf extends down to the maximum depth where littoral sediments are found (that can be regarded as the sedimentological depth of closure), and is characterized by finer sands frequently mobilized but only transported under high energy wave events. At the mid shelf, whereas the bottom energy induced by waves decreases, the grain size of bottom sediments increases, consisting of medium to coarse sand. Sediment remobilization within this domain is significant, but net sediment transport is very low and dominated by an alongshelf component. Finally, the abrupt contact with muddy sediments (mudline) marks the beginning of the outer shelf where sediments are in equilibrium with the milder hydrodynamic regime.

The proposed conceptual model constitutes a step forward in the harmonization of the sedimentological and oceanographic settings affecting the inner, mid and outer continental shelf domains. The coupled behaviour between sediment distribution and hydrodynamic

processes allowed the prediction of the depth limits between nearshore domains through theoretical calculations solely based on wave conditions. Still, and despite the valuable contribution to the understanding of nearshore sediment dynamics made by this work, further efforts are needed regarding this subject. The incorporation of wave-related sediment transport due to wave streaming into numerical models, as well as more sediment transport measurements are improvements to be prioritized. These improvements, associated with the predictive capacity of numerical models, can constitute a powerful tool for the coastal management of natural resources, especially with regard to the current sea level rise scenario and the consequent potential coastal sediment budget imbalances.

keywords: sediment transport; nearshore zonation; coastal sediment budget; continental shelf.

Resumo

Os problemas ligados à gestão costeira estão geralmente associados a desequilíbrios no balanço sedimentar costeiro. As preocupações a cerca deste tema aumentaram significativamente nos últimos anos, uma vez que dentre as principais consequências desses desequilíbrios está a erosão costeira, que em médio a longo prazo compromete a estabilidade do litoral (recuo da linha de costa). Assim sendo, compreender o movimento de entrada e saída de sedimentos do sistema de praia é considerado fundamental para a compreensão de como a zona costeira evolui e de como a mesma responde às intervenções de engenharia costeira. No entanto, a existência do conceito de profundidade de fecho (DoC) levanta algumas dúvidas quanto à importância das trocas sedimentares entre a praia e a plataforma continental. A falta de dados relativos a natureza e magnitude do transporte de sedimentos na zona *nearshore*, especialmente ao largo da DoC, é provavelmente a principal causa das incertezas associadas à atividade sedimentar neste ambiente.

Este trabalho tem como objetivo avançar na compreensão da dinâmica sedimentar da zona *nearshore* e identificar sua relação com os mecanismos forçadores, especialmente ao largo da profundidade de fecho. Para tal, foi realizada uma abordagem multidisciplinar envolvendo dados de transporte e remobilização sedimentar assim como dados oceanográficos, sedimentológicos e morfológicos.

O transporte sedimentar foi estimado através de medições *in situ* e modelação numérica. As medições foram realizadas na plataforma média através de uma experiência de areias marcadas em que se injetou 400 kg de traçador e cujo deslocamento foi monitorado durante um ano. A abordagem da modelação numérica foi conduzida através da aplicação de um modelo de camada limite onda-corrente, desenvolvido no âmbito deste trabalho, tendo sido a sua validação realizada com base nos dados obtidos pela experiência com traçadores.

Os dados oceanográficos, que também suportam o modelo de transporte de sedimentos, foram baseados em medições de ondas e correntes complementadas pela modelação da propagação das ondas. Os dados *in situ* estão representados por medições realizadas através de ADCP (ondas e correntes) e dados de boias-ondógrafo, sendo o conjunto de dados oceanográficos considerado representativo das condições anuais. A modelação foi levada a cabo através do modelo de propagação SWAN, cujas condições de fronteira foram

impostas pelos dados das boias-ondógrafo ao largo das áreas de estudo. O conjunto de dados sedimentológicos baseia-se em amostras adquiridas no âmbito deste trabalho, bem como em mapas pré-existentes de distribuição texturais na plataforma . Por fim, a análise morfológica do fundo é feita sobretudo com base em dados de feixe-simples e multifeixe, complementados com estudos morfodinâmicos pré-existentes.

A abordagem multidisciplinar acima descrita foi replicada para dois ambientes costeiros energicamente contrastantes. O primeiro, representativo de um ambiente de energia moderada, localiza-se na costa sul de Portugal, ao largo da ilha barreira de Tavira. O segundo, representativo de um ambiente altamente energético, localiza-se na costa oeste portuguesa, ao largo da praia da Almagreira, Peniche. As condições modais são caracterizadas por alturas significativas de onda ao largo de 0.92 e 2.2 m, e períodos de pico de 8.2 e 10.4 s, para os ambientes de energia moderada e alta, respectivamente.

Apesar do caráter energeticamente distinto dos ambientes abordados neste trabalho, a análise integrada dos dados evidencia características comuns entre eles. Estas semelhanças, representadas sobretudo pela textura dos sedimentos e dinâmica neles induzida, levaram à definição de limites de profundidade que distinguem domínios com características intrínsecas, sendo eles: plataforma interna superior e inferior, plataforma média e plataforma externa. A análise integrada dos dados também permitiu o desenvolvimento de um modelo conceptual da dinâmica sedimentar para o ambiente *nearshore* dominado por ondas e com pouco aporte sedimentar. Neste modelo, a dinâmica sedimentar dentro de cada domínio nearshore é descrita e suportada sobretudo pelos resultados obtidos no âmbito deste trabalho, complementada com dados externos.

De acordo com o modelo conceptual, a plataforma interna é caracterizada por depósitos litorais com tendência de diminuição do tamanho das partículas em direção ao largo. Estes sedimentos, por sua vez, são mantidos pelos processos de remobilização e redistribuição induzidos pelo regime hidrodinâmico atual. De uma maneira geral, o transporte de fundo é considerado o mecanismo que leva as areias mais grosseiras em direção à costa, enquanto que o transporte das areias mais finas em direção ao largo é realizado em suspensão. Este domínio pode ser dividido em dois setores: 1) a plataforma interna superior; 2) a plataforma interna inferior. O primeiro é marcado por uma intensa remobilização e troca frequente de sedimentos com a praia sub-aérea, traduzindo-se em mudanças morfológicas mensuráveis que se estendem até a profundidade de fecho, limite exterior deste setor. A plataforma interna inferior se estende até a profundidade máxima onde os sedimentos litorais são encontrados (neste trabalho denominada profundidade sedimentológica de fecho) e caracteriza-se por areias mais finas, frequentemente remobilizadas, mas transportadas apenas em eventos de alta energia. Na plataforma média, enquanto a energia junto ao fundo induzida pelas

ondas diminui, o tamanho dos sedimentos aumenta, sendo estes constiuídos por areia média a grosseira. A remobilização sedimentar neste domínio é significativa, mas o transporte residual de sedimentos é muito baixo e dominado por uma componente paralela à costa. Por fim, o contato abrupto com a *mudline* marca o início da plataforma externa onde os sedimentos estão em equilíbrio com o regime hidrodinâmico pouco energético.

O modelo conceptual proposto constitui um passo em frente na harmonização das características sedimentológicas e oceanográficas que dominam os diversos setores da plataforma continental compreendidos na zona *nearshore*. O acoplamento entre a distribuição de sedimentos e os processos hidrodinâmicos permitiu a previsão dos limites de profundidade entre os domínios da zona *nearshore* através de cálculos teóricos baseados exclusivamente nas condições de agitação. Ainda assim, e apesar do valioso contributo para a compreensão da dinâmica sedimentar dado por este trabalho, são necessários esforços adicionais no âmbito desta temática. A incorporação e validação do transporte de sedimentos induzido pelas ondas nos modelos numéricos, bem como mais medições diretas de transporte de sedimentos em zonas estratégicas, são avanços a serem priorizados. Estes progressos, associados à capacidade preditiva dos modelos numéricos, podem constituir uma ferramenta poderosa para a gestão costeira dos recursos naturais, especialmente no que diz respeito ao atual cenário de aumento do nível médio do mar e os potenciais desequilíbrios no balanço sedimentar costeiro associados.

palavras-chave: transporte sedimentar; zonamento costeiro; balanço sedimentar costeiro; plataforma continental.

Table of contents

List of figures

List of tables

Chapter 1

Introduction

1.1 Motivation and scope of the thesis

Concerns regarding coastal management issues associated to imbalances in the coastal sediment budget have been significantly increased in recent years. One of the main consequences of these imbalances can be reflected in coastal erosion, which in medium to long-term compromises the stability of the coastline. With sea level rise rates becoming faster than they have been over the past several millennia (Antunes and Taborda, 2009; Vermeer and Rahmstorf, 2009), changes in sediment budget can be a primary driver of coastal evolution. Understanding the movement of sediment in and out of the beach system is a key to understand how the coast evolves and how does it responds to coastal engineering interventions such as the implementation of offshore wave energy acquisition systems, beach fill design, sediment extraction/placement and also the installation of submarine cables (Ortiz and Ashton, 2016).

On sandy coasts, the continental shelf is often identified as a potential sediment source/sink to the coastal system (Batten, 2003; Niedoroda et al., 1985; Schwab et al., 2000), although the time scale on which it acts remains a source of great uncertainty. However, the existence of the depth of closure (DoC) concept[1] cast some doubts regarding the importance of the sedimentary exchanges between the beach and the continental shelf. The assumption that a quantifiable DoC exists, where there is no significant transport of sediment seaward of this point, is frequently used on coastal sediment budget analyses (e.g. Brunn, 1962; Hallermeier, 1981; Rosati, 2005; Rosati et al., 2013). Therefore, it is a common practice to assume that because insignificant profile changes occur offshore the DoC, sand mining seaward of this depth has theoretically minimal impacts on the beach (Robertson et al., 2008). However this assumption can be questioned as the absence of significant morphological changes does

[1] The empirical measure of the seaward limit for significant morphological variations. (Nicholls et al., 1998)

not necessarily implies on a lack of sedimentary activity which should be expected to occur seaward of the profile closure especially during high-energy wave conditions (Gracia et al., 1998; Nicholls et al., 1998; Wright et al., 1991).

The wave-induced bottom activity is commonly associated to the effective wave base concept which describes the depth at which nearbed wave orbital velocities become able to reach the threshold value for the initiation of sediment motion (Immenhauser, 2009). Specially within continental shelves with low continental supply of sediments, this phenomena is translated to bottom sediments texture as an abrupt sand-mud transition, being this depth also known as mudline (Immenhauser, 2009; Selley, 2000) or simply sand-mud transition (George and Hill, 2008). Thus, this work will focus on the nearshore environment comprised between the DoC and the mudline, thus encompassing the continental shelf domain where bottom sediments are under the action of wave-induced forces.

The nearshore zone links the subaerial beach to the offshore domain (see domain definition on Chapter 2), thus encompassing boundaries which comprehension is of main importance for the coastal sediment budget. Although sediment transport within the surf zone (upper nearshore) have been extensively addressed in the literature (de Vries et al., 2014; Kraus et al., 1982; Wang et al., 1998), the nearshore zone offshore the DoC, that includes the inner and the mid continental shelf, still faces a lack of information regarding the nature and magnitude of sediment transport. This can be partially attributed to the complexity of the processes driving sedimentary dynamics. Furthermore, the logistical constraints on the acquisition of sediment transport data seaward the DoC is often conditioned by highly energetic conditions marked by the influence of waves and currents (e.g. Kleinhans and Grasmeijer, 2006; Williams, 2012). This translates in the scarcity of works reporting measurements of the total (suspended and bedload) sediment transport, especially at monthly or larger time scales. So far, most of works dealing with the sediment transport estimations seaward the DoC are based on numerical models (e.g. Ferré et al., 2010; van Rijn, 1997), focus on short time scales (hours to days) and rarely reports quantitative estimates. These limitations prevents the complete understanding of the processes that controls the long-term nearshore morphodynamics and consistent evaluation of the sedimentary dynamics. Furthermore, the discrepancy among estimated sediment transport rates reported on the literature (up to two orders of magnitude), reinforce the need of sediment transport in situ measurements, preferably on a time scale compatible with the forcing mechanisms.

Besides the importance of in situ sediment transport measurements, also the specific role played by waves and currents on the sedimentary dynamics and the sediment response to different oceanographic conditions are critical to understanding the behaviour of coastal systems. However, this is still a poorly understood topic, mainly at the most seaward region

of the nearshore zone (Backstrom et al., 2015; Nittrouer and Wright, 1994; Schwab et al., 2000). In this context, numerical models (properly calibrated) appear as a powerful tool on the comprehension of these processes due to its predictive capacity and ability to evaluate the individual contribution of each forcing mechanism to the sedimentary dynamics (Taborda, 1999).

In order to contribute to significant advances on the understanding of the nearshore sedimentary dynamics, this work aims to understand the variation of sediment dynamic processes according to depth and their relationship with forcing mechanisms from the depth of closure down to the mudline. To reach this objective, in situ sediment transport measurements were performed with simultaneous hydrodynamic data acquisition complemented with numerical modelling data. A wide overview regarding the framework of this thesis is represented on Figure 1.1.

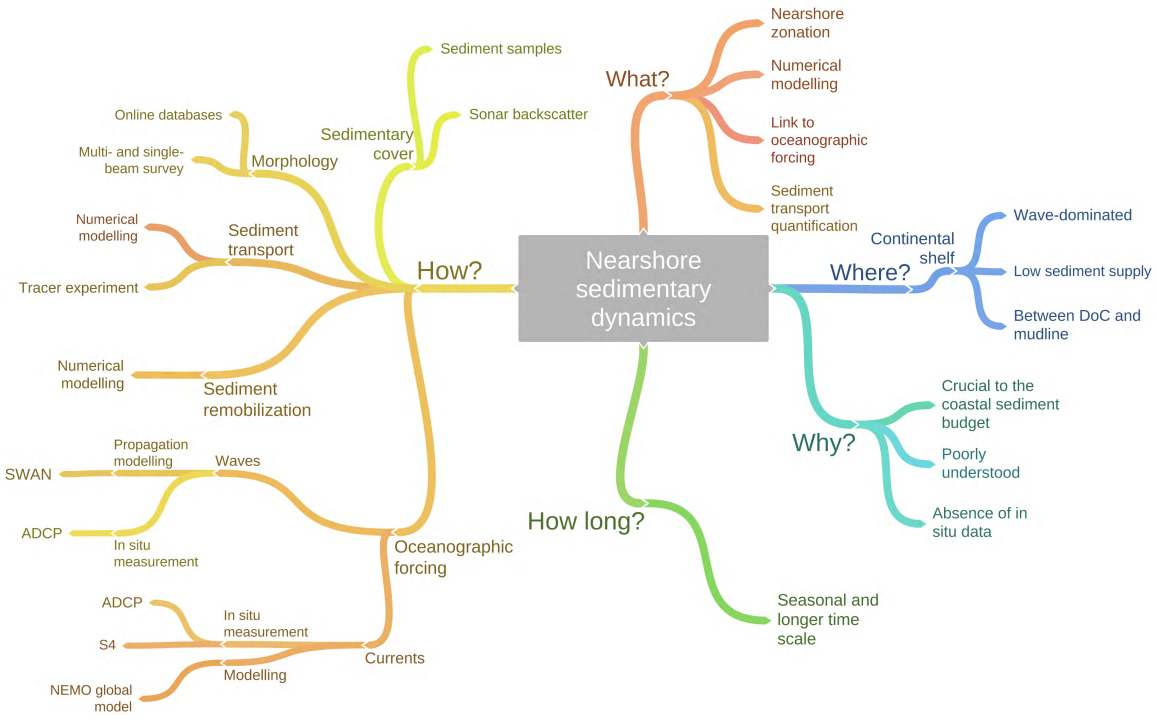

Figure 1.1 Graphical introduction.

1.2 Thesis outline

This thesis is organized in seven chapters. The description of the contents of each chapter is given in the following paragraphs.

Chapter 1 Introduction: provides a general introduction describing the motivation and objectives of the present work, as well as an outline of the thesis.

Chapter 2 Literature Review: presents a bibliographic review of the most relevant terminologies and concepts for the present work as well as a state of the art of the nearshore sedimentary dynamics.

Chapter 3 Bottom boundary layer and sediment transport modelling: describes the numerical model developed in this work including the main formulations and parametrizations regarding the bottom boundary layer and sediment transport approximations.

Chapter 4 Sedimentary dynamics in a moderate-energy environment: discusses the nearshore sedimentary dynamics in a moderate-energy environment (offshore Tavira, southern Portugal), under a multidisciplinary approach with emphasis to the sand tracer experiment carried out on this site coupled with oceanographic monitoring and modelling data. This chapter also includes the calibration of the numerical model described on **Chapter 3** using the sediment transport results obtained through the sand tracer experiment.

Chapter 5 Sedimentary dynamics in a high-energy environment: focus on the application of the numerical model described on **Chapter 3** to a high-energy environment represented by the nearshore zone off Almagreira beach (Portugal's western coast).

Chapter 6 Final discussion: proposes a zonation of the nearshore zone based on sedimentological and oceanographic data from **Chapters 4** and **5**. Also, it is proposed a conceptual sediment dynamic model involving the nearshore domains defined through its zonation.

Chapter 7 Conclusions and future research: provides the conclusions of this work and gives insights regarding future nearshore sediment transport studies.

Chapter 2

Literature review

2.1 Introduction

The frequent lack of consistency found on the literature regarding a wide variety of coastal concepts led to the production of this literature review. In this chapter, the coastal features and terminologies considered of main relevance to the present work are discussed in order to well define the terms cited herein. So, firstly it is approached the concept of a wave-dominated environment as well as its main characteristics, features and domains, giving emphasis to the nearshore zone. Later, the temporal and spatial scales variability on coastal processes are approached, followed by the main techniques for estimating nearshore sediment transport. Finally, it is presented a brief state of the art of the nearshore sedimentary dynamics.

2.2 The wave-dominated environment

The geomorphological and sedimentological characteristics of coasts reflect a wide range of controlling factors and forcing mechanisms which exert their influence over various spatial and temporal scales (Davidson-Arnott, 2011). The term "wave-dominated", as the name suggests, it is used to define an environment subject to physical processes that are dominated by wave-induced energy (Davis and Hayes, 1984). One of the first definitions found on the literature describes a wave-dominated system as consisting primarily of sandy sediments. However, as in situ sediments may contain a large range of sizes, this definition has been adapted over the years by several authors (e.g. Davidson-Arnott, 2011; Davis and Hayes, 1984; Roy et al., 1994; Short, 1999). Therefore, in a broader sense and based on these more recent definitions, a wave-dominated environment is a classification applied to coastal environments with an abundance of sediment (mainly sand but also including gravel and

cobbles) where contemporary coastal evolution is shaped through erosion, transport, and deposition processes primarily forced by waves and wave-generated currents. These coasts are also influenced by tides and tidal currents, but they play a subordinate role compared to waves.

Also, wave-dominated environments are subject to various levels of energy, being commonly classified into: low-, moderate- or high-energy environments. According to Otvos (1982), a **low-energy** environment is usually sheltered from storms and swells by adjacent topographic features, by their relative position to prevailing wind direction, by gentle bottom topography or by a combination of these factors. A **moderate-energy** environment in turn is exposed to moderate wave energy conditions, being usually associated to barrier islands, sandy beaches, spits, etc. A more rigorous work is the one of Tanner (1960) where a moderate-energy environment is characterized by mean breaker heights between 10–50 cm. Finally, **high-energy** environments are those totally exposed to strong, steady, zonal winds and fronts with high wave energy (Davies, 1973).

2.2.1 Sediment distribution

According to Carter (1988), the boundary between wave-worked and non-wave-worked sediment may be apparent from the sediment size, grain preservation or faunal community structure. Nearshore sands on the upper inner shelf are generally well sorted and often (but no always) similar to the subaerial beach sediments, although there is usually a decrease in the mean grain size in the seaward direction. In many places, such as US Atlantic Coast (Swift et al., 1971) and south-east Australia Roy and Stephens (1980), seaward fining of sediments occurs down to an abrupt transition to coarser and poorly sorted sand. This grain size discontinuity marks the offshore limit of the inner shelf environment and it is generally interpreted to correspond to the limit at which wave-induced sediment remobilization is more frequent as well as the boundary of rip transported sediments (Carter and Carter, 1986; Hilton and Hesp, 1996). The mid shelf is marked by medium to coarse sand often containing mollusc shells and with oxidised surficial sediments which are described by Swift et al. (1971) as relict deposits[1]. The seaward limit of the mid shelf environment, which also marks the end of the nearshore zone, is represented by the abrupt transition to finer sediments containing a significant amount of mud (>25%). This transition is commonly referred on the literature as the mudline (Immenhauser, 2009) or simply as the sand-mud transition (SMT - George and Hill, 2008). A scheme describing the sediment distribution across the continental is shown in Figure 2.1.

[1]Sediments remnant from a different earlier environment which are undergoing modification in response to their present environment, especially the hydraulic regime, although could not be currently supplied.

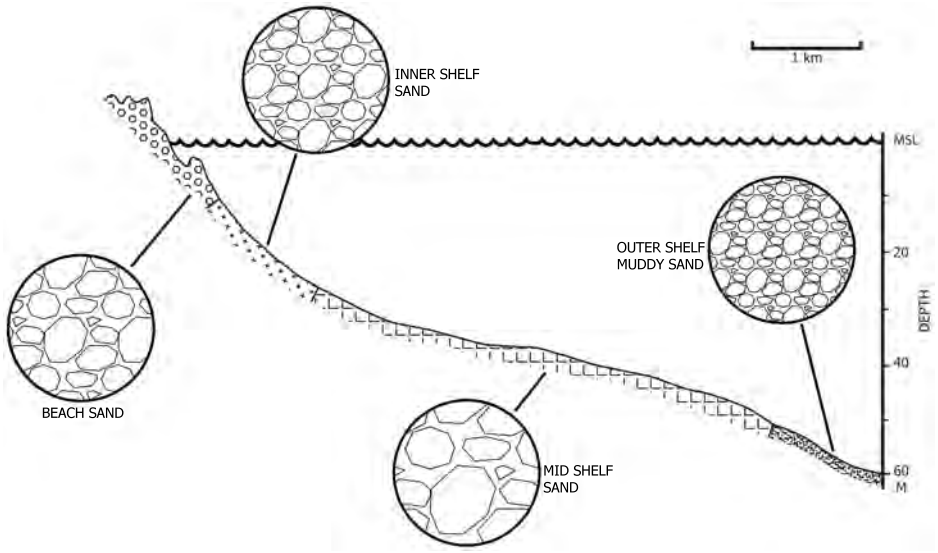

Figure 2.1 Bottom sediment distribution along a cross-shelf profile (Adapted from Roy and Stephens, 1980).

Other patterns regarding the textural distribution of nearshore sediments are reported on the literature since the coarse-grained sand zone does not occur on all coasts (Short, 1999). According to Niedoroda et al. (1985), for example, on the Mississippi coast sands fine progressively across the nearshore zone down to offshore fine silts and clays. Also, on the south-east Australian coast the nearshore zone is marked by very well sorted sand with a constant modal grain size from de shoreline down to water depths of 50 to 60 m where it mixes with muddy sediments of the outer shelf (Roy et al., 1994).

2.2.2 Depth of closure and wave base

There is a frequent misunderstood on the literature regarding the wave base and depth of closure concepts. Some authors even consider these two limits as synonymous (e.g. Ashton et al., 2007; Guisado et al., 2013). However, a clear distinction must be made between these depths specially in order to better understand the dynamic processes considered in the definition of the nearshore domains (Figure 2.2).

According to Immenhauser (2009), wave propagation over unconsolidated seabeds has three possible effects that can be represented by the following depths, from the offshore to the shore: wave base, effective wave base and depth of closure. These boundary depths are better described below.

Wave base

As a wave approaches shallower zones, there is a depth where it starts to "feel" the bottom, i.e. a depth at which seabed starts affecting the wave (and not where the wave starts affecting bottom dynamics). According to Davies (1973), this is the shoreward limit for the so called *deep-water waves*. By convention, this limit is taken to be where the water depth is half the deep water wavelength ($h = \frac{L_0}{2}$). Some authors even call this depth as the **hydrodynamic wave base** (e.g. Flores, 2011; Immenhauser, 2009). In sedimentary geology, this boundary depth has no significance. As the wave moves into increasingly shallow waters, the near-bottom orbital velocity exceeds the threshold of motion, but a still higher threshold is not yet reached (see depth of closure definition). This depth is known as the **effective wave base** and it is where waves starts affecting bottom dynamics, being this limit therefore of major relevance on sediment dynamic studies within the continental shelf (Immenhauser, 2009).

Depth of closure

Following the rationale of Immenhauser (2009), as wave continuous to approach the coast, a higher threshold is passed and vigorous grain transport occurs over the sea bottom. When even higher hydrodynamic levels are reached, the seafloor is modified by deep-cutting erosion currents. In the terminology of coastal engineers, this water depth is referred to as the depth of closure (DoC - Hallermeier, 1981). Thus, the DoC describes the seaward limit of measurable bed elevation changes, being therefore considered a morphological boundary (Hallermeier, 1978; Nicholls et al., 1996). According to Birkemeier (1985), this depth can be interpreted as a boundary between the active cross-shore sediment transport zone and a deeper zone of negligible sediment movement, thus playing a major role on coastal engineering interventions such as the placement of mounds of dredged material, beach fill design and the calculation of sedimentary budgets (Morang and Birkemeier, 2005).

The DoC is commonly estimated empirically by examining seabed elevation changes measured by repetitive cross-shelf bathymetric surveys and identifying the depth at which changes become insignificant (usually less than 0.15 m, see Kraus et al., 1998; Nicholls et al., 1998; Robertson et al., 2008). The first theoretical definition of DoC came from a study by Hallermeier (1978, 1981) where it was stablished a direct relationship between the DoC and the wave climate. This work came out with the definition of two dynamically distinct boundaries: the inner and outer DoCs. The inner limit marks the seaward extent of the littoral zone where the bed experiences extreme activity caused by waves breaking and their related currents. Whereas the outer limit denotes the limit of the shoal zone where

waves induce little sediment transport, implying on neither a strong nor negligible effect on the bed Hallermeier (1981).

2.2.3 The nearshore

The nearshore zone, as well as a many other of terms used on the literature for defining coastal domains, also experiences the tradition of inconsistent terminology. This lack of consistency is mainly due to the variety of processes (and time scales) and features considered by the authors for defining both landward and seaward limits.

Komar (1998) defines the nearshore as the region extending from the shoreline to just beyond the waves breaking zone. On the other hand, Svendsen (2006) and Davidson-Arnott (2011) use both the same definition of nearshore zone where the shoreline (represented by the low water line) is considered its landward limit and the seaward boundary is defined by a fictive offshore limit where the depth becomes so large (equivalent to approximately half the wave length) that the bottom is no longer influenced by storm waves . Lastly, Short (1999) classifies the nearshore as the region lying between the waves breaking zone and the depth which waves stop interacting with the seabed preventing sediment entrainment and shoreward transport.

Despite the noticeable divergence on defining the nearshore zone, which can be also aggravated by discrepancies on shoreline definitions and the time scales considered, it is clear that the nearbed wave-induced force plays a major role on establishing nearshore physical boundaries.

In this work, the nearshore is defined as the region lying from the low water line down to seaward limit of wave-worked sediments. However, instead of using an oceanographic approach, this limit is defined using as a proxy the bottom sediment texture characteristics, which in turn reflects the long-term wave near bottom activity.

Following this definition, the nearshore zone ends up encompassing coastal domains of main importance for the coastal sedimentary budget: the submerged beach and the inner and mid continental shelves (Figure 2.2).

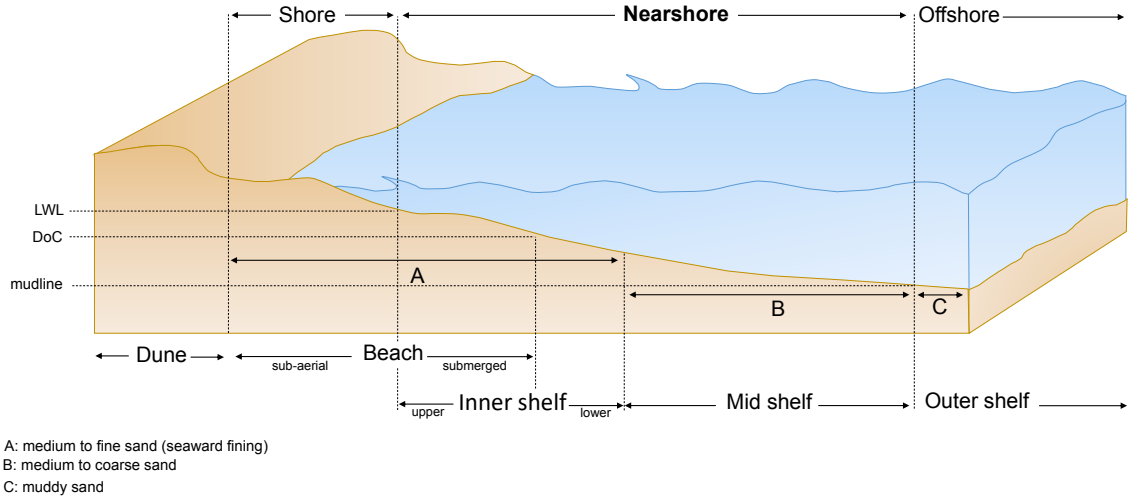

Figure 2.2 Description of wave-dominated coastal domains according to the across-shelf sediment distribution.

2.3 Temporal and spatial variability on coastal processes

The interplay between the forcing mechanisms that occur over different spatial and temporal scales adds complexity and heterogeneity to the comprehension of coastal evolution. Thus, understanding these complexities and the impact of the time-variable coastal processes is of main importance in managing the nearshore zone in the future (Carlin et al., 2015).

Niedoroda et al. (1985) stated "Coastal processes occur in time scales that vary from nearly instantaneous to geological intervals. A comprehensive discussion of the processes that dominate and control a coastal environment needs to consider all of these scales and to distinguish the combination of processes that are most relevant to operation of the physical system at each time scale". Thus, matching the dynamic length of the forcing mechanism to the time and spatial scales of a specific study is of main importance for the correct interpretation of coastal dynamics.

The nearshore zone is primarly controlled by the local waves and currents. While waves usually occur in a relatively narrow range of frequencies, coastal currents have a wide range of time scales which depends on the relative magnitude of the forcing mechanisms such as waves, tide, and/or baroclinic/barotropic processes (Niedoroda et al., 1984). However, across the nearshore zone, the baroclinic mode is reduced as the stratification is often weak due to wave mixing. In this environment there is often a "well-organized" coastal flow coupled to the surface wind stress which requires at least a day of nearly steady conditions to develop.

Still, over shallower depths of the nearshore zone (e.g. surf zone) the response to wind forcing is reduced due turbulence increasing.

There is often an apparent periodicity of the forcing mechanisms controlling coastal sediment transport processes. Thus, the temporal scale should be able to represent the periodicity that is relevant to the specific study. Additionally, the spatial scale should be adequate to describe the characteristics of the specific coastal environment. Generally speaking, appropriate temporal and spatial scales depends on the objectives of the sediment transport measurement, and also different measurement methods are suitable for different spatial and temporal scales. As an example, finer scales may provide more accurate measurement during the study period. However, fine scale studies tend to be short-term and may not entirely capture regional characteristics and yield a representative regional long-term sediment transport rate (Wang, 2005).

Coastal sediment transport and associated morphological changes can be analysed at many spatial and temporal scales. These scales range from instantaneous movement of single grains on a time scale of the local turbulence to long-term evolution of barrier islands chains associated to sea level rise time scale (Larson and Kraus, 1995). These processes are frequently classified based on the temporal and spatial scales of the forcing mechanisms and system responses. According to Larson et al. (2002), coastal processes can be described as a regional or a local scale process (Figure 2.3). The regional scale refers to coastal processes at time scales of 10-250 years and spatial scales between 1 and 100 km. On the other hand, local scale includes coastal processes with time periods of 0.01-30 years and spatial length of 0.1-10 km.

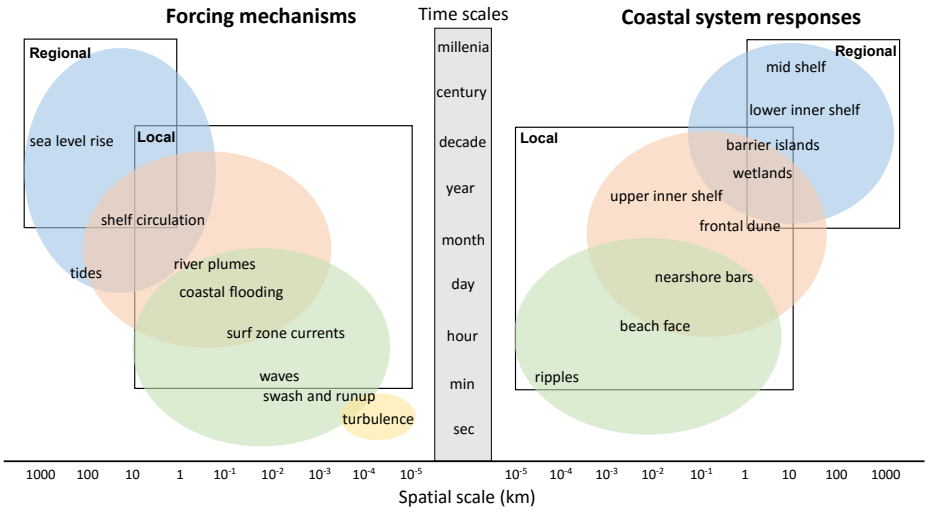

Figure 2.3 Spatio-temporal scales of coastal evolution. Adapted from Elko et al. (2014).

2.4 Techniques on sediment transport estimation

Estimates of the sediment transport can be obtained from a wide range of techniques based on in situ measurements, analytical formulas, numerical and physical modelling. Each method has its (dis)advantages which are mostly linked to the absence of adequate calibration/validation data and to the spatial and temporal scales of interest of the specific study.

Determining proper temporal and spatial scales comprises an important part of the nearshore sediment transport measurement. As mentioned earlier, coastal sediment transport demonstrates various periodicities, so it is important define in which of them the specific study will focus, especially when time-average values are to be calculated.

In this section it will be made a synthesis of the main techniques used for the sediment transport estimation by briefly describing its main advantages and drawbacks in order to understand the potentialities of the methods used on the present work.

2.4.1 Numerical modelling

Numerical models are an attempt to simulate natural phenomena through the implementation of mathematical formulations and parametrizations. A reliable application of this method depends not only on the quality of these formulas but also on the availability of field data for proper calibration/validation of the model results. Since this requirement is met, the numerical modelling can act as a powerful tool on the study of sedimentary dynamics due to its predictive capacity and ability to isolate processes and to estimate its individual contribution to the system (Taborda, 1999).

The acquisition of proper in situ data for numerical model calibration is one of the main difficulties faced by this method. The poor accessibility of the nearshore zone, specially offshore the closure depth, usually prevents sediment transport data acquisition for periods longer than hours/days. This fact results on unreliable numerical model calibration thus frequent implying on unrealistic sediment transport rates at longer time scales.

2.4.2 Physical modelling

Sediment transport estimation through physical modelling is still a challenging task due to restrictions imposed by the scaling laws. Although microscale pieces of physical models can be built correctly (including sand-scale sediments), these models still faces two major limitations: 1) simultaneously model both suspended and bedload mode of transport and 2) basin-size limits require to model cohesionless sediment with cohesive sediment (White,

1998). These two drawbacks still affect the reliability of this technique, which led Hughes (1993) to state that "there will probably never be a ‘completely correct’ sediment transport physical model at any scale other than prototype".

2.4.3 Field measurement

2.4.3.0.1 Bedform migration

The bed form migration can provide a means of quantifying the bedload transport (Masselink et al., 2007). Estimates of ripple displacement are mostly performed through echo sounders surveys (Knaapen et al., 2005) and video imagery (Becker et al., 2007), thus covering a wide range of temporal and spatial resolutions. However, this technique strongly depends on the weather conditions and rarely reaches regions deeper than 3 m.

As in other techniques, the transport rates evaluated in this types of study are time-averaged measures of the response of the bed to the flow and can be generalized if the flow conditions during the period of study is assumed to be typical of a longer time duration and a larger area (Goud and Aubrey, 1985). The fact that this method does not account with the suspended load is a relevant disadvantage on field sites where this mode of transport represents a significant part of the total load.

2.4.3.0.2 Trench filling (sandpit)

The seabed morphology and morphodynamics are strongly affected by bottom disturbances such as a local depression due to excavation (Gonçalves et al., 2014). Thus, trench filling experiments are frequently carried out on the nearshore environment in order to evaluate the local sedimentary dynamic (e.g. Blondeaux and Vittori, 2005; Gonçalves et al., 2014). This technique assumes that the trench act as a sink for sediments originating from the surrounding areas, which will often results in deposition. This continuous deposition along the time can be translated into a sediment flux per unit of time, giving then sediment transport rates (van Rijn and Walstra, 2004). However, the difficulty in distinguishing some physical processes inherent to the system adds complexity to the method which frequently ends up being used under a qualitatively approach (e.g. Gonçalves et al., 2014). Also, a sandpit experience is an expensive intervention that must be followed by several bathymetric surveys with high spatial resolution, further increasing the costs associated with the method.

2.4.3.0.3 Particle tracking

The particle tracking technique offers a practical solution to the assessment of transport pathways and to the estimation of sediment transport rates. This method implies on tagging and tracking natural sediment in the system (Black et al., 2007). A number of different signature have been used to label natural sand, being the most common ones through radioactivity (e.g. Drapeau and Long, 1984; Inman and Chamberlain, 1959) and fluorescent ink (e.g. Ciavola et al., 1997; Duane and James, 1980; Duarte et al., 2014; Komar and Inman, 1970; Silva et al., 2007). Although, due to the potential environmental impacts and also to the cost implications of the radioactive tracers, this technique has been banned from this type of study.

According to White (1998), one of the main restriction of using sand tracers on the understanding of sedimentary dynamics is the cost associated to the method. Moreover, the same author refers as one of the main practical problems the "tedious methods of determining tracer concentration in samples". However, recent advanced on image analysis techniques concerning the automated identification of fluorescent particles have significantly improved the efficiency of the laboratory work, drastically reducing the costs of the method.

There are three main methods referred on the literature for estimating sediment transport through a sand tracer experiment:

1. The Continuous Injection Method (CIM): also known as dilution method, implies on the continuous injection of a certain mass of tracer, at a constant rate, over a period of time that allow the stabilization of the flux of tracer. The sampling method is performed through the continuous sediment sampling downdrift the injection point.

2. The Temporal Integration Method (TIM): it is an eulerian method where a known mass of tracer is released and the variation of the tracer concentration with time is monitored in a point downdrift the injection.

3. The Spatial Integration Method (SIM): in this lagrangian method, a known mass of tracer is injected and the dispersion cloud of tracers is monitored in time and space.

According to Madsen (1987), the success of these methods relies on the following assumptions: 1) the sand tracers behave as the native sediment whose transport rate is to be estimated, 2) the advection mechanism dominates diffusion/dispersion and 3) no tracer leaves or enters the transport system that must be steady and uniform.

As the CIM and TIM must be applied to well-oriented sedimentary fluxes such as on the surf zone (longshore transport) or river flows, the SIM appears to be the most appropriate

method available for estimating the sediment transport using sand tracers in nearshore areas seaward the surf zone.

In the SIM method, the sediment transport rates are obtained through the product between the mean velocity of the center of mass ($\bar{V}$) and the active layer thickness (δ_{mix} also known as transport thickness) as described in Equation 2.1.

$$Q_t = \bar{V} \times \delta_{mix} \tag{2.1}$$

Estimates of δ_{mix} have progressed from simply observing the depth of penetration of tracer within the core sample (Inman and Chamberlain, 1959; King, 1951) to objective semi-empirical estimators for application on the surf zone (Kraus et al., 1982; Sunamura and Kraus, 1984) and on deeper nearshore areas (Harris and Wiberg, 1997).

2.4.3.0.4 Physical sensors

The deployment of optical, eletromagnetic and/or acoustic sensors is probably the most common method for measuring coastal sediment transport. As the measurement of the sediment flux imply on the simultaneous acquisition of sediment concentration and flow velocity data, this frequently imply on the deployment of more than one instrument. For example, it is a common practice to use the combination of an Eletromagnetic Current Meter (EMCM) with an Optical Backscatter (OBS) in order to obtain the sediment flux, specially on the surf zone. In this case, the spatial coverage along the water column if often limited to a single-point measurement, which is considered a reasonable approximation for estimations of the sediment transport on the surf zone (Aagaard, 2014). However, field experiments carried out seaward this region usually require a more detailed vertical discretization, as the absence of breaking waves significantly reduces the vertical mixing. This is more conveniently done using profile sensors such as acoustic doppler profilers, which are capable of simultaneously measure the sediment concentration (through backscatter data properly calibrated) and the flow velocity along the water column. This technique has suffer significant advances over the last years and its application on the evaluation of the suspended load has given good results (e.g. Santos et al., 2014; Styles and Glenn, 2005; Thorne and Hurther, 2014). However, still bedload measurement is missing by using these physical sensors.

2.5 Nearshore sedimentary dynamics: state of the art

Studies concerning the nearshore sedimentary dynamics have a historical concentration on shallower areas, namely on the surf zone (Aagaard et al., 2002; Beach and Sternberg, 1996;

Kraus et al., 1982; Thornton, 1972; Wang et al., 1998). Research efforts on the region seaward of the depth of closure have been long neglected due to its poor accessibility. Also, field experiments frequently experiences a broad array of logistical problems specially including sampling performance and instrument deployment. This translates on a scarcity of good quality in situ data, thus preventing a well-based understanding of the sedimentary dynamics within this area.

The logistical constraints experienced on the field frequently results on short-term (hours to weeks) observational datasets often restricted to a single-point measurement and/or focusing on only one mode of transport (suspended or bedload). Styles and Glenn (2005), for example, evaluates the sedimentary dynamics of New Jersey inner shelf exclusively based on suspended load measurements. Kleinhans and Grasmeijer (2006) in turn evaluates the inner shelf sediment transport through bedload-only measurements carried out over a single tidal cycle. Further, in situ observations of a sandpit experiment reported by Gonçalves et al. (2014) was able to simultaneously account on suspended and bedload. However, the local sedimentary dynamics was evaluated only under a qualitative approach and no quantitative estimates were reported.

Most of work dealing with the evaluation of the sedimentary dynamics outside the surf zone is based on numerical models (e.g. Oberle et al., 2014; Ortiz and Ashton, 2016). The semi-empirical nature of such models and the high uncertainty of their predictions highlight the role of, and need for, proper observational datasets (Nugzar et al., 2012). Also, the above-mentioned fieldwork limitations led to the development of poorly calibrated models. On the work of Soulsby and Whitehouse (2005a), for example, the calibration data is based on results from a river experiment, while the numerical modelling approach described in Ribberink (1998) is calibrated with physical modelling data. Even the more recent work of Aagaard (2014), although calibrated with in situ measurements, could not manage to a fully reliable sediment transport model as its calibration was performed based solely on suspended load field data.

Overall, despite the recent advances in nearshore sedimentary dynamics, this region is still a poorly understood environment, specially seaward the closure depth (Backstrom et al., 2015). The lack of proper field measurements prevents a more realistic evaluation of the sedimentary dynamics in this area, where more research efforts should be done in order to better understand the process-response mechanisms across this complex environment. Those efforts should focus on the acquisition of in situ data (both oceanographic and sedimentological) through methods capable of accounting on both suspended and bedload and preferably at monthly or higher time scale.

Chapter 3

Bottom boundary layer and sediment transport modelling

3.1 Introduction

The nearshore dynamics is mainly driven by the combined action of slowly varying currents and oscillatory waves. The layer inside which the wave-current induced flow is significantly influenced by the bed is known as the bottom boundary layer (Nielsen, 1992). Therefore, a thorough understanding of the hydrodynamic forces acting on this layer is of crucial importance for qualitative and quantitative assessments concerning the nearshore sedimentary dynamics.

In essence, waves are responsible for stirring up the sediment and currents for transporting it. More specifically, the near-bed orbital velocities generated by surface gravity waves act as the main driving force for sediment mobilization while low frequency currents are the major driver of sediment advection (Grant and Madsen, 1986). However, in particularly cases, waves can also act as the main moving force. These episodes are frequently associated to asymmetries in wave orbital velocity which can induce cross-shelf sediment transport in both onshore and offshore directions (e.g. Aagaard, 2014; Crawford and Hay, 2003; Grasso et al., 2011; Holmedal et al., 2015; Patterson, 2012), however being more frequently associated to an onshore component.

The fundamental theory behind the sediment transport mechanism is to relate the frictional force exerted by the fluid on the bottom (bed shear stress) to the sediment response that may be translated into a transport rate. However, this is a challenging task as sediment transport is a complex, multidimensional, and dynamic process that results from the interactions of coastal hydrodynamics and non-uniform sediment particles (Amoudry and Souza, 2011).

This complexity is enhanced by the non-linear nature of the interaction between waves and currents, which means that their combined behaviour is not a simple sum of their individual actions.

In this context, the numerical modelling appears as a powerful predictive tool capable of individually analyse the influence of waves and currents on sediment dynamics, thus contributing to a better understanding of the bottom boundary layer processes and sediment transport. However, large discrepancies regarding the quantitative estimates of the sediment transport evidences the need of coupling this information with observational data in order to minimize model inaccuracies.

The purpose of this chapter is to present the modelling approach developed for the evaluation of the bottom boundary layer dynamics as well as the theory behind the model. This approach is represented by a one-dimensional bottom boundary layer model driven by waves and nearbed current measurements.

The governing equations and theories behind the numerical model are described in the next section (**3.2. Bottom boundary layer dynamics**), while an overview of the model implementation is presented in section **3.3. Numerical model overview**.

3.2 Bottom boundary layer dynamics

According to Nielsen (1992) the thickness of the bottom boundary layer (BBL) follows the general expression $\delta \propto \sqrt{\upsilon_t T}$ where υ_t is the eddy viscosity and T the flow period. This means that the boundary layer of a tidal flow is much more wider than that associated to superficial waves. The cohexistence of flows of different time scales and hence different boundary layer scales results in the wave BBL (in the order of centimeters) nested within a thicker BBL (of a few meters) associated to the steady flow (Madsen and Wood, 2002). Since thinner boundary layers translates in larger bed shear stress, waves tends to dominate sediment entrainment process. However, due to the "forward-backward" nature of wave motion, currents still play a relevant role on the net sediment transport (Nielsen, 1992).

The bed shear stress (τ_0) is the friction exerted on the seabed by the fluid, thus being the primary force controlling sediment dynamics (Equation 3.1). The shear stress (N/m^2) can also be written in velocity units (m/s), being represented by the friction velocity (u_*) as described in Equation 3.2.

$$\tau_0 = \rho u_*^2 \tag{3.1}$$

$$u_* = \sqrt{\frac{\tau_0}{\rho}} \tag{3.2}$$

where ρ is the density of the water.

The total bed shear stress (τ_0) results from the contribution of forces produced by (and acting on) sediment particles, by the pressure field associated with the flow over ripples and by the momentum extracted by the flow to move sediment particles (Soulsby, 1997). These three components are also known as skin friction (τ_{0s}), form drag (τ_{0f}) and sediment-transport contribution (τ_{0t}), respectively, thus giving:

$$\tau_0 = \tau_{0s} + \tau_{0f} + \tau_{0t} \tag{3.3}$$

In this work, bottom boundary layer dynamics will be evaluated seaward the depth of closure, where sediment transport is in general relatively low so its contribution to the total bed shear stress was neglected. Thus, the Equation 3.3 was simplified to:

$$\tau_0 = \tau_{0s} + \tau_{0f} \tag{3.4}$$

Attention must be given to the fact that the cohexistence of various components of bed shear stress often causes confusion. In that context, it is important to highlight that, in the next sections, only the skin friction (τ_{0s}) contribution is used for calculating the threshold of motion, reference concentration and bedload transport. The total bed shear stress (τ_0) in turn corresponds to the overall resistance of the flow and it is considered for the determination of turbulence intensities that influence the vertical diffusion of suspended sediment (Soulsby, 1997).

3.2.1 Current boundary layer

The bed friction experienced by low frequency nearbed currents normally forms a boundary layer of some meters or tens of meters thick. While in shallow waters the current BBL may occupy the entire depth, whereas in deep waters it only fills the lower part of the water column. The current speed within this layer increases with the distance from the bottom, where the faster current increase takes place near the bed. Equation 3.5 describes the variation of current velocity with a distance z from the bed according to the classic logarithmic vertical profile expressed in terms of z_0 (Figure 3.1).

$$u(z) = \frac{u_*}{k} ln(\frac{z}{z_0}) \tag{3.5}$$

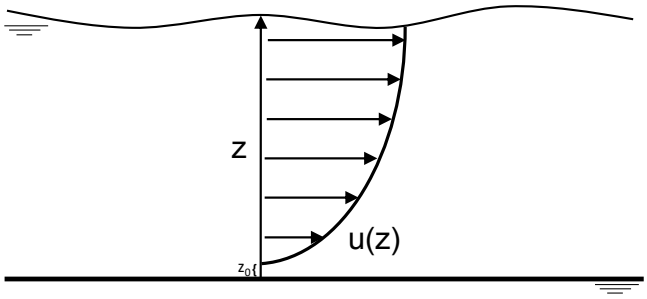

Figure 3.1 Schematic of the logarithmic velocity profile over the bed.

where $u_* =$ friction velocity

$z_0 =$ bed roughness length

$k =$ von Karman's constant = 0.4

The bed roughness length experienced by the currents depends on the current speed, on the viscosity of water (υ) and on the physical bed roughness (bedforms). A simplified method for determining z_0 proposed by Colebrook and White (1937) is:

$$z_0 = \begin{cases} \dfrac{\upsilon}{9u_*} & \text{for hydrodynamically smooth flow, i.e. when } \frac{u_* k_s}{\upsilon} < 5, \quad (3.6a) \\ \dfrac{k_s}{30} & \text{for hydrodynamically rough flow, i.e. when } \frac{u_* k_s}{\upsilon} > 70. \quad (3.6b) \end{cases}$$

The k_s equivalent Nikuradse sand grain roughness is assumed by Soulsby (1997) to be:

$$k_s = 2.5 d_{50} \tag{3.7}$$

where d_{50} is the median grain size.

As mentioned in Soulsby (1997), for mathematical simplification, it is a common practice to treat all flows over sandy bottoms as being hydrodynamically rough, which is also assumed in the present work.

By merging Equations 3.6b and 3.7, a grain-size related bed roughness length is obtained:

$$z_{0s} = \frac{d_{50}}{12} \tag{3.8}$$

According to Madsen and Wood (2002), for the estimation of the sediment transport, it is often convenient to express the bottom shear stress (τ_c) based on a known flow speed (at a specific distance from the bottom z) in terms of a current friction factor (f_c):

$$\tau_c = 0.5\rho f_c u(z)^2 \tag{3.9}$$

The friction factor is given on Eq. 3.10 by assuming the logarithmic profile for current velocity as described in Smyth and Li (2005).

$$f_c = 2\left[\frac{k}{ln(\frac{z}{z_0})}\right]^2 \tag{3.10}$$

3.2.2 Wave boundary layer

Contrasting with the relative steadiness of low frequency currents, the wave boundary layer is inherently unsteady due to its oscillatory nature. This periodic behaviour is clearly observed through the oscillations of the bottom wave orbital velocity. This motion, in deep waters, is described by circular paths along the water column that are not influenced by the bottom. However, in sufficiently shallow waters [1] the wave starts "feeling the bottom" and this interaction gradually changes the orbital motion along the water column to elliptic paths and then to a back and forward movement just above the seabed (Figure 3.2). This nearbed oscillatory motion acts as the main force driving fluid-sediment interaction, thus of crucial importance to the bottom boundary layer dynamics and consequently to the sediment transport.

[1] A condition that is usually considered satisfied when water depth is less than half the wavelength of surface gravity waves.

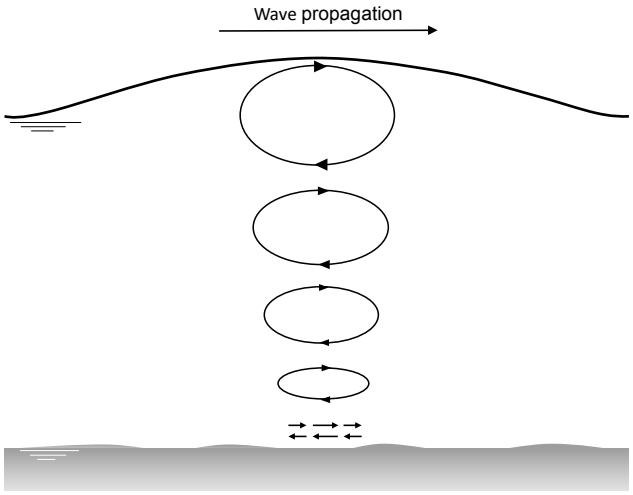

Figure 3.2 Description of the path of the wave orbital velocity along the water column over shallow depths.

The oscillatory nature of the wave BBL is described by the successive increase and decrease of its thickness. Basically, the boundary layer grows and diminishes each half of wave period, thus preventing its development and resulting in a layer of only a few centimeters (Figure 3.3).

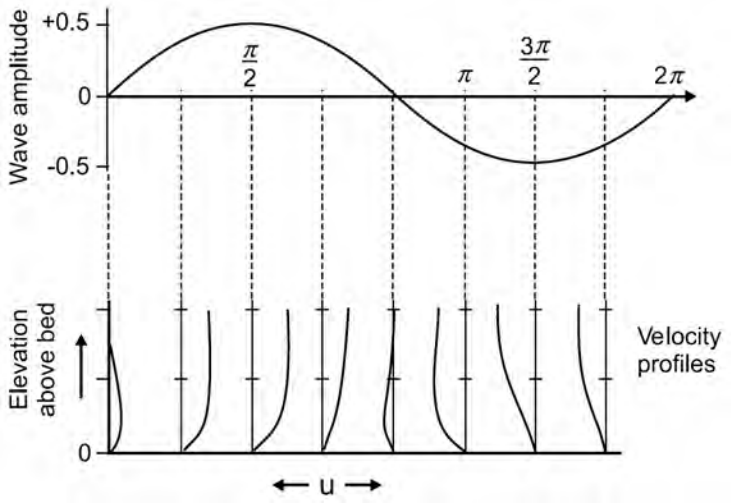

Figure 3.3 The changing profile shape of the oscillatory wave bottom boundary layer for a single wave cycle (reprinted from Davidson-Arnott, 2011).

The time-varying wave orbital velocity results in a time-varying bed shear stress. Thus, it is a common practice to characterize wave-generated bed shear stress (τ_w) in terms of the maximum/significant value of the wave bottom orbital velocity (u_w), which is represented on the top of the wave BBL. Also, as on the analogous expression for current-alone action (Equation 3.10), the wave-induced bed shear stress depends on a friction factor (f_w):

$$\tau_w = \frac{1}{2}\rho f_w u_w^2 \tag{3.11}$$

For a single frequency (monochromatic) wave of height H a period T in water of depth h, the amplitude u_w is described according to the following equation.

$$u_w = \frac{\pi H}{T \sinh(kh)} \tag{3.12}$$

where $k = 2\pi/L$ is the wave number, being L the wavelength

However, a naturally occurring random sea will have a broad spectrum of frequencies. Thus, Soulsby and Smallman (1986) have developed a better approximation to calculate the representative orbital velocity (u_{rms}) based on statistical wave parameters and by assuming a JONSWAP[1] spectrum:

$$u_{rms} = \frac{0.25 H_s}{T_n(1+At^2)^3} \tag{3.13}$$

where H_s = significant wave height

$A = \left[6500 + (0.56 + 15.54t)^6\right]^{1/6}$

$t = \frac{T_n}{T_z} = \frac{1}{T_z}(\frac{h}{g})^{1/2}$, being T_z the average zero-crossing period and T_n the natural scaling period.

From Equation 3.13 the significant orbital velocity u_w can be obtained according to the following relationship:

$$u_w = \sqrt{2} u_{rms} \tag{3.14}$$

The wave friction factor f_w depends on the type of flow (laminar, smooth turbulent or turbulent) and also on the type of bed (smooth or laminar). According to Soulsby (1997), by assuming a rough turbulent flow the f_{wr} can be obtained based on the ratio between the semi-orbital excursion (A) and the grain-related bottom roughness (z_{0s}) as described in

[1] Joint North Sea Wave Project spectra: an empirical relationship that defines the distribution of wave energy with frequency.

Equation 3.15. While for a smooth turbulent flow the friction factor is determined is given by 3.16

$$f_{wr} = 1.39(\frac{A}{z_{0s}})^{-0.52} \tag{3.15}$$

where $A = \frac{u_w T}{2\pi}$ is the semi-orbital excursion.

$$f_{ws} = BR_w^{-N} \tag{3.16}$$

where B = 0.521, N = 0.187 and $R_w = \frac{u_w A}{\nu}$ is the Reynolds number.

The determination of the final friction factor (f_w) follows Soulsby (1997) definition where:

$$f_w = max(f_{wr}, f_{ws}) \tag{3.17}$$

3.2.3 Wave-current boundary layer

As the sediment dynamics over the nearshore zone is mainly controlled by the combined effect of waves and currents, numerical approximations of this interaction are of main importance on the sediment transport estimation. However, waves and currents interact with each other hydrodynamically and its combined effect can not be explained by a linear sum of their individual behaviours (Figure 3.4). This fact adds complexity to the bottom boundary layer models, making the quantification of the wave-current induced shear stress a challenging task.

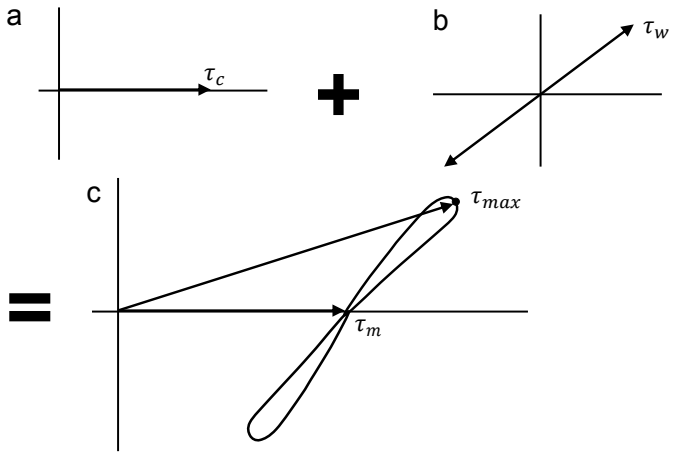

Figure 3.4 Scheme of the bed shear stress enhancement due to non-linear interaction between waves and currents. a) Current-alone stress (τ_c). b) wave-alone stress (τ_w). c) wave-current bed shear stress with mean (τ_m) and maximum (τ_{max}) values (reprinted from Soulsby et al., 1993).

As shown in Figure 3.4c, in a combined flow the bed shear stress varies over a wave cycle. Thus, the key-parameters in sediment transport calculations are represented by the mean (τ_m) and maximum (τ_{max}) values of bed shear stress over a wave cycle. While the particle threshold of motion and entrainment is determined by τ_{max}, the current velocity and diffusion of suspended sediment are driven by τ_m (Soulsby et al., 1993).

There are a wide variety of approximations (over 20) proposed to describe the non-linear behaviour within the wave-current bottom boundary layer and therefore for determining τ_m and τ_{max}, being most of them concentrated on the case of a rough turbulent flow. Examples of some major contributions to this area are represented by the analytical models of Bijker (1967), Grant and Madsen (1979), Fredsøe (1984), van Kesteren and Bakker (1984), Christoffersen and Jonsson (1985), Myrhaugh and Slaattelid (1989) and the numerical models of Huynh-Than and Temperville (1991 in Soulsby et al., 1993) and Davies et al. (1988). Soulsby et al. (1993) have performed an intercomparison of these models based on the estimated values of τ_{mean} and τ_{max} which gives a good overview of the overall performance displayed by the BBL models (Figure 3.5). Emphasis should be given to the time-invariant eddy viscosity model of Grant and Madsen (1979) which have been successfully applied to numerous studies on the continental shelf (e.g. Cacchione and Drake, 1982; Condie and Sherwood, 2006; Styles and Glenn, 2005; Taborda, 1999) and will be therefore used in this work. The application of this model is based on the parametrization derived by Soulsby et al. (1993) (accurate to $\pm 5\%$).

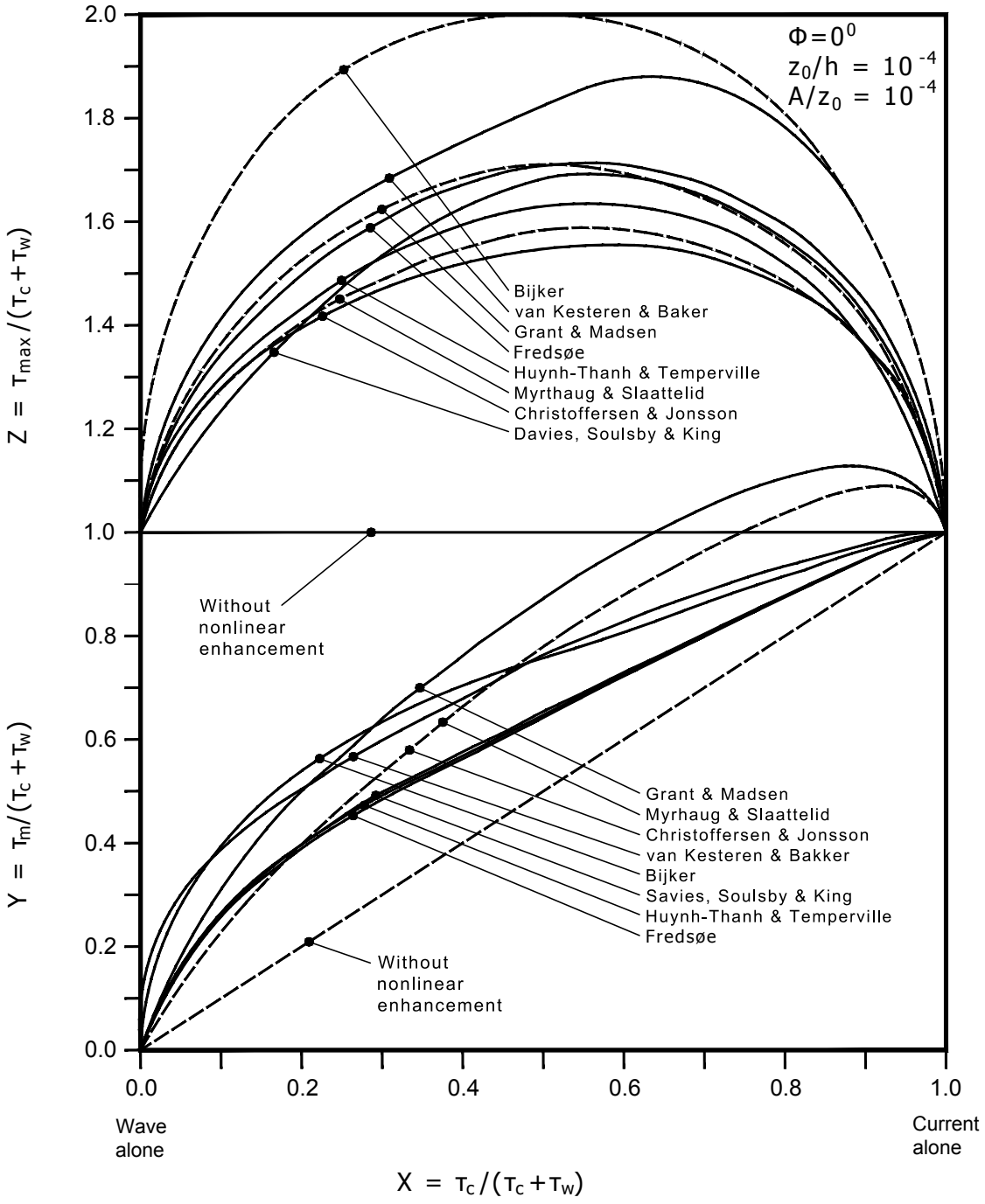

Figure 3.5 Intercomparison of 8 wave-current bottom boundary layer models for the prediction of mean (τ_m) and maximum (τ_{max}) shear stresses (reprinted from Soulsby et al., 1993).

3.2.4 Threshold of particle motion

The threshold for the initiation of motion can be defined as the minimum force/velocity required to move a sediment particle and it is reached when driving forces exceed the stabilizing ones. For non-cohesive sediments this limit is usually given in terms of the bed shear stress. This approach, developed by Shields (1936) for steady currents, can be extended to wave-current induced flows as verified by Soulsby (1997). The Shield's theory is based on the ratio between the force exerted by the bed shear-stress on the sediment particle and the submerged weight of the grain counteracting this. Thus, the critical Shields parameter (θ_{cr}) is given through:

$$\theta_{cr} = \frac{\tau_{cr}}{g(\rho_s - \rho)d} \tag{3.18}$$

The empirical results obtained by this author are originally described by the Shield curve in Shields (1936) where the θ_{cr} are ploted against the grain Reynolds number[1]. Later, a more practical parametrization is found in Soulsby (1997) where the critical Shields (θ_{cr}) is plotted against the dimensionless grain size D_* (equation).

$$D_* = \left[\frac{g(s-1)}{v^2}\right]^{1/3} d \tag{3.19}$$

Based on this new curve, Soulsby and Whitehouse (1997, in Soulsby, 1997) have proposed an improved formulation for the threshold bed shear stress:

$$\theta_{cr} = \frac{0.30}{1+1.2D_*} + 0.055\,[1 - exp(-0.020D_*)] \tag{3.20}$$

3.2.5 Bedforms

The dynamics within the bottom boundary layer are dictated by the resistive mechanisms imposed by the various roughness scales that compose the seabed boundary. Over a flat sediment bed, for example, the roughness scales are given solely by the median grain diameter, which momentum transfer between the fluid and the sediment particles is known as skin friction. However, unconsolidated sea bottoms are commonly formed into ripples, thus adding more resistance to the flow and affecting the turbulence intensities which in turn influences the diffusion of suspended sediment.

The quantitative estimation of bedforms are still not well understood under the individual action of waves or currents and several formulas for estimating the wave-related and current-

[1] $Re = \frac{u_{*cr}d}{v}$

related bedform geometry have been developed over the years. Soulsby and Whitehouse (2005a,b), for example, listed 28 prediction methods of which 18 are for wave-alone, 5 for current-alone and 5 for combined wave-current action. Uncertainties regarding this field are greater when dealing with the combined action of these forcing agents, which are the conditions for the generation of bed features on the nearshore environment. In this case, it is convenient to adopt the simple criteria described in Soulsby et al. (2012) that assumes the relative intensity of waves and currents acting on the bottom for determining which expression to be used:

$$\text{if } \tau_w \geq \tau_c \text{ use wave-generated expressions}$$
$$\text{if } \tau_c \geq \tau_w \text{ use current-generated expressions}$$

As this work focus on a wave-dominated nearshore environment, the estimation of bedform geometry through the ripple wavelength (λ) and height (η) will follow the wave-generated expressions developed by Soulsby and Whitehouse (2005b):

$$\lambda = \frac{A}{1 + 1.87 \times 10^{-3}\Delta(1 - exp(-(2 \times 10^{-4}\Delta)^{1.5}))} \tag{3.21}$$

$$\eta = \lambda \times 0.15(1 - exp(-(\frac{5000}{\Delta})^{3.5})) \tag{3.22}$$

where $\Delta = \frac{A}{d_{50}}$, being A the semi-orbital excursion and d_{50} the median grain size.

These expressions are valid when the threshold of motion is exceeded, i.e., if $\tau_w > \tau_{cr}$.

Finally, the form drag component z_{0f} can be related to ripple wavelength (λ) and height (η) through the following relationship described in Soulsby (1997):

$$z_{0f} = \alpha \frac{\Delta^2}{\lambda} \tag{3.23}$$

where α ranges between 0.3 and 3 with a typical value of 1.0 which is assumed in this work.

3.2.6 Sediment transport

When the threshold for the initiation of motion is exceeded, the sediment particles starts to move. In general terms, when the wave-current induced bed shear stress is slightly higher than its critical value, the sediment particles are predominantly transported by rolling, sliding and/or saltating, i.e. as bedload. On the other hand, when the bed shear velocity increases and exceeds the fall velocity of the grains, the sediment starts to move in the form of suspended load (Figure 3.6). These two modes of transport usually coexist on the nearshore environment,

thus a better evaluation of the sedimentary dynamics is achieved when both suspended and bedload are considered on the modelling approach.

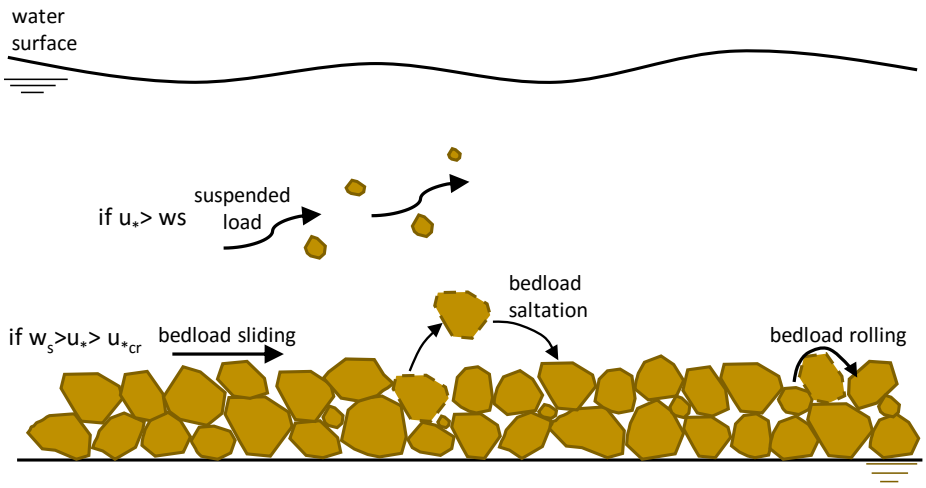

Figure 3.6 Suspended and bedload modes of transport.

However, there is a particularity on the threshold for the initiation of motion on particles with texture between silt ($10^{-5} - 10^{-6}$m) and very fine sand (10^{-4}m). For these grain sizes, the critical shear stress to get into suspension is theoretically lower than the threshold to be transported as bedload. In this particular situation, when the threshold of particle motion is exceeded, sediment particles are immediately transported as suspended load, without going through the bedload mode of transport (Figure 3.7).

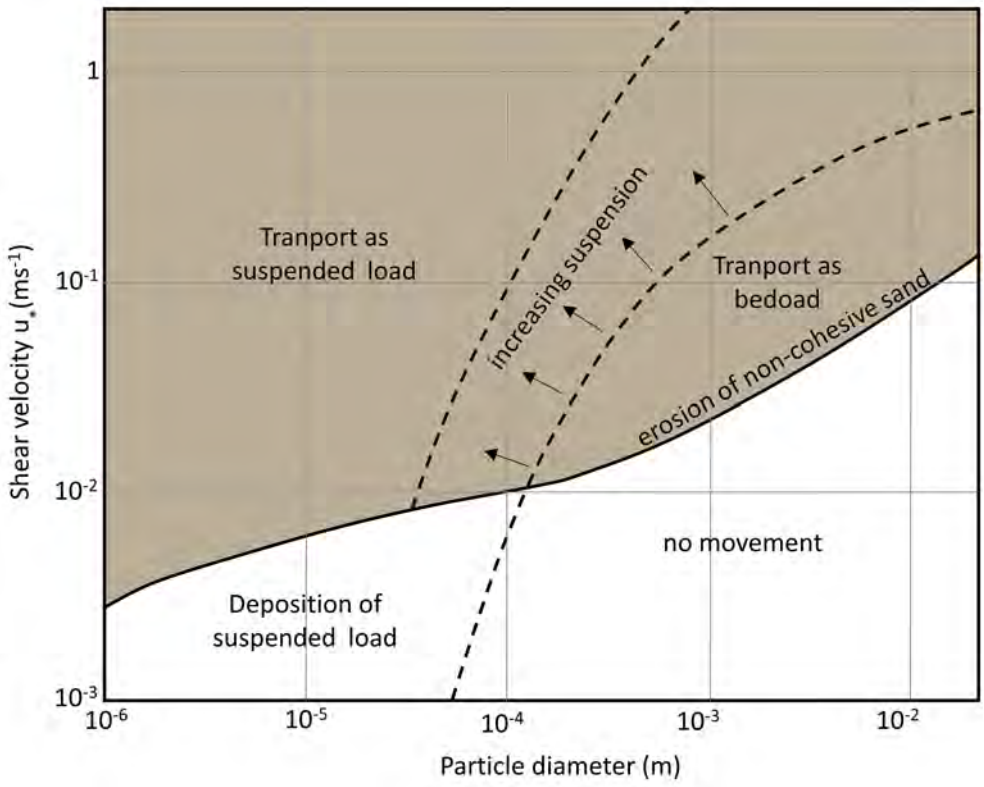

Figure 3.7 Diagram comparing the shear velocity at which sediment particles of different sizes are transported in suspension or as bedload. Broken lines represent gradational boundaries. The parameters used in the compilation of this graph are: density of quartz:2.65×10^3 kg m^{-3}; density of sea water: 1.025×10^3 kg m^{-3} at 15°; viscosity: 10^{-3} N s m^{-2}; and acceleration of gravity: 9.8 m s^{-2} (adapted from Brown et al., 1994).

3.2.6.1 Bedload

This is the part of the total sediment transport which occurs in a thin nearbed layer of high sediment concentration. According to Bagnold (1956, in Nielsen, 1992) the bedload, under a modelling approach, can be defined as the mode of transport supported by intragranular forces, thus being dependent on the skin friction force.

Some of the more commonly methods for estimating the bedload transport rate are empirical formulae developed for steady uniform flows, i.e. for use in rivers, such as the works of Meyer-Petter and Muller (1948), Bagnold (1963, in Soulsby, 1997), Nielsen (1992) and van Rijn (1984). All these formulas relates a dimensionless transport rate (Φ) to a power of the excess bed shear stress with respect to its critical value for initiation of motion which is usually in the form of Equation 3.24. These formulas, which are still widely used for river applications, have been adapted to marine coastal environments, i.e. to a combined

wave-current flow on the later works such as the ones of Ribberink (1998), Soulsby (1997) and Kleinhans and Grasmeijer (2006).

$$\Phi = m\theta^n(\theta - \theta_{cr})^p \tag{3.24}$$

where $\Phi = \frac{q_b}{[g(s-1)d^3]^{0.5}}$

θ = Shields parameter

θ_{cr} = critical Shields

q_b = volumetric bedload rate per unit width

g = acceleration due to gravity

ρ = water density

s = ratio of densities between sediment and water

d = grain size

m, n and p = empirical constants

In the present work, the estimation of the bedload transport is evaluated in terms of a steady current superimposed on sinusoidal waves which asymmetry is not considered. For this, it is applied the formula of Soulsby (1997), better described in Soulsby and Damgaard (2005), which is an approximation to the bedload transport obtained by integrating the formula of Nielsen (1992) (same as Equation 3.25) through one wave cycle (Equations 3.25 to 3.28).

$$\Phi_{x1} = 12\theta_m^{0.5}(\theta_m - \theta cr) \tag{3.25}$$

$$\Phi_{x2} = 12(0.95 + 0.19cos2\phi)\theta_w^{0.5}\theta_m \tag{3.26}$$

$$\Phi_x = max(\Phi_{x1}, \Phi_{x2}) \tag{3.27}$$

$$\Phi_y = \frac{12(0.19\theta_m\theta_w^{0.5}sin2\phi)}{\theta_w^{1.5} + 1.5\theta_m^{1.5}} \tag{3.28}$$

subject to $\Phi_x = \Phi_y = 0$ if $\theta_{max} \leqslant \theta_{cr}$

The mean volumetric bedload transport rate in the direction of the current (q_{bx}) and at right angle to the current (q_{by}) is given through the relationship $\Phi_{x,y} = \frac{q_{bx,y}}{[g(s-1)d^3]^{0.5}}$ already mentioned in Equation 3.24.

3.2.6.2 Suspended load

When the hydrodynamic forces are significantly higher than the threshold of motion and exceeds the fall velocity of the sediment, the transport of sediment particles instead of being associated to the intergranular forces governed by skin friction shear stress (τ_{0s}), starts to be supported by the fluid turbulence associated to the total bottom shear stress (τ_0). This transition characterizes the change from the bedload to the suspended load mode of transport (see Figure 3.7). Basically, the larger the flow velocity, the larger is the relative contribution of the suspended load to the total transport.

According to Bagnold (1966), for sediment particles to remain in suspension, and consequently enabling their transport in suspension, there must be an upward turbulent component of velocity (which relates to the u_*) higher than the particle fall velocity (w_s).

The fall velocity of sediment particles in water is given by their diameter and density together with the viscosity of water. Many formulas (e.g. Hallermeier, 1981; van Rijn, 1984) assume different formulations for different values of the dimensionless grain size D_*(Equation 3.19). A more simplified and better performed method for estimating the fall velocity is described in Soulsby (1997) where a single formulation is applied to all D_* (Equation 3.29).

$$w_s = \frac{\nu}{d_{50}}[(10.36^2 + 1.049D_*^3)^{1/2} - 10.36] \tag{3.29}$$

where ν : kinematic viscosity of water

g : acceleration due to gravity

s : ratio of densities between sediment and water

d_{50} : median grain size

According to Styles and Glenn (2005), a commonly used method to model sediment resuspension in continental shelf environments is to prescribe the nearbed concentration in terms of a reference value (C_r) that is a function of the excess shear stress based on skin friction. In this case, if the eddy diffusivity of the sediment is assumed to increase linearly with height above sea bed (z), the corresponding profile of concentration is given by a power-law profile:

$$C(z) = C_r(\frac{z}{z_r})^{-b} \tag{3.30}$$

where z_r is the nearbed reference height described in Equation 3.33

In the nearshore environment which is under the combined action of waves and currents, the sediment is suspended within the wave boundary layer (z_w) and redistributed along the

water column by the turbulence associated to the currents. In these conditions, Soulsby (1997) describe the form of the concentration profile according to:

$$C(z) = C_r(\frac{z}{z_r})^{-b_{max}} \qquad if \quad z_r \leq z \leq z_w \tag{3.31}$$

$$C(z) = C(z_w)(\frac{z}{\delta_w})^{-b_m} \qquad if \quad z_w < z \leq h \tag{3.32}$$

where $b_{max} = \frac{w_s}{k u_{*max}}$: Rouse number associated to the maximum shear velocity u_{*max}, being k : von Karman's constant = 0.40

$b_m = \frac{w_s}{k u_{*m}}$: Rouse number associated to the mean shear velocity u_{*m}

$z_w = \dfrac{u_{*max} T}{2\pi}$

$C(z)$: sediment concentration at height z

z_r : nearbed reference height

C_r : reference concentration at height z_r

The reference nearbed sediment concentration (C_r) is a key feature to describe the entrainment of sediment in suspension and its prediction can be performed through several formulations. Garcia and Parker (1991) tested seven of them against a large dataset concluding that the approximations of van Rijn (1984) and Smith and McLean (1977) have the best performances, being the last one used in this work and given by the following equations:

$$\begin{aligned} C_r &= \frac{C_b \gamma_0 T_s}{1 + \gamma_0 T_s} \\ \text{at height } z_r &= \frac{26.3 \tau_{cr} T_s}{\rho g (s-1)} + \frac{d_{50}}{12} \end{aligned} \tag{3.33}$$

where $C_b = 1 - \varepsilon$: maximum sediment concentration, being ε the sediment porosity.

γ_0: empirical resuspension coefficient

$T_s = \frac{(\tau_{0s} - \tau_{cr})}{\tau_{cr}}$: normalized excess bed shear stress

Estimates of γ_0 resuspension coefficient from field and laboratory studies have revealed a large variation ranging essentially between 10^{-2} and 10^{-5} values (e.g. Drake and Cacchione, 1989; Hill et al., 1988; Li et al., 1996; Smith and McLean, 1977; Vincent and Green, 1990). Despite estimated γ_0 from these studies differs more than an order of magnitude, they all present a systematic decrease in γ_0 values with the increase of the excess of shear stress. In this work the default value of 2.4×10^{-4} assumed by Smith and McLean (1977) will be used for the resuspension coefficient.

The concentration of sediment in the bed (C_b) is frequently set to a default values of 0.65, thus assuming a sediment porosity of 0.35.

The general principle for the calculation of the total suspended load transport rate (q_s) is to depth-integrate the sediment flux given by the product between the velocity u and concentration c associated to a depth z as described in Equation 3.34.

$$q_s = \int_{z_r}^{h} u(z)c(z)dz \tag{3.34}$$

3.3 Numerical model overview

3.3.1 Introduction

The model developed in this work (available at https://github.com/ivanabosnic/Transed2016) consist on a unidimensional numerical model based on sets of mathematical equations (discussed in section 3.2) that overall describe the physical processes within the wave-current bottom boundary layer.

The modelling approach carried out on this work is set on class-based object-oriented programming (OOP) principles that simplify programming tasks involving specialized data structures or large numbers of functions behaving interactively, thus being suitable for this work.

In the class-based OOP approach, programming procedures rely on three basic concepts: class, object and methods. The class is the template or set of instructions to build a specific type of object. The object in turn is a self-contained entity with its own identity containing properties and methods needed to process object data. Finally, the methods can be described as a programmed procedure usually based on a set of functions that process the data known to the object.

3.3.2 Model classes

The object-oriented model is built around 8 classes supported by wave, current and sediment data. Each class generate a object containing data (properties) and procedures (methods) for processing data. However, some of these entities do not have any property associated as they depend only on methods from other objects (Figure 3.8).

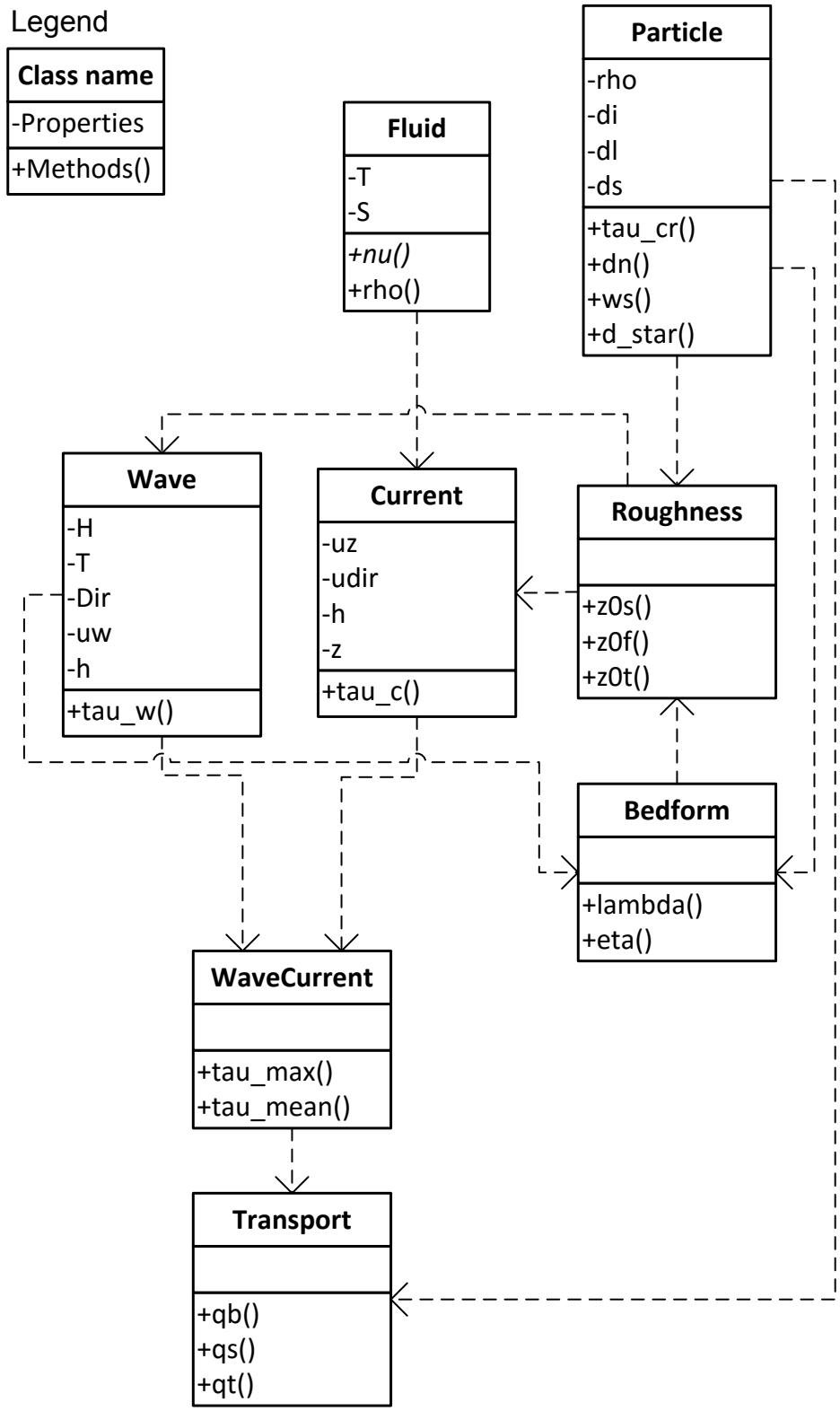

Figure 3.8 Class diagram of the developed numerical model.

A synthetic description of each class is carried out on the next sections.

3.3.2.1 Fluid

The class Fluid holds the water temperature and salinity and compute the kinematic viscosity (ν) and density (ρ) using the algorithms of Unesco (1983). It computes the physical properties of the fluid, namely the kinematic viscosity (ν) and density (ρ), based on water temperature and salinity using the algorithms of Unesco (1983).

3.3.2.2 Particle

The class Particle describe the sediment properties based on the representative diameters (smaller ds, intermediate di and larger dl) of the grain and on the sediment density (ρ_s).

Class methods include:

1. nominal diameter (dn): equal to the intermediate diameter (di) and assumed to be equal to the median grain size (d_{50}).

2. critical shear stress (tau_cr): calculated according to the Equation 3.20

3. dimensionless diameter (d_star): calculated according to Equation 3.19

4. fall velocity (ws): calculated according to the Equation 3.29.

3.3.2.3 Roughness

The class Roughness compute the roughness length ($z0$) based on the grain size and/or bedform geometry which are given by Particle and/or Bedform classes, respectively. Thus, it calculates the grain-related roughness, bedform roughness as well as total roughness depending on the input parameters.

Class methods include:

1. Grain-related roughness (z0s): calculated according to Equation 3.8.

2. Bed form roughness (z0f): calculated according to Equation 3.23.

3. Total roughness (z0): z0s + z0f

3.3.2.4 Current

The class Current compute the current-related bed shear stress (tau_c) in terms of a friction factor according to Equation 3.9 as described in Madsen and Wood (2002). This calculation is based on nearbed current measurements including current speed and direction at a specific distance z from the bottom, fluid properties and roughness length, being the last two items given by Fluid and Roughness objects, respectively.

3.3.2.5 Wave

Analogous to the Current class, the class Wave compute the wave-related bed shear stress (tau_w) in terms of a friction factor according to Equation 3.11 as described in Soulsby (1997). This calculation is based on the wave significant parameters H, T, Dir, and u_w and also on the water depth, direction of the bathymetry and roughness length given by the Roughness object.

3.3.2.6 WaveCurrent

The class WaveCurrent computes the wave-current non-linear interaction using the bottom boundary layer model of Grant and Madsen (1979) parametrized by Soulsby et al. (1993) in order to give the following methods:

1. Mean shear stress (tau_m)
2. Maximum shear stress (tau_max)

3.3.2.7 Bedform

The class Bedform calculates the bedform geometry using the method of Soulsby and Whitehouse (2005b).

Class method includes:

1. Bedform wave length (lambda): calculated according to the Equation 3.21
2. Bedform wave height (eta): calculated according to the Equation 3.22

3.3.2.8 Transport

The class Transport calculates the sediment transport associated to the bedload and suspended load modes of transport as well as the total sediment transport.

Class method includes:

1. Bedload (qb): calculated according to the approximation of Soulsby (1997) adapted from Nielsen (1992) and described in the Equations 3.25, 3.26, 3.27 and 3.28.

2. Suspended load (qs): calculated according to the general Equation 3.34 where the concentration profile is described according to Equations 3.31 and 3.32 as in Soulsby (1997). Finally, the reference concentration follows the method of Smith and McLean (1977) described in Equation 3.33.

3. Total load: qb + qs

3.3.3 Model algorithm

The modelling strategy developed on this work consist on automatically process large wave and current data for evaluating the bottom boundary layer conditions which are in turn crossed with sediment data in order to assess the BBL dynamics and induced sediment transport. The overall modelling procedure is described in Figure 3.9.

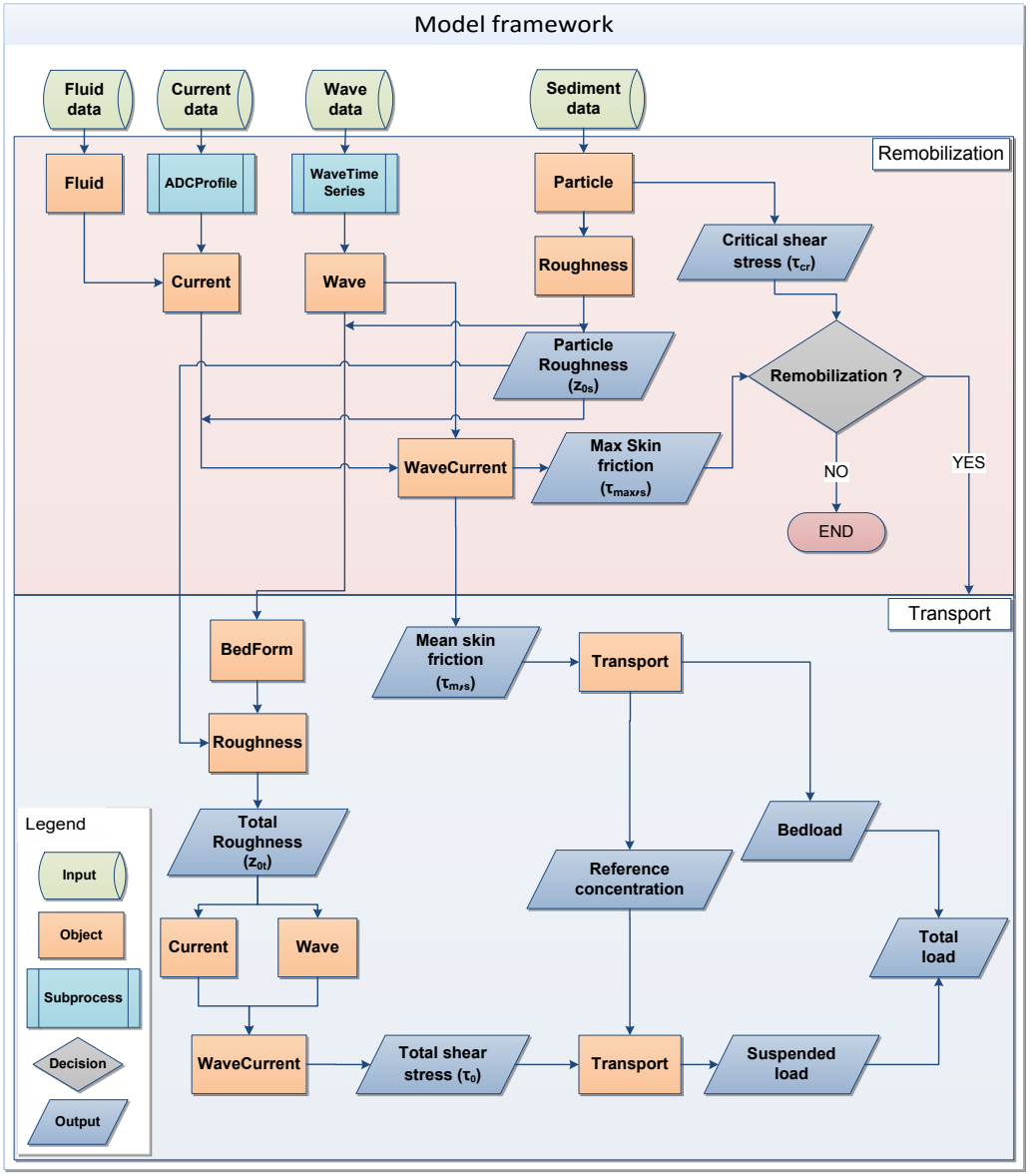

Figure 3.9 Modelling strategy for the evaluation of the bottom boundary layer dynamics and sediment transport.

Chapter 4

Sedimentary dynamics in a moderate-energy environment

Modified from Bosnic, I., Cascalho, J., Taborda, R., Drago, T. Hermínio, J., Rosa, M., Dias, J. and Garel, E. (2017). Nearshore sediment transport: Coupling sand tracer dynamics with oceanographic forcing, Marine Geology, 385:293-303, ISSN 0025-3227, https://doi.org/10.1016/j.margeo.2017.02.004.

4.1 Introduction

The importance regarding the understanding of the nearshore sedimentary dynamics relates mainly to its influence on the coastal sediment budget and the further implications of it (see Chapter 1). The impact of this dynamics on bottom instrument installation as well as on benthic ecosystems also highlights the relevance of this theme (Markert et al., 2015). However, despite sediment transport studies within the surf zone are well documented in the literature (e.g. de Vries et al., 2014; Kraus et al., 1982; Wang et al., 1998), this process is still poorly understood deeper than the depth of closure (DoC) owing greatly to the lack of direct sediment transport measurements at seasonal and longer time scales. In order to contribute to fulfil this gap, the present chapter aims at evaluating the sedimentary dynamics seaward of the DoC under a multiproxy approach involving sediment transport numerical modelling (see Chapter3) and measurement (sand tracer experiment) and its relationship with the oceanographic forcing, bottom morphology and sedimentary cover.

4.2 Study area

The study area is located at Tavira (Portugal) nearshore zone offshore the eastern sector of the Ria Formosa barrier system (Figure 4.1). At this location, the continental shelf, up to 30 m depth, is characterized by a gentle slope with approximately 1:170 NE-SW oriented.

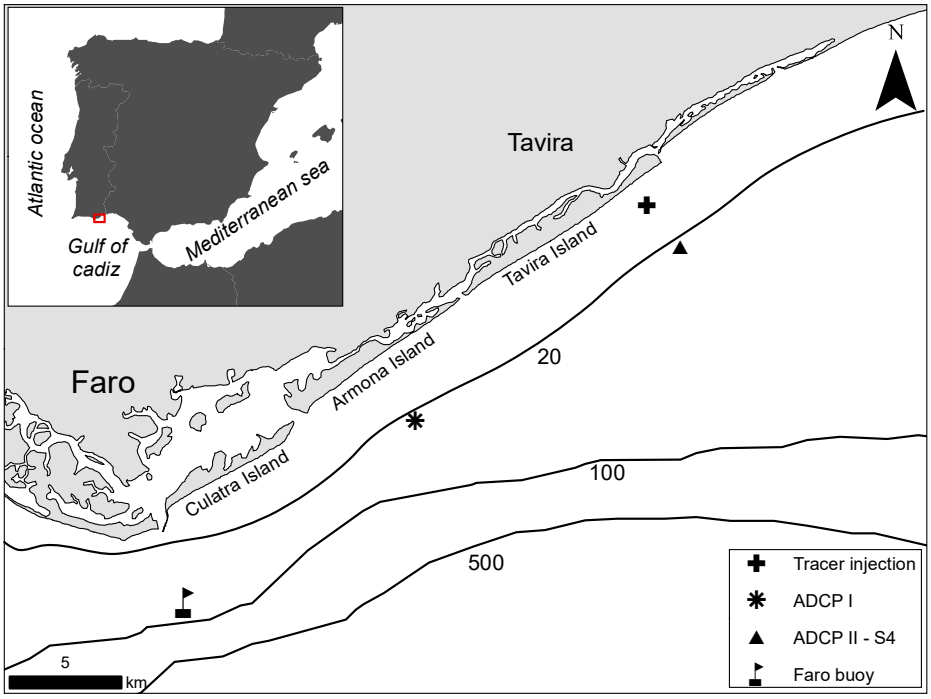

Figure 4.1 Study area and field instrumentation sites.

Bottom sediment is largely dominated by fine to medium sand down to 10 m water depth; in deeper areas (10 to 15 m) gravel-sized sediments become important representing between 10 to 30 % of the total sediment as well as the presence of mollusc shells that comprises 30 to 45 % (Rosa et al., 2013; Rufino et al., 2008). The depth of closure on this region was estimated to be around 10 m depth by Almeida et al. (2010), while the work of López-Doriga et al. (2015) developed specifically in the study area of the present work revealed a DoC of about 6 m depth below mean sea level.

The tidal regime is semi-diurnal with average ranges of 1.3 and 2.8 m for neap and spring tides, respectively. According to Costa et al. (2001), wave climate is characterized by an offshore average significant wave height of 0.92 m and average mean and peak wave period of 4.7 and 8.2 s, respectively, with incident waves predominantly from W-SW (71% of occurrences). A particular condition called "Levante", marked by short period waves generated by SE winds, represents 23% of the occurrences. The storm regime within this

region is characterized by significant wave heights higher than 3.5 m which occurrences are mainly from SW (64%) and SE (32%) directions.

The study area constitutes the equatorward extremity of the Iberian upwelling system. The nearshore circulation is predominantly alongshelf, characterized by northeastward coastal upwelling jets alternating with coastal counter-currents of opposite direction (Relvas and Barton, 2002). Various studies suggest a significant control of large-scale wind conditions on this coastal circulation (Garel et al., 2016; Sánchez et al., 2006). Recent analyses of multiyear current observations have indicated that the alongshelf flow is mainly barotropic, reaching (depth-averaged) magnitudes up to 0.4 m/s, with a predominance of northeastward currents ($\approx$ 60% of time) and no seasonal variability (Garel et al., 2016). Cross-shelf currents are one order of magnitude lower and mostly tidal.

4.3 Materials and methods

The nearshore sedimentary dynamics was evaluated based on a multiproxy approach involving sedimentological, morphological and oceanographic features. This characterization was based on both in situ and modelling data (e.g. tracer experiment and numerical model application) further described on the next sections.

4.3.1 Oceanographic monitoring

4.3.1.1 In situ measurement

Local hydrodynamic conditions were measured at two sites at the nearshore zone (Figure 4.1). The first one was located offshore Armona Island where waves and currents were measured using an upward-looking ADCP (Workhorse 600 kHz, TRDI) bottom mounted on top of an 1.4 m-height artificial reef, at 23 m water depth (ADCP I in Figure 4.1). Several deployments were performed during the studied period, with durations from 35 up to 98 days (Figure 4.2). Current velocities along the water column were measured for at least 15 minutes every 60 minutes within 0.5 m cells where first valid ADCP record is placed 3.60 m above bottom. Waves were registered during a minimum period of 10 minutes every 3 hours. The vertical distribution of the flow velocities was also measured by an upward-looking ADCP (Sentinel V 500 kHz, TRDI) bottom-mounted offshore Tavira Island during a shorter period (84 days - see Figure 4.2) using the same configuration above-mentioned (ADCP II - in Figure 4.1). At this site, an electromagnetic current meter (S4A from InterOcean Systems Inc.) was also deployed together with the ADCP at 0.65 m from the bed. The S4 provided 2

minute-averaged current measurements every 30 minutes, and wave parameters every hour computed from 10 minutes-long current measurements at a 2 Hz sampling rate.

In order to compare the oceanographic conditions to the sediment dynamics data obtained through the sand tracer experiment, oceanographic data is displayed according to the time periods (P1 to P4) between tracer surveys (C1 to C4, Figure 4.2). Also, due to gaps on the ADCP I deployment, current data represents 100 %, 63 %, 33 % and 76 % of the encompassed time on observation periods P1, P2, P3 and P4, respectively (see Figure 4.2).

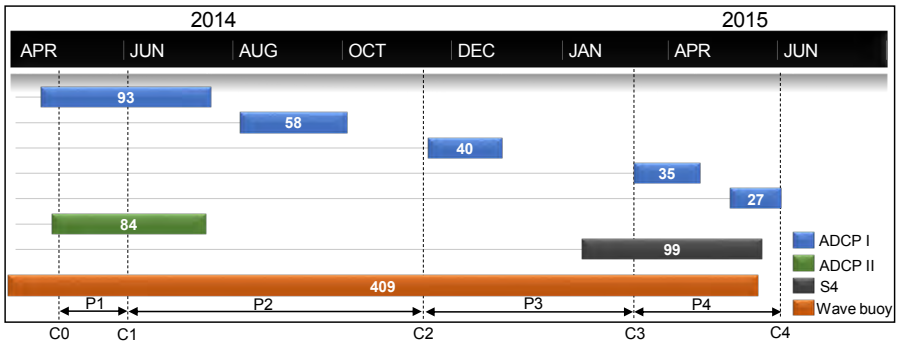

Figure 4.2 Time of deployment for each instrument and respective days of observation (inside the coloured bars). Sea missions for tracer survey (C0 to C4) and periods of oceanographic monitoring (P1 to P4) are also marked on the timeline.

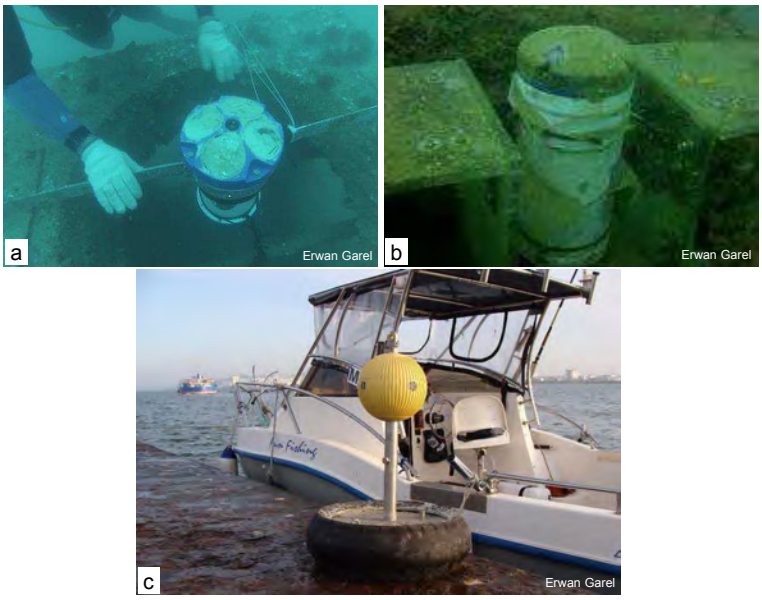

Figure 4.3 Oceanographic instrumentation: a) ADCP I b) ADCP II c) S4 current meter.

Along and cross-shelf near bottom current components were calculated according the angle of maximum variance of the flow using non-filtered current data. Positive values of the two components are oriented northeastward (alongshelf) and onshore (cross-shelf).

The spatial representativeness of the current data acquired offshore Armona was checked through current data comparison between ADCP I and II and through data supplied by the 3D global ocean model NEMO[1].

4.3.1.2 Wave modelling

Offshore wave regime recorded at Faro buoy, between April 2014 and April 2015, was propagated using SWAN 3rd generation model (Booij et al., 1999) under stationary mode over a 4.32 km x 5.10 km local grid nested into a 42.5 km x 50.5 km regional grid with cell sizes of 20 m and 500 m respectively. The larger grid is based on the Iberian Coast and the Bay of Biscay digital terrain model provided by European Marine Observation and Data Network (EMODnet) available at http://www.emodnethydrography.eu/, while the nested one is build from high-resolution bathymetric data acquired in the scope of SHORE project (Figure 4.4). The wave modelling strategy was validated against in situ data collected by the ADCP I and also by comparing significant nearbed orbital velocities estimated from SWAN model against S4 current meter records.

Wave-induced bottom dynamics was computed at 4 points placed seaward of the depth of closure taking place at the following water depths: 10 m, 14 m (sand tracer injection), 20 m and 32 m below mean sea level (MSL). Simulation points are represented on Figure 4.4.

[1]Nucleous for European Modelling of the Ocean: an ocean modelling framework which is composed of 'engines' nested in an 'environment'. The 'engines' provide numerical solutions of ocean, sea-ice, tracers and biochemistry equations and their related physics (Madec, 2012). More information in http://www.nemo-ocean.eu/.

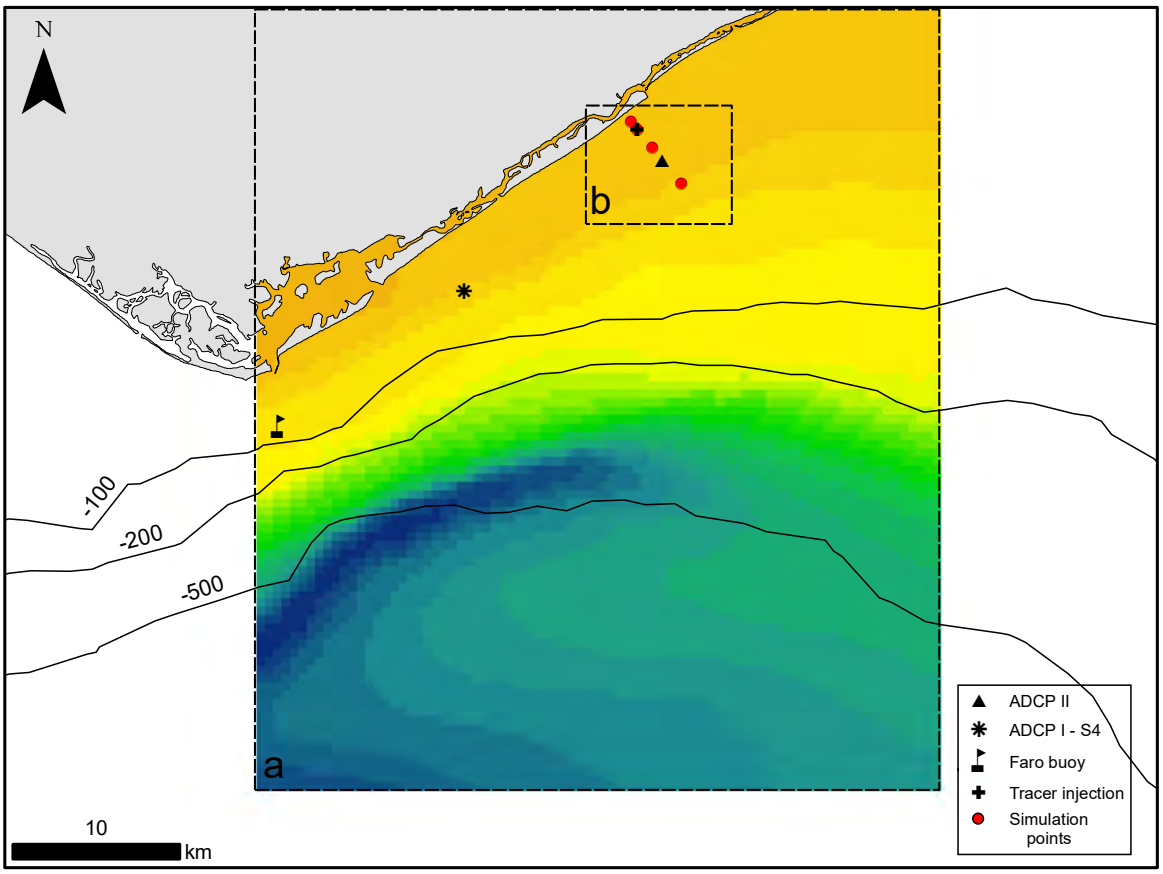

Figure 4.4 Representation of SWAN computational grids: a) regional domain (500 m resolution) and b) local domain (20 m resolution). Simulation points are located at 10 m, 14 m, 20 m and 32 m depth below mean sea level.

4.3.2 Morpho-sedimentary data

The seabed morphology and sediment distribution of the study area were surveyed in the scope of SHORE project over several transects oriented alongshelf and cross-shelf as described on Figure 4.5. The sea missions were headed by Teresa Drago and Marco Silva from IPMA (Instituto Português do Mar e da Atmosfera) with the help of the skipper Isidoro Costa.

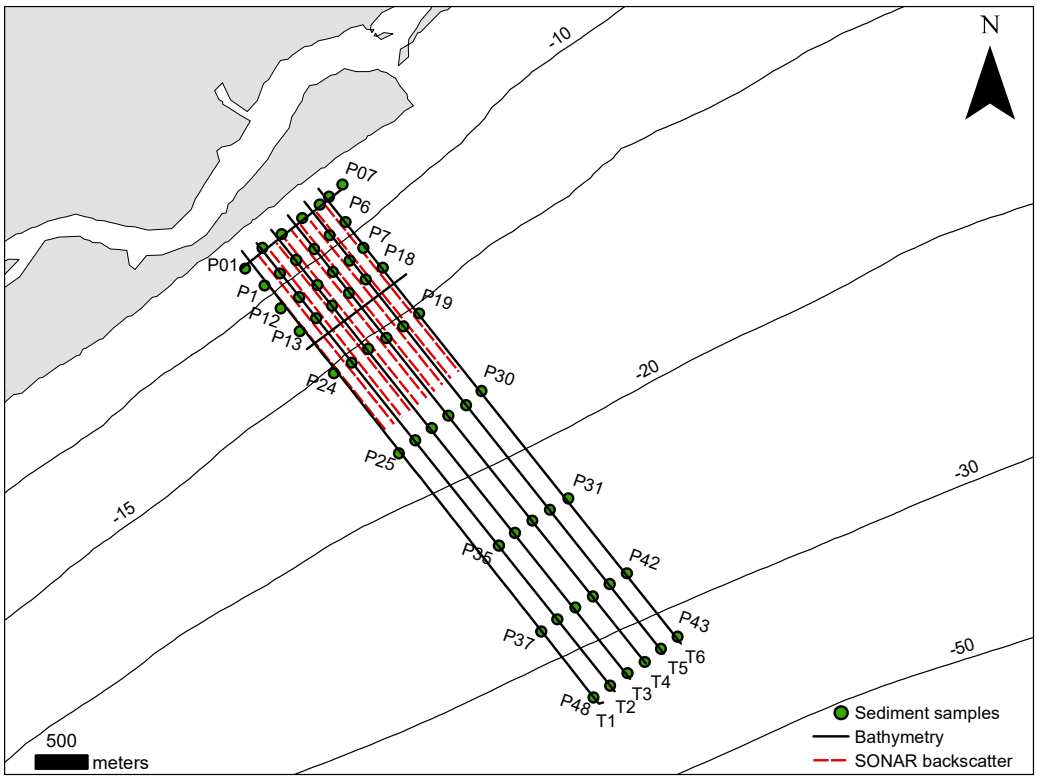

Figure 4.5 Bathymetric (T1 to T6) and SONAR survey transects (dashed lines) and sediment samples (P01 to P07 and P1 to P48) sites.

4.3.2.1 Backscatter

Bottom acoustic backscatter data was collected on January 2014 using a sidescan sonar (Starfish operating at 400 kHz) along 9 cross-shelf transects extending from about 7 meters depth down to approximately 18 m below MSL (Figure 4.5). Data interpretation focus on bottom sediment texture since sediments with different reflectance properties can be distinguished by changes in the strength of the sidescan return sign. According to Barnhardt et al. (2005), in general, the low-backscatter region (darker) within the sidescan sonar data represents finer-grained sediment, while the high-backscatter regions (lighter) represent coarser-grained sediment.

4.3.2.2 Morphology

The bathymetric survey was performed on February 2014 along six cross-shelf transects (T1 to T6) spaced 200 m apart and extending from 4.5 down to 32 m below MSL (Figure 4.5). Measurements were conducted during spring tide using an echo-sounder combined with the

RTK-DGPS, operating at 1Hz. Estimated errors related to equipment and field operation comprise a vertical error up to 10-15 cm.

4.3.2.3 Sediments

Bottom sediment sampling was performed on February 2014 according to a pre-defined grid in which a total of 55 samples were collected using a van Veen grab sampler from 4.5 m down to 32 m water depth (Figure 4.5). Sediment textural analysis was performed in the scope of SHORE project through dry sieving method. Grain-size classification and the statistical parameters were performed using Gradistat® (Blott and Pye, 2001) by applying the Method of Moments.

4.3.3 Sand tracer experiment

A sand tracer experiment was conducted on the scope of SHORE project in order to evaluate the sediment transport seaward the depth of closure. The evaluation of the tracer pathway and mass center movement since tracer injection enabled a quantitative estimation of the sediment transport and validation of the sediment transport model.

4.3.3.1 Preparation of the fluorescent sand tracer

Prior to the field experiment, 400 kg of sand collected at Tavira inlet, was first washed with fresh water and then well-spreaded on the ground for drying it. The dry sediment was then dyed with an orange fluorescent ink in a concrete mixer according to the methodology described in Silva et al. (2007), and represented in Figures 4.6a, b and c.

Figure 4.6 Sand tracer methods: a) sediment dry b) coating process c) marked sand d) sand tracer bags and CCMAR vessel e) tracer injection.

The textural comparison between traced and natural sediment shows that tracer is representative of the most mobile fraction of the in situ sediment (Figure 4.7).

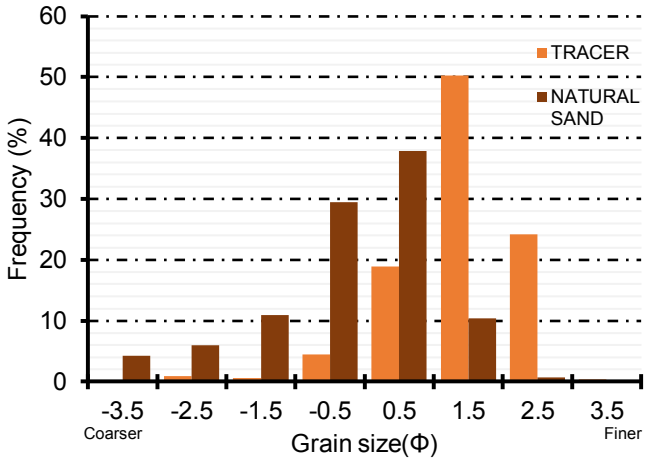

Figure 4.7 Textural characterization of both traced and natural sediment.

4.3.3.2 Tracer injection and sampling surveys

On the 24th of April 2014 the marked sand was released by divers over the seabed at 14 m water depth (referred to the MSL). To release the painted sand, 27 bags containing marked sand were lowered with a rope from the boat at the injection point (Figures 4.6d and 4.6e). These bags were distributed "randomly" within a distance of some meters around the injection point. For each bag, the sand tracers were released by divers forming a layer of about 1 m^2 and 1 cm thick. Additional information concerning tracer release is available through an online video at https://youtu.be/YKho0KvddrA.

After injection the sand tracer displacement was monitored through four sea missions performed on June 2014 (C1), November 2014 (C2), March 2015 (C3) and June 2015 (C4). During the surveys sediment samples were collected over an irregular grid surrounding the injection point by using van Veen grab sampler with a 0.05 m^2 sampling area (Figure 4.8). Positioning was performed using a DGPS in RTK mode with an accuracy better than 0.5 m. The error in sampling location was mainly the result of boat drift which can be estimated to be less than 3 m.

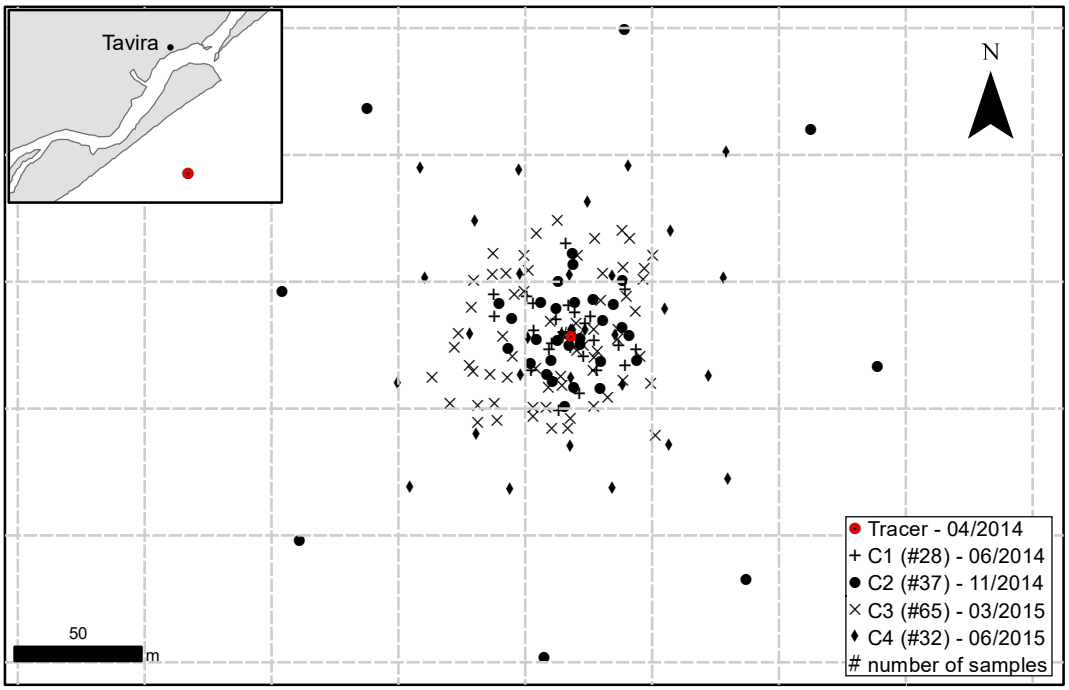

Figure 4.8 Sampling points for all field surveys.

4.3.3.3 Tracer detection

In laboratory, all samples were carefully inspected using ultra-violet (UV) light in order to identify samples containing marked sand. After the visual inspection, each selected sample was washed, dried, well mixed and then spread over a 39 x 29 cm black tray. Digital images of the sediment were acquired under UV lights by using a standardized image acquisition system with a fixed 18 megapixel digital SLR camera (Figure 4.9).

Tracer detection and counting of tagged grains were performed automatically through an image processing routine developed in the scope of SHORE and Beach to canyon [1] projects and available at http://sandcode.fc.ul.pt/.

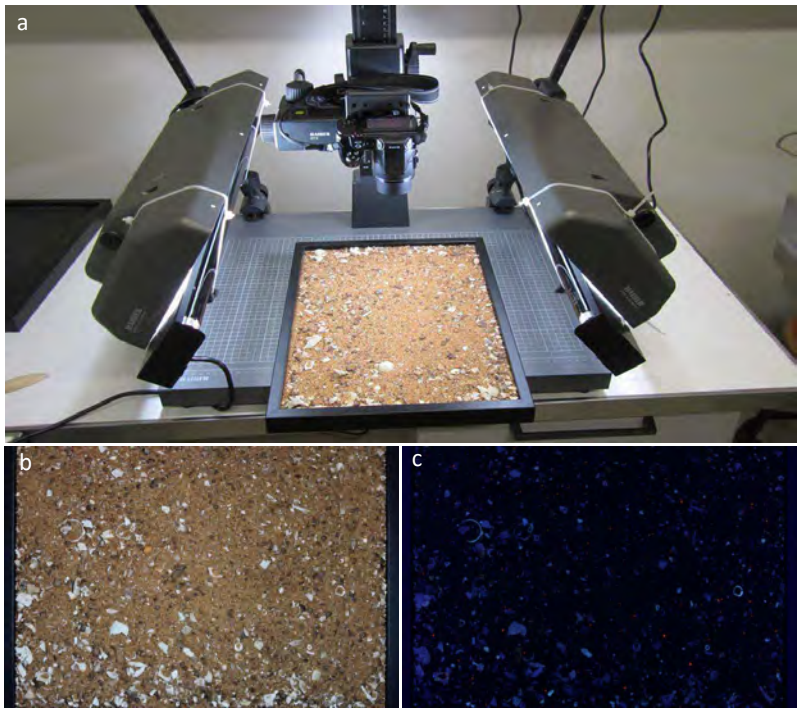

Figure 4.9 Image acquisition system (a) and digital images of a sediment sample containing tagged grains under visible (b) and UV (c) lights.

The relation between tracer concentration detected on digital images (area filled by tagged grain\total image area) and tracer mass concentration was estimated in laboratory using standards dilutions for successive injections of a known mass of tracer (3 images for each injection – Figure 4.10).

[1] Beach to Canyon Head Sedimentary Processes project funded by Fundação para a Ciência e Tecnologia (PTDC/MAR/114674/2009), more information at http://beachtocanyon.fc.ul.pt/.

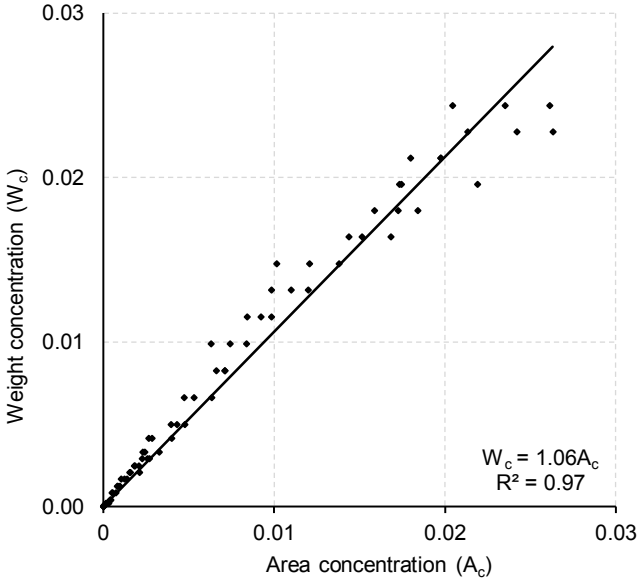

Figure 4.10 Ratio between weight of tracer and sample total weight versus the ratio between areas of tagged grains and total image.

4.3.3.4 Estimation of tracer recovery rates

Tracer recovery was computed by integrating tracer weight across the target area using the Thiessen polygon technique. Tracer weight at each Thiessen polygon was computed by the product between the tracer dimensionless concentration, the polygon area and the mixing layer thickness. The depth of the mixing layer (δ_{mix}) was assessed according to the formulation described in Harris and Wiberg (1997):

$$\delta_{mix} = 0.07(\tau_{max} - \tau_{cr}) + 6D_{50} \tag{4.1}$$

where D_{50} is the in situ particle median grain size (0.66 ϕ) and τ_{max} and τ_{cr} can be translated into velocity units through $u_* = (\frac{\tau}{\rho})^{\frac{1}{2}}$, being ρ the density of the water.

4.3.3.5 Sediment diffusion

On the sand tracer experiment carried out by Miller and Komar (1979), both theoretical and experimental evidences has shown that, after an initial short period of rapid dispersion, longitudinal and transverse diffusion coefficients can be reached through the concentration variance provided by tracer distribution. In order to compute the magnitude of this process,

diffusion coefficients (m^2/s) were calculated for both cross-shelf and alongshelf directions according to the following equation:

$$D_x = \frac{\frac{\sum cx^2}{\sum c^2}}{\triangle t} \tag{4.2}$$

where c is the tracer mass concentration (dimensionless), x is the distance alongshore/cross-shore from the injection point (m) and Δt the time interval(s) between campaigns.

4.3.3.6 Sediment advection

The sediment transport rate was estimated based on the spatial integration method (SIM), a Lagrangian method that analyzes the behavior of a cloud of tracers in space and time (Madsen, 1987). Mean velocity ($\bar{V}$) was computed through the displacement of the center of mass over time:

$$\bar{V} = \frac{x_{cm}(t_2) - x_{cm}(t_1)}{t_2 - t_1} \tag{4.3}$$

where x_{cm} is the centre of mass location in the alongshelf or cross-shelf direction at t instant.

The sediment transport rate (Q_t in m^2/s) was estimated by the product between the mean velocity and the depth of the mixing layer:

$$Q_t = \bar{V} \times \delta_{mix} \tag{4.4}$$

4.3.4 Wave modelling validation

The significant wave height and zero-crossing period calculated using SWAN propagation model were validated against in situ data measured by the ADCP I. Results show an excellent fit between observed and modeled significant wave height with a correlation (r) of 0.97 and a root-mean square (RMS) of 0.18 m. Zero-crossing period validation is strongly affected by the ADCP acquisition performance. Observed ADCP data clearly overestimates the wave period when the sea state is characterized by low amplitude high frequency waves as observed in the first half of the validation time-series (Figure 4.11). When the wave amplitude is higher (in the second half of the validation period), it is observed a good match between observed and modeled zero-crossing period.

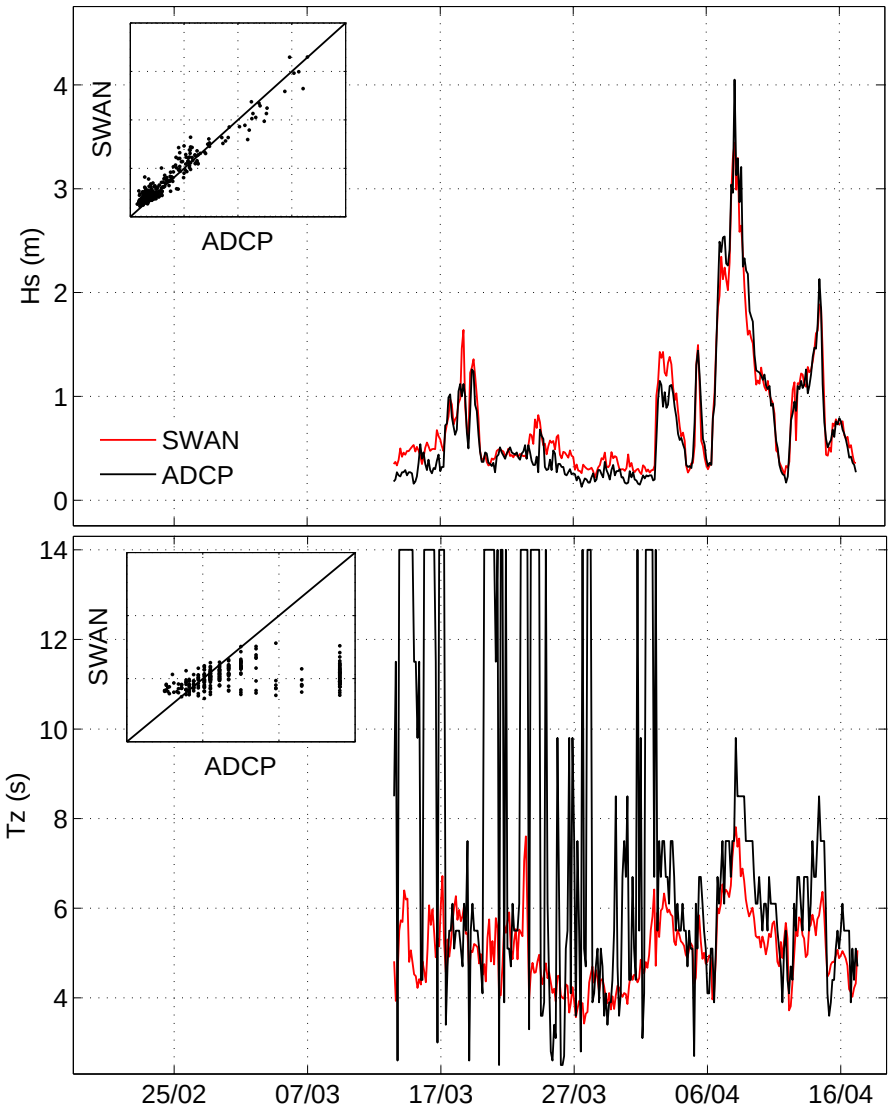

Figure 4.11 Wave propagation validation against ADCP I values of significant wave height (top) and zero-crossing period (bottom).

Estimated bottom significant orbital velocities ($_w$) were also validated against S4 current meter observations. Results show that the modeled u $_w$ values are in line with S4 measurements (r = 0.79) with an underestimation trend during low energetic periods. On the other hand, the estimated orbital velocity for high energetic periods, when remobilization occurs, shows an excellent fit to the observed data (Figure 4.12).

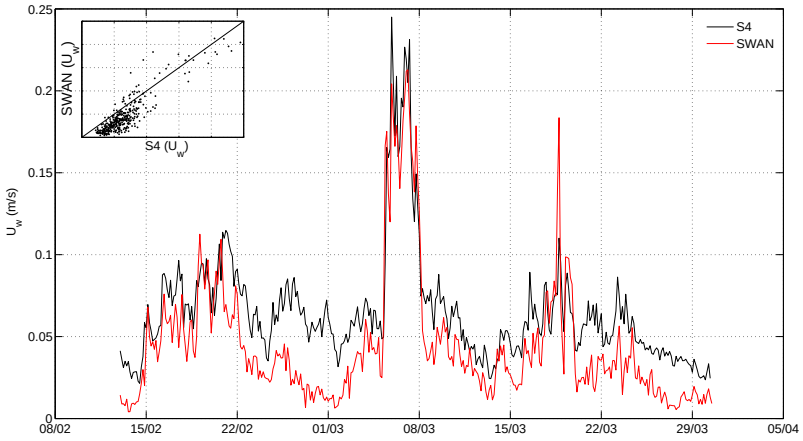

Figure 4.12 Bottom orbital velocity validation against S4 observations.

4.3.5 Spatial representativeness of current data

Results from NEMO ocean currents as well as the comparison between both flow velocities acquired by ADCP I (Armona) and II (Tavira) revealed a relatively uniform spatial circulation over the continental shelf on both alongshelf and cross-shelf directions with minor variations regarding its magnitude and direction (Figures 4.13 and 4.14). This observation allowed to use current data from ADCP I to characterize the flow pattern over the study area.

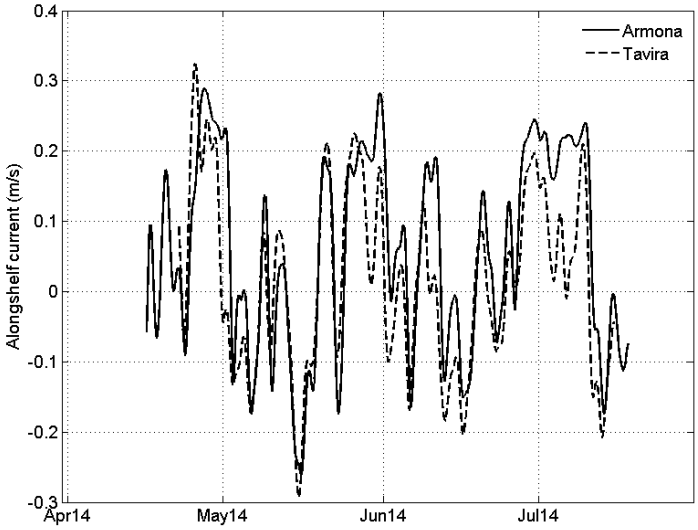

Figure 4.13 Comparison between the alongshelf current component measured by the ADCP at Armona and Tavira continental shelf.

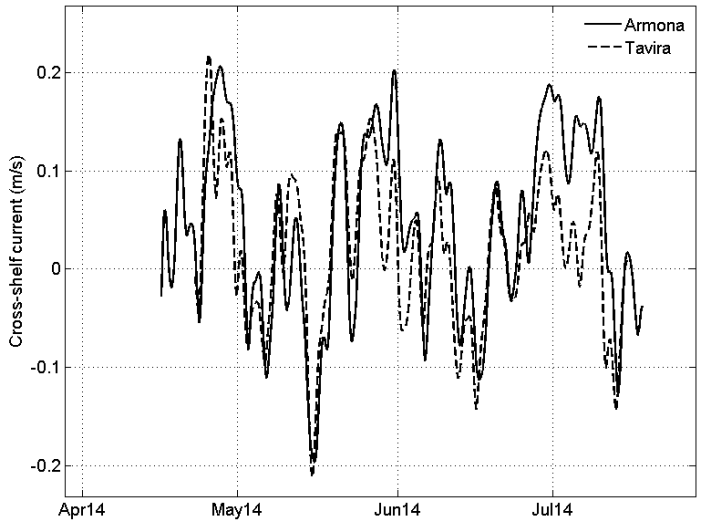

Figure 4.14 Comparison between the cross-shelf current component measured by the ADCP at Armona and Tavira continental shelf.

4.3.6 Bottom boundary layer modelling

The sedimentary dynamics within the bottom boundary layer was evaluated through the application of the numerical model described in Chapter 3 which calculates sediment remobilization and transport. The model was supported by nearbed current data from ADCP I (section 4.3.1.1) and wave modelling data from SWAN propagation model (section 4.3.1.2), being the wave-current non-linear interactions only calculated when both wave and current data were available (see Figure 4.2).

For a wider comprehension of the nearshore sedimentary dynamics, the sediment remobilization and transport rates were computed for each sand class (very coarse to very fine sand). This was performed by considering sand particles between -0.5 and 3.5 ϕ with 1 ϕ step, thus accounting for 5 grain sizes.

4.4 Results

4.4.1 Oceanographic forcing

4.4.1.1 Currents

Nearbed currents measured offshore Armona Island (ADCP I - Figure 4.1) displays an alongshelf-dominated pattern with an average speed of 0.08 m/s being northeast directed

during 56 % of the total observation period. Overall cross-shelf currents present an average speed of 0.04 m/s but are not dominated by either northwestward (onshore) or southeastward (offshore) component (Table 4.1).

The first observational period (P1) is dominated by a northeastward flow (62 %) with an average speed of 0.10 m/s, while cross-shelf currents presents an average magnitude of 0.03 m/s (54 % directed onshore). During the second observational period (P2) alongshelf currents are northeastward 59 % of the time with an average speed of 0.06 m/s and cross-shelf average current speed is of 0.05 m/s without trend on its direction. Currents during the third observational period (P3) are clearly dominated by its alongshelf component which is mainly northeast directed (60 %) with an average speed of 0.10 m/s, while the cross-shelf component present an average speed more than three times smaller (59 % directed onshore). The last period (P4) is marked by a slight dominance of southwestward currents (56 %) with flow velocities up to 0.3 m/s and cross-shelf currents with an average speed of 0.03 m/s (Figure 4.15).

Table 4.1 Average speed (m/s) and percentage of occurrence for the NW (onshore) and SW components of cross-shelf and alongshelf directions, respectively.

		P1 to P4	P1	P2	P3	P4
Cross-shelf	Speed (m/s)	0.04	0.03	0.05	0.03	0.03
	% NW	49	54	48	41	50
Alongshelf	Speed (m/s)	0.08	0.09	0.06	0.10	0.08
	% SW	44	38	41	40	56

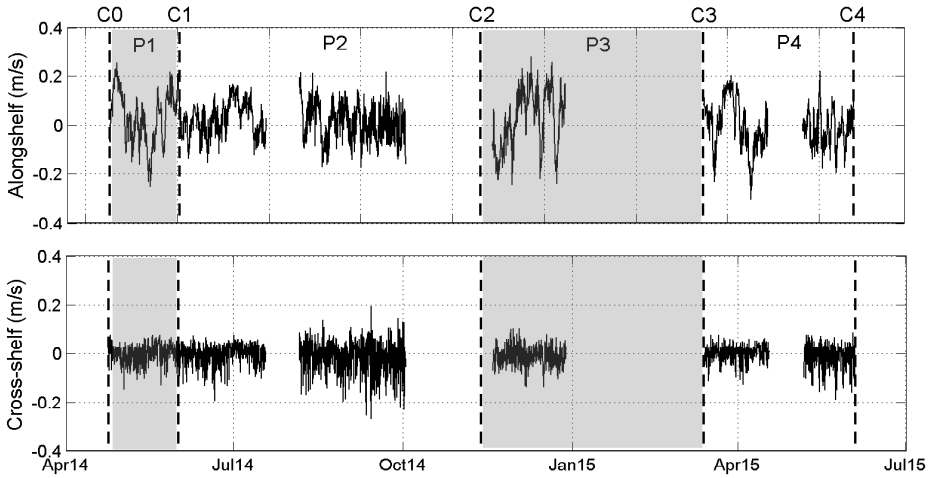

Figure 4.15 Time-series of alongshelf (top) and cross-shelf (bottom) current components. C0 to C4 corresponds to sand tracer sea missions (C0: tracer injection; C1 to C4: tracer sampling) and P1 to P4 are the oceanographic monitoring periods between surveys.

4.4.1.2 Waves

Average significant wave height (H_s) ranged from 0.39 m during summer months (P2) up to 0.57 m during winter months (P3). Values of time-average zero-crossing periods (T_{02}) do not have significant variations, being mainly between 4 and 5 seconds (Table 4.2).

Offshore waves propagated up to the tracer injection point show a bimodal behaviour of the wave conditions (Figure 4.16). The first and most representative one is characterized by short waves with average zero-crossing period of about 4 s coming from southwest that rarely exceed 1 m. The second one ("Levante") is represented by higher waves coming from southeast which frequency of occurrence do not exceed 15 %, being more frequent on periods P1 and P4, mainly represented by spring months.

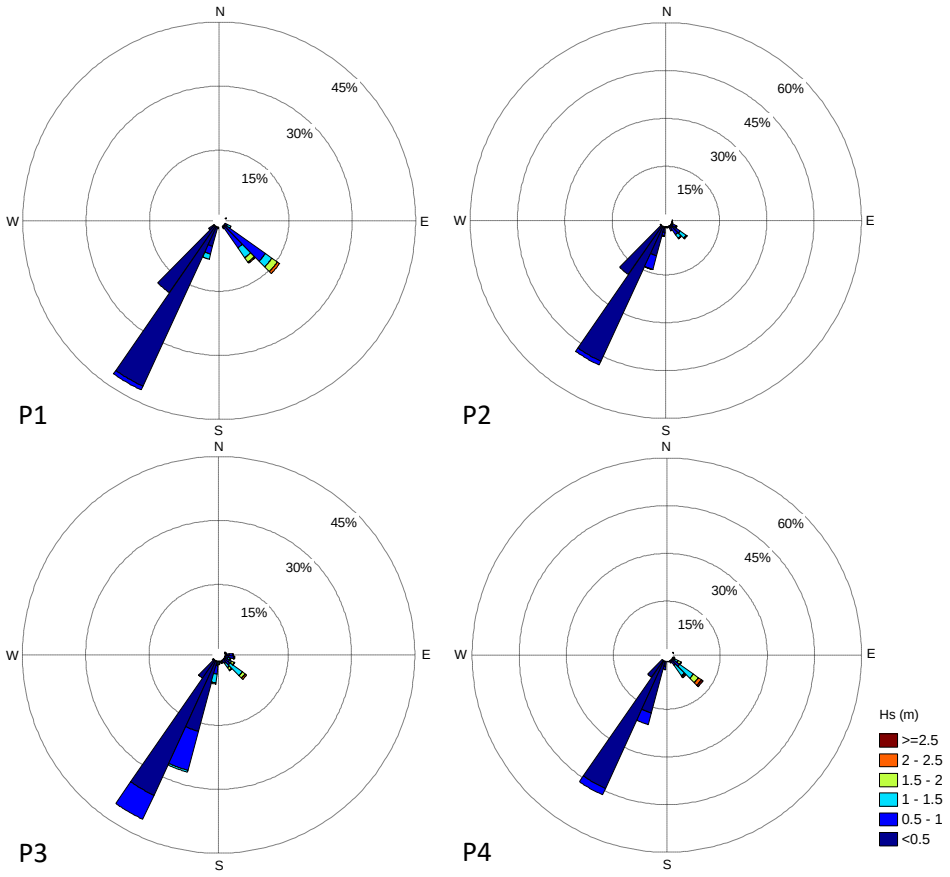

Figure 4.16 Frequency of occurrence of wave direction and height at 14 m depth offshore Tavira for the observation periods P1 to P4.

Table 4.2 Time-averaged wave parameters. H_s: mean significant wave height; T_{02}: mean zero-crossing period; U_w: significant orbital velocity; MP_{dir}: mean power direction.

Observation period	H_s (m)	T_{02} (s)	U_w (m/s)	Dir (°)	MP_{dir} (°)
P1	0.49	4.46	0.05	192	143
P2	0.39	4.39	0.03	200	162
P3	0.57	4.86	0.06	193	157
P4	0.55	4.87	0.07	192	138

The first observation period (P1) shows a time-averaged H_s of 0.49 m mainly coming from southwest. In this period it was registered a strong "Levante" event with significant wave heights higher than 2 m. The period P2 shows the mildest wave conditions with an average H_s of 0.39 m where the most energetic wave event did not reach 2 m. During P3 period the time-averaged significant wave height was of 0.57 m, thus representing the most energetic observation period with waves frequently exceeding 1 m height. The last period (P4) presents an average H_s of 0.55 m and it is marked by the strongest wave event registered in this work with waves coming from southeast and significant wave heights exceeding 3 m (Figure 4.17).

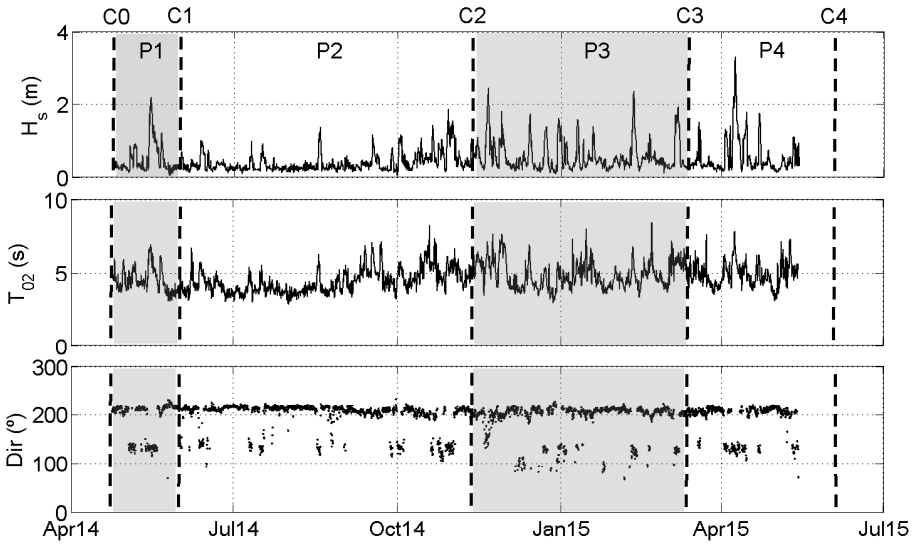

Figure 4.17 Wave conditions at the sand tracer injection point (modelling results). Top: significant wave height; middle: average zero-crossing period; bottom: wave mean direction.

Despite the higher frequency of occurrence of waves coming from southwest, mean power direction is from southeast for all periods. The time-averaged wave parameters for the observation periods (P1 to P4) are summarized on Table 4.2 and the wave conditions time series are described on Figure 4.17.

4.4.2 Morpho-sedimentary features

4.4.2.1 Backscatter

The side-scan sonar data revealed the seabed composed by unconsolidated sediment without the presence of rocky outcrops. The spatial resolution of the sonar survey did not allow the identification of bed forms, thus only characteristics regarding the sediment texture were evaluated.

The shallower part of the surveyed area is marked by dark patches (finer sand) interleaves with lighter ones (coarser sand) reaching almost 12 m depth at the center of the surveyed area and less than 10 m depth on the north-eastern sector. Seaward 12 m depth results reveals homogeneous light pattern (Figure 4.18).

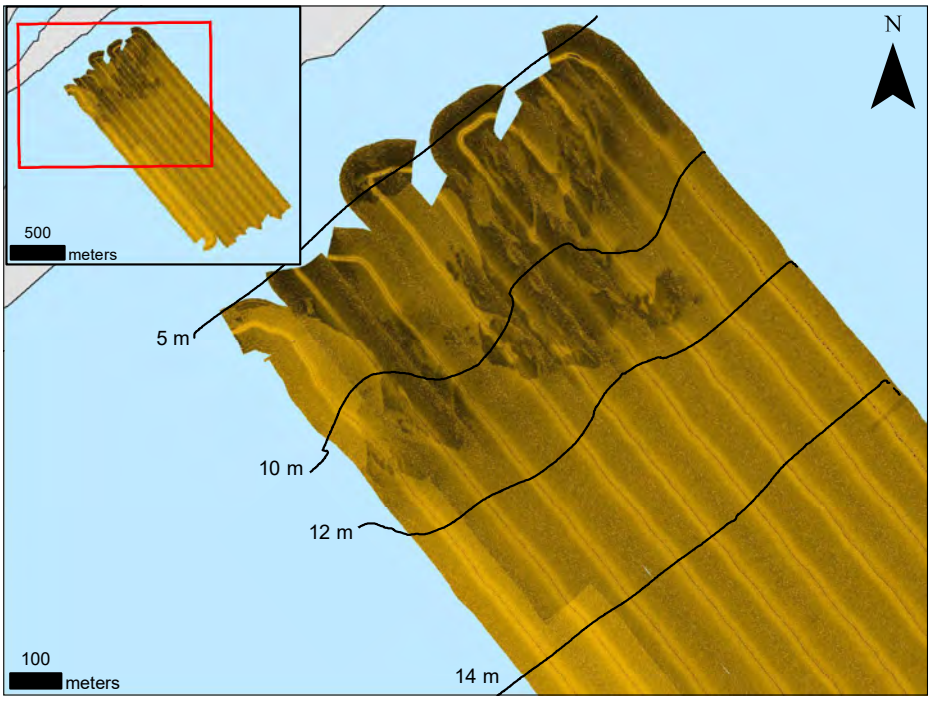

Figure 4.18 Side-scan sonar seabed imagery.

4.4.2.2 Morphology

The shelf morphology is marked by a narrow roughened area of about 600 m extending down to 10-12 m depth. A smoother bottom is observed seaward this point (Figure 4.19).

From 5 to 8 m depth, the shelf is marked by a steep slope that can reach up to 11 % followed by a break in the slope that marks the transition to a flatter bottom but also with slope oscillations down to approximately 12 -13 m depth (Figure 4.20). On the profiles transects represented in Figures 4.21 (T1 to T3) and 4.22 (T4 to T6) the break(s) on the slope are easily observed, occurring between 10 m and 12 m depth on transects T1 and T2 (southwestern sector) and around 10 m depth or shallower on transects T3 to T6. Transects T4 and T5 also present irregularities on bottom morphology below 10 m depth.

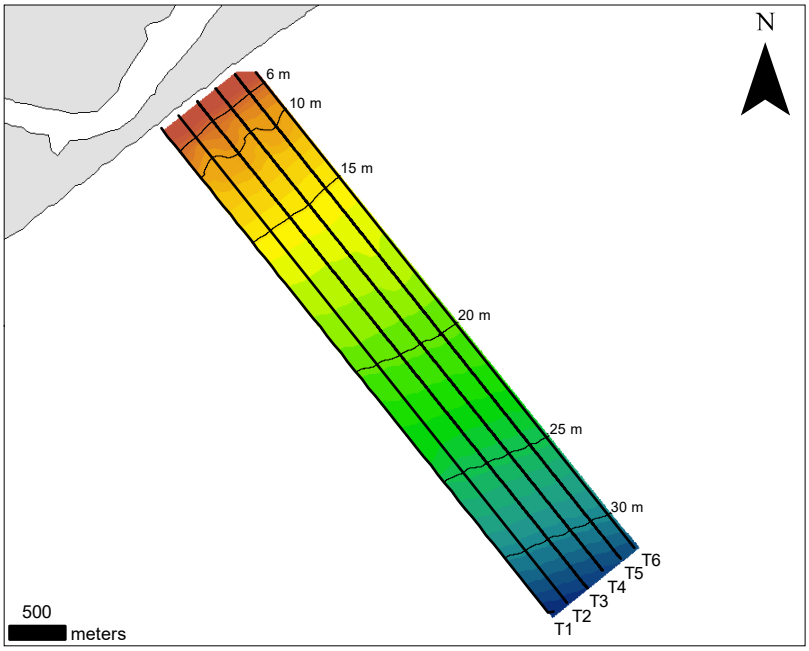

Figure 4.19 Bottom morphology and the transects (T1 to T6) represented on Figures 4.21 and 4.22.

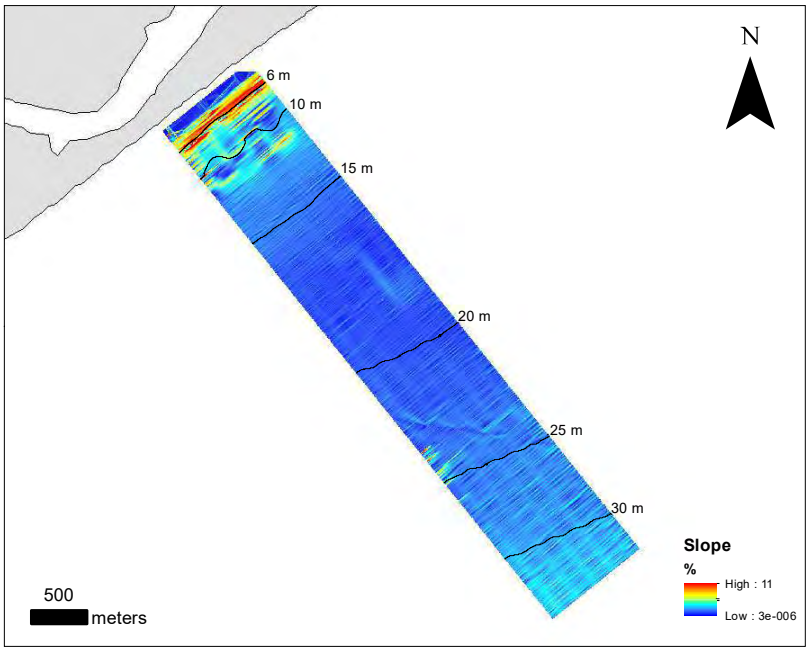

Figure 4.20 Spatial distribution of the slope over the study area.

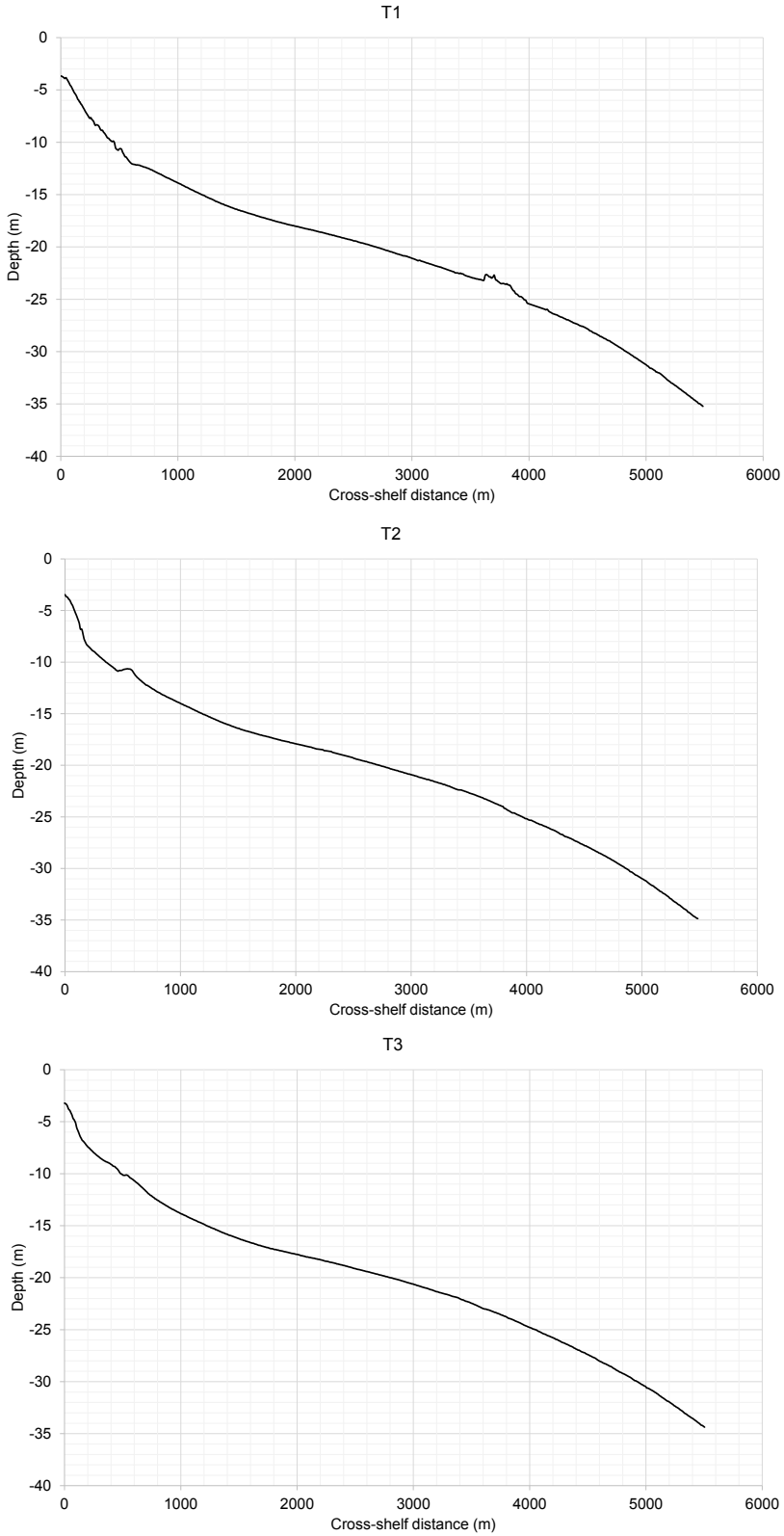

Figure 4.21 Bathymetric profiles of transects T1 to T3.

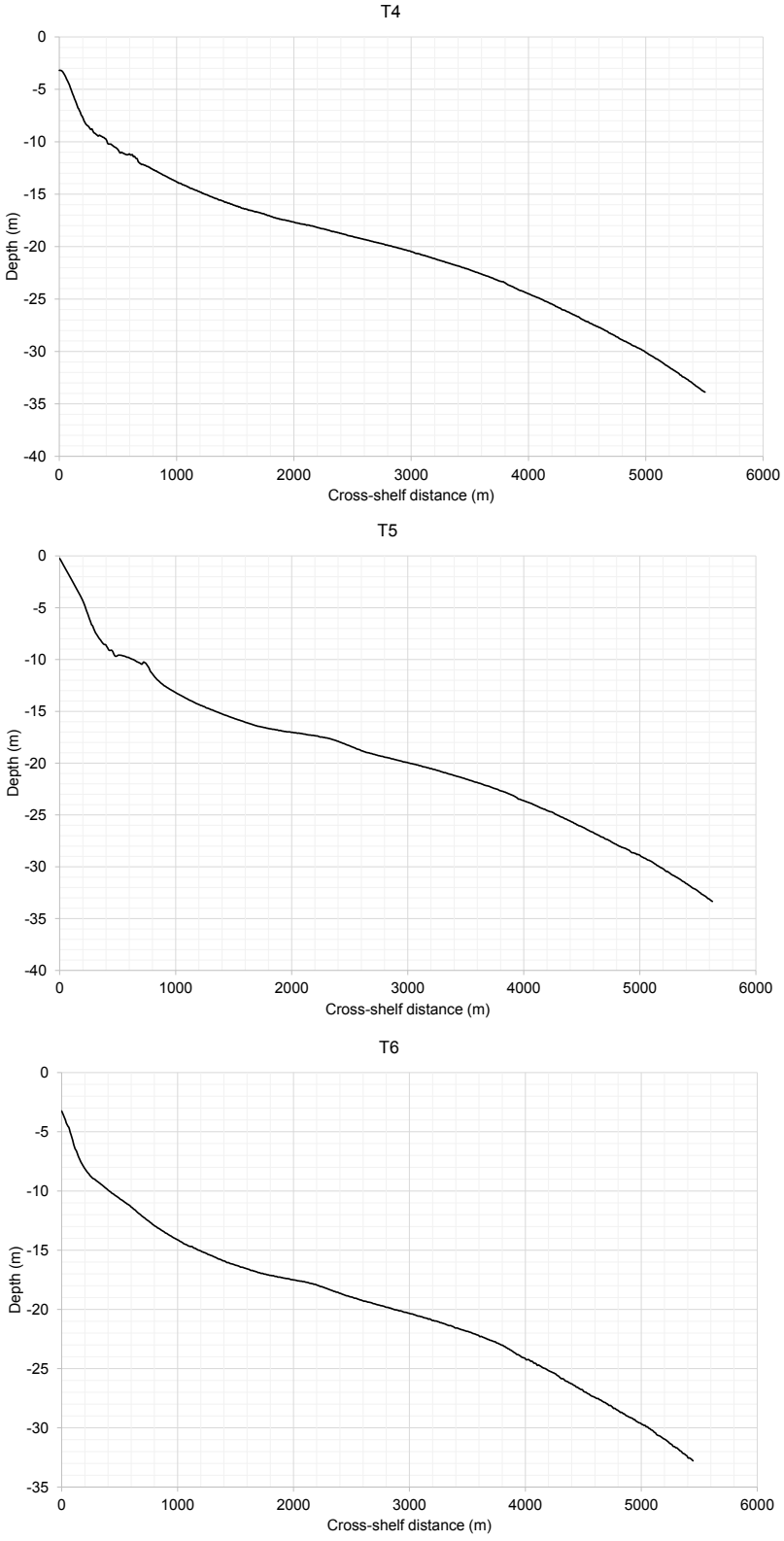

Figure 4.22 Bottom morphology of transects T4 to T6.

4.4.2.3 Sediments

Textural analysis revealed bottom sediments dominated by moderate to well-sorted fine to medium sand without fragment of shells between 5 and 10 m water depth and becoming coarser with increasing depth. From 10 down to about 25 m depth the shelf bottom is composed basically by coarse to very coarse sand with a reddish coat and containing fragment of shells. Also an offshore coarsening trend is observed. Seaward 25 m depth sediments starts to become finer being composed mainly by medium and coarse sand at about 28 m depth where the sedimentary cover is followed by an abrupt transition from sandy to muddy sediments at about 30-32 m depth. A general overview regarding sediment textural distribution over the study area is given on Figure 4.23 and further details of some sediment samples considered representative of its depth are described below.

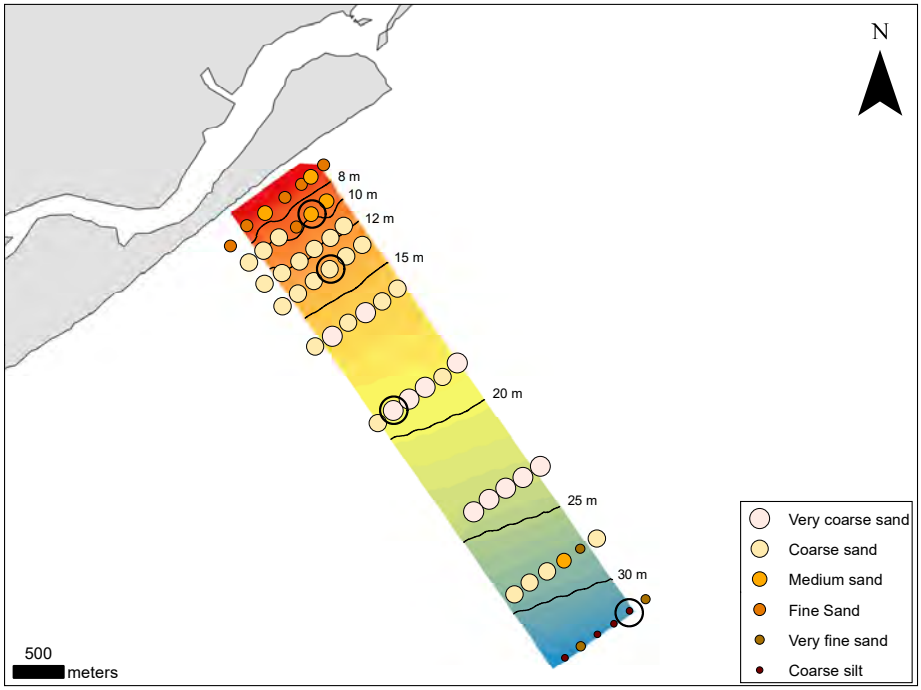

Figure 4.23 Textural distribution of bottom sediments across the study area. Black circle marks the sediment samples selected from each analysed depth.

$\approx$ **10 m depth**: sediments are mostly classified as medium to coarse sand moderately sorted, however with a substantial presence of fine sand. Fragments of shells are very rare and no coat on sediment particles is observed (Figure 4.24).

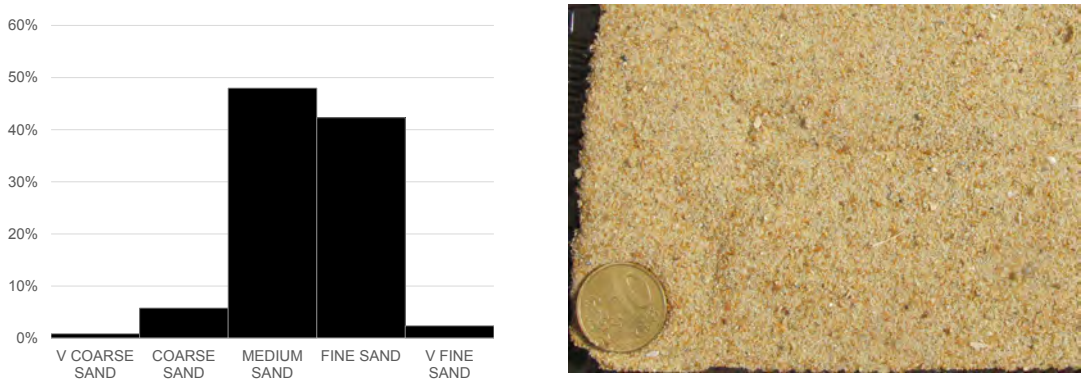

Figure 4.24 Grain size distribution and sediment sample image from 10 m depth.

≈ **14 m depth**: bottom sediment is marked by poorly sorted coarse sand with an apparent reddish coat. A significant amount of gravel-sized particles is observed, being mostly represented by fragments of shells (Figure 4.25).

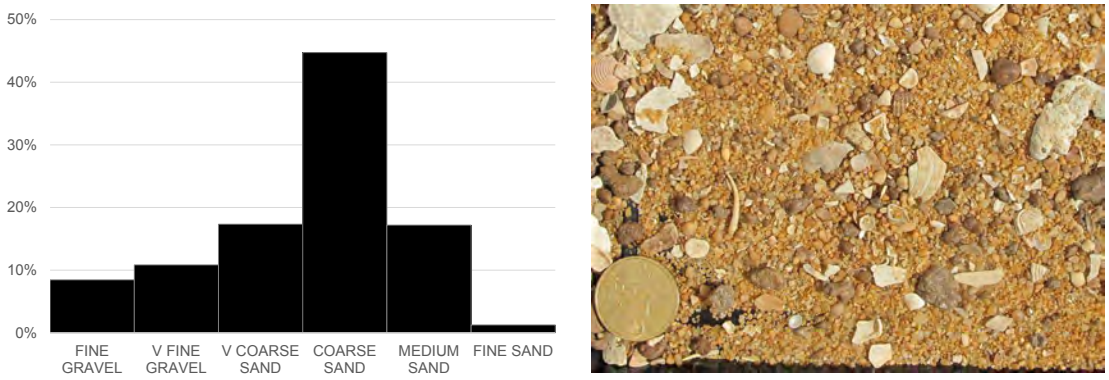

Figure 4.25 Grain size distribution and sediment sample image from 14 m depth.

≈ **20 m depth**: sediment is composed by moderate and poorly sorted coarse to very coarse sand also with a reddish coat. The presence of gravel-sized particles is even more frequent, being mostly represented by shell fragments (Figure 4.26).

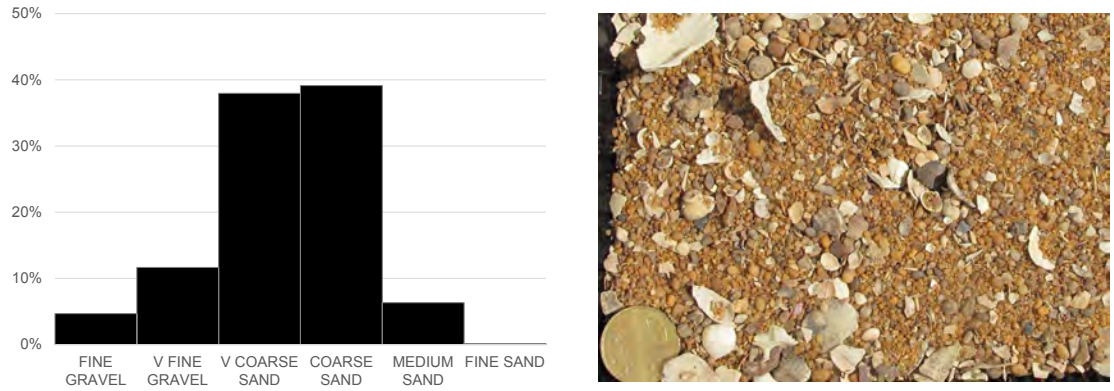

Figure 4.26 Grain size distribution and sediment sample image from 20 m depth.

$\approx$ **32 m depth**: bottom sediment is classified from very fine sand to coarse silt, being the mud fraction very significant (up to 60%). Fragments of shells are also observed (Figure 4.27).

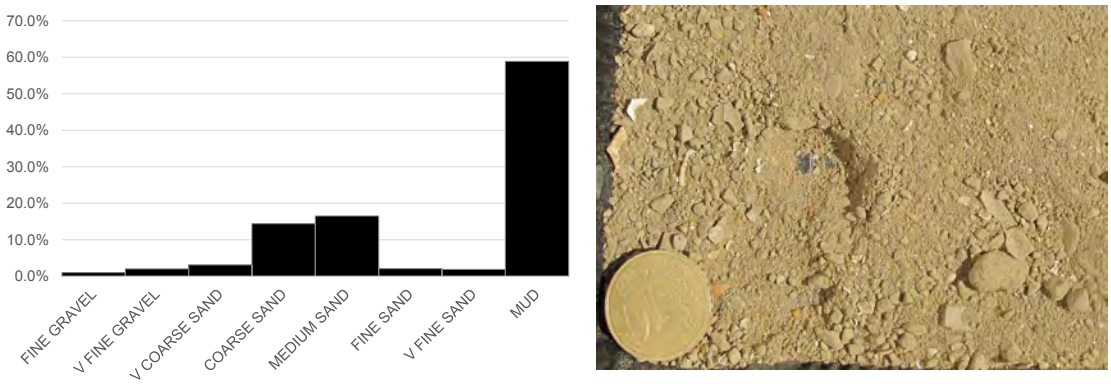

Figure 4.27 Grain size distribution and sediment sample image from 32 m depth.

4.4.3 Sand tracer distribution

4.4.3.1 Tracer concentration

Estimated tracer recovery rates ranged between 7 and 38 %. The lowest rate relates to C4 field data while the highest one concerns the field campaign C2. The other two field surveys C1 and C3 displayed recovery rates of 18 and 10 %, respectively.

The concentration distribution of tagged grains for each field survey is represented on Figure 4.28. Results show that sand tracer was mainly found westward from the injection point. On the first campaign tracer concentration exceeds 40.000 tagged grains/m^2 . The

highest concentrations are found in the vicinity of the injection point, with most of the tracer being located northwestward from this point up to a distance of 35 m towards the northwest. The second field survey revealed the highest concentrations westward and southwestward from the injection point with over 5000 grains/m^2. On the sea mission C3 tracer concentrations ranged between 36 and 981 grains/m^2 where lower and higher values are within a distance of 45 and 10 m from the injection point, respectively. The last field survey displayed only 7 out of 32 samples containing sand tracer with concentrations ranging between 18 and 718 tagged grains/m^2. The highest and lowest tracer concentrations are found within a distance of 25 and 87 m towards southwest, respectively.

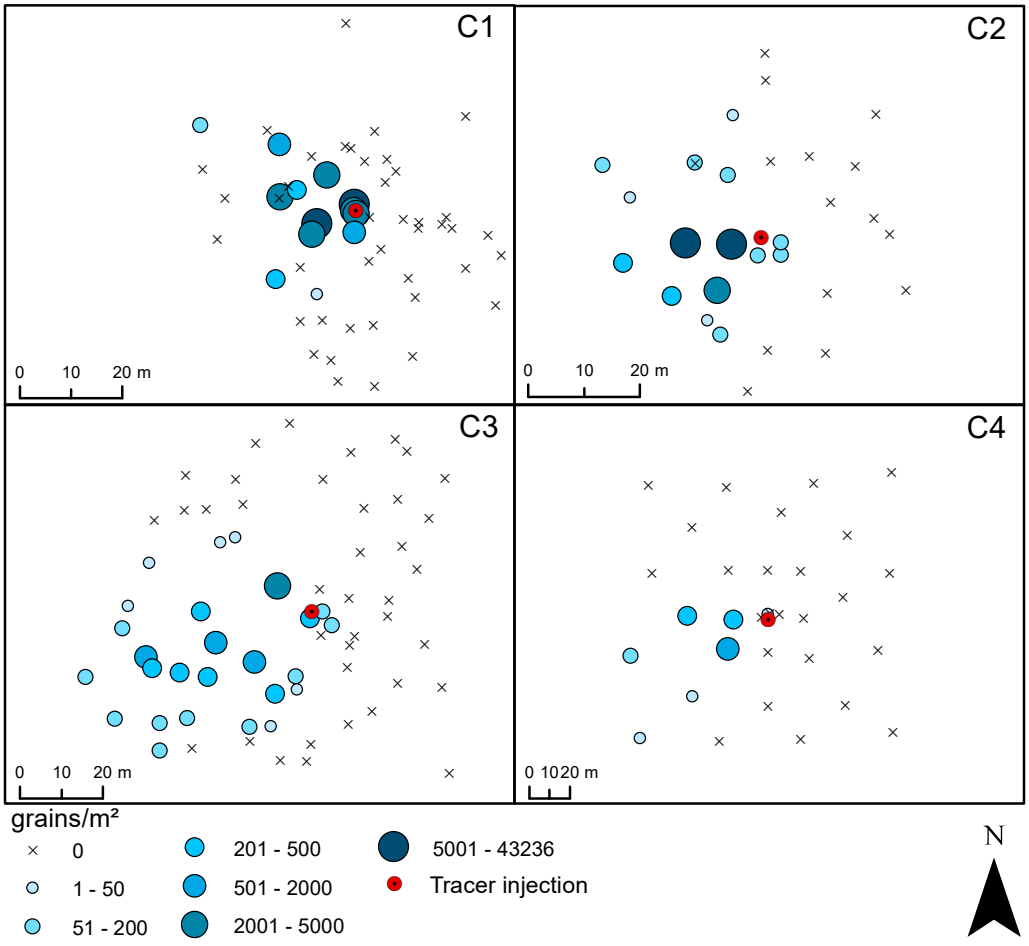

Figure 4.28 Concentration distribution of tagged grains for each field survey presented in number of grains per square meter (note: each map has a different spatial scale).

Tracer centroid movement along the 4 field campaigns shows a good consistency, being dominated by a southwestward alongshelf-component (Figure 4.29). On sea missions C1, C2 and C3 tracer results reveals the predominance of an alongshelf displacement displaying

averages velocities of 0.08, 0.02 and 0.10 m/day, respectively. In the last field survey centroid movement revealed a comparatively slightly stronger cross-shelf displacement with an average velocity of 0.05 m/day while the average alongshelf displacement was of 0.04 m/day.

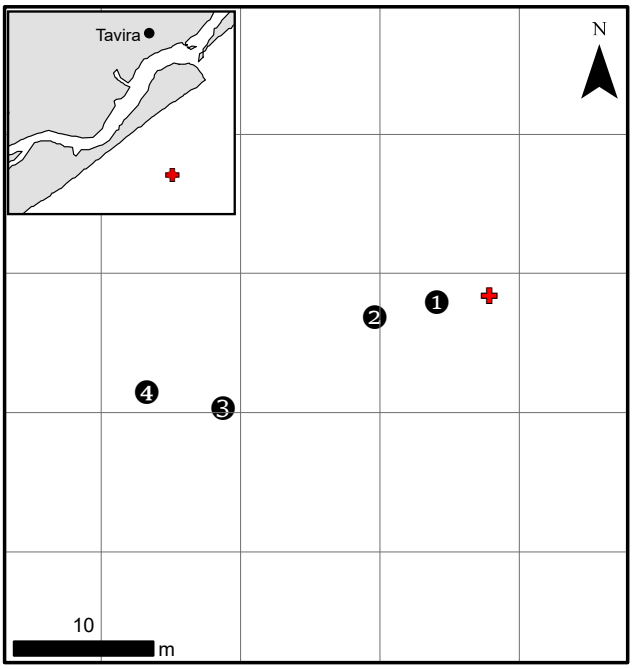

Figure 4.29 Tracer center of mass estimated for each field survey.

4.4.3.2 Sediment diffusion

The spatial distribution of the tracer concentration allowed the computation of diffusion coefficients. The first sea mission (C1) is marked by intense diffusion, represented by diffusion coefficients of $3.52e^{-05}$ m^2/s and of $2.42e^{-05}$ m^2/s along alongshelf (d_{as}) and cross-shelf (d_{cs}) directions, respectively. The diffusion coefficients reach their lowest values on sea mission C2, with a d_{as} of $0.26e^{-05}$ m^2/s and d_{cs} of $0.97e^{-05}$ m^2/s. Overall, results (Table 4.3) show that the cross-shelf diffusion coefficient tends to be slightly higher than its alongshelf component, except for sea mission C1.

4.4.3.3 Sediment advection

Estimations of the sediment transport rates shows the predominance of the alongshelf-directed transport with rates ranging from 0.87e^{-08} to 3.54e^{-08} m^2/s southwestward while cross-shelf rates are between 0.44e^{-08} and 1.96e^{-08} m^2/s onshore directed (Table 4.3).

Table 4.3 Results concerning the tracer experiment. d_{as} and d_{cs} are the alongshelf and cross-shelf diffusion coefficients and Q_{as} and Q_{cs} are the alongshelf and cross-shelf sediment transport rate.

Sea mission	Tracer recovery (%)	d_{as} (10^{-5}m^2/s)	d_{cs} (10^{-5}m^2/s)	Q_{as} (10^{-8}m^3/m/s)	Q_{cs} (10^{-8}m^3/m/s)
C1	18	3.52	2.42	-2.63	1.81
C2	38	0.26	0.97	-0.87	0.44
C3	10	1.08	1.30	-3.54	0.75
C4	7	1.57	2.35	-1.33	1.96

4.4.4 Bottom boundary layer dynamics

Results from one-year bottom boundary layer modelling at 14 m depth (same as sand tracer experiment) revealed that the current-alone shear velocity presented an average value of 3.4 $\times 10^{-3}$ m/s, exceeding 1.0 $\times 10^{-2}$ m/s only once. On the other hand, average wave-alone shear velocity is 7.9 $\times 10^{-3}$ m/s, reaching up to 4.6 $\times 10^{-2}$ m/s (Figure 4.30). Naturally discrepancies between wave- and current-alone induced forcing are even more evident when dealing with shear stress values ($\tau = \rho u_*^2$) as shown in Figure 4.31 where current bed shear-stress is always within 0 to 0.15 N/m^2, while wave-induced bed shear stress attained values higher than 2.00 N/m^2.

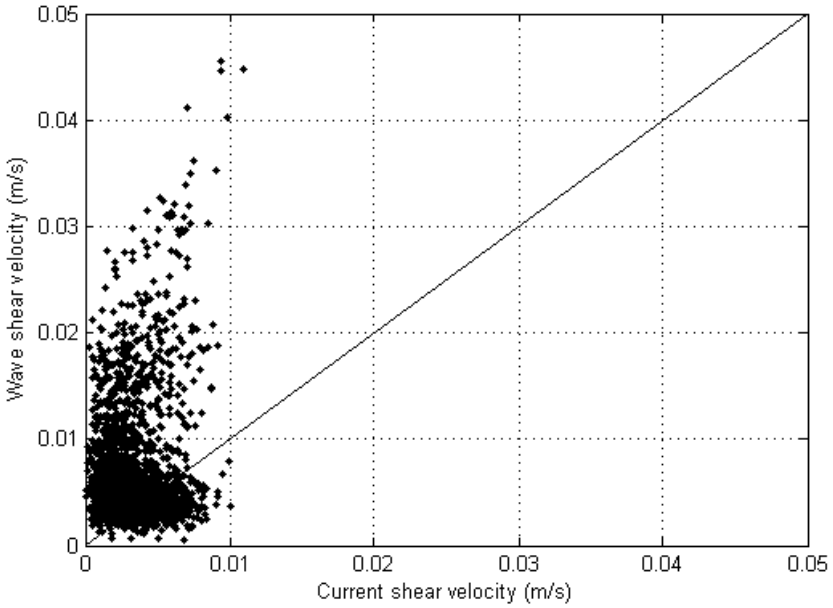

Figure 4.30 Wave-alone versus current-alone bed shear velocity at 14 m water depth.

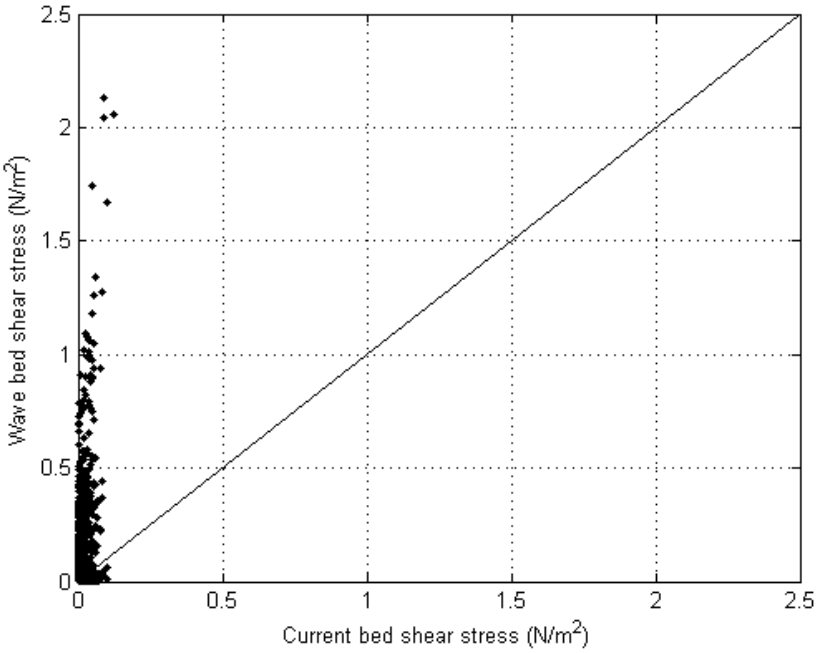

Figure 4.31 Wave-alone versus current-alone bed shear stress at 14 m water depth.

The maximum combined wave-current shear velocity ranges between 4.0×10^{-3} and 4.6×10^{-2} m/s, with an average value of 8.8 $\times 10^{-3}$ m/s (Figure 4.32). These values are

similar to those computed by using wave-alone approach, being those obtained by using a current-alone approach much lower (see Figure 4.30). On the other hand, mean combined wave-current shear velocity varies from 1.5×10^{-4} up to 1.9×10^{-2} and present an average of 4.1×10^{-3}, values that are in turn similar to the current-alone shear velocities.

The mean shear velocity in combined wave-current conditions frequently exceeds the current alone shear velocity in 50 % or more (Figure 4.33). Figure 4.34 shows that the maximum bed shear velocity in wave-current conditions is frequently one order of magnitude greater than current alone bed shear velocity.

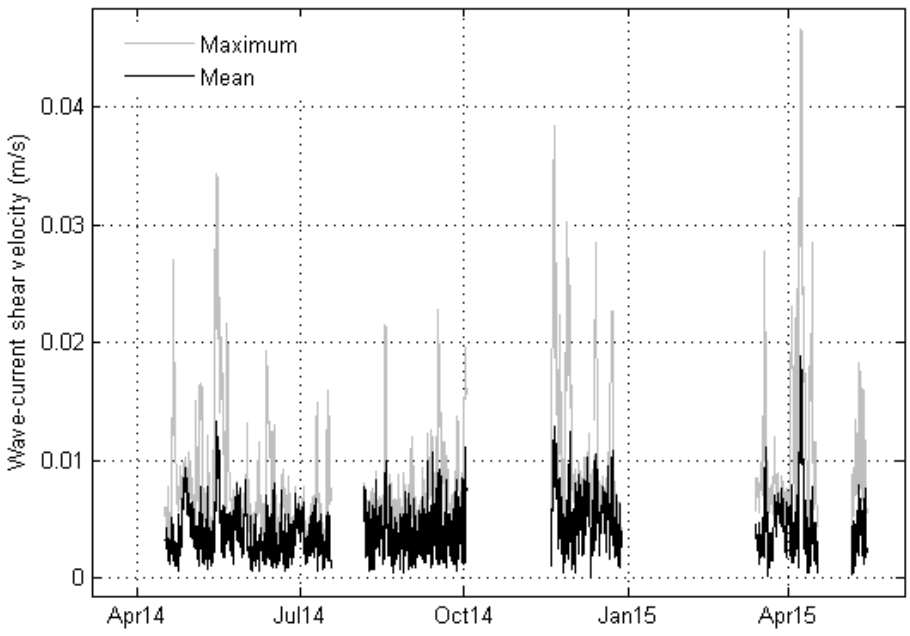

Figure 4.32 Time series of mean and maximum wave-current bed shear velocity from April 1st, 2014 to May 15th, 2015 at 14 m water depth below MSL.

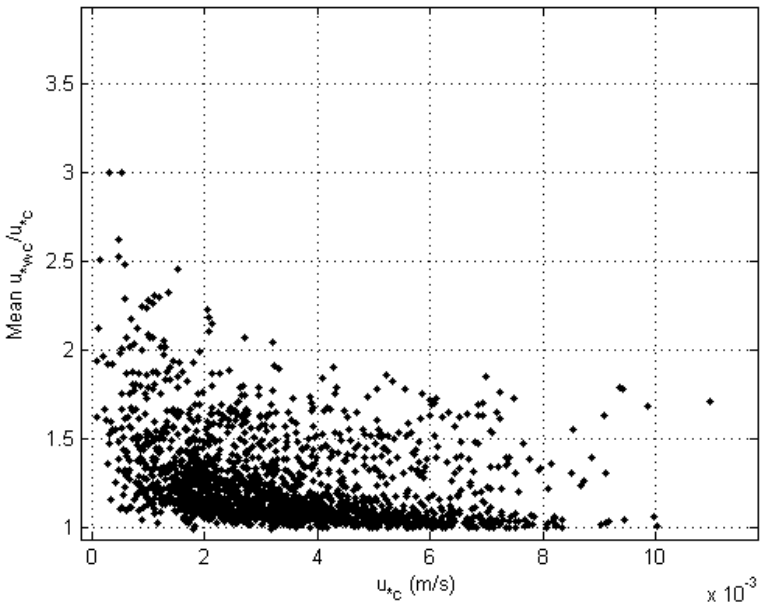

Figure 4.33 Relation between mean bed shear velocity under combined wave-current conditions (mean u_{*wc}) and current-alone bed shear velocity (u_{*c}).

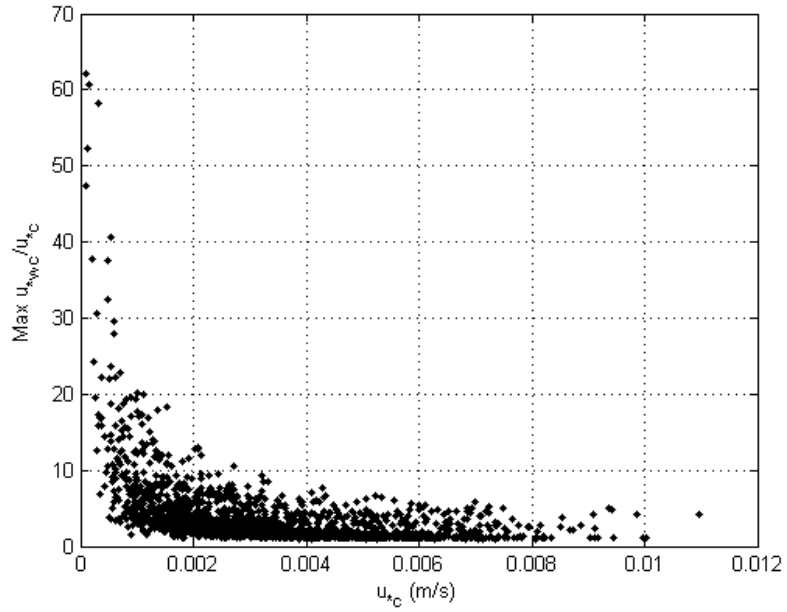

Figure 4.34 Relation between maximum bed shear velocity in wave-current conditions (mean u_{*wc}) and current-alone bed shear velocity (u_{*c}).

4.4.4.1 Sediment entrainment

The sediment remobilization is described using two approaches concerning sediment grain size. The first one evaluates sand tracer particles ($d_{50} = 0.35$ mm or 1.5 ϕ) remobilization according to the periods of observations P1 to P4 (Figure 4.2). The second one evaluates sediment entrainment for 5 grain sizes ranging from very fine to very coarse sand in water depths of 10 m, 14 m, 20 m and 32 m for the entire observational period.

4.4.4.1.1 Tracer particles

The comparison between maximum wave-current shear velocity and the threshold of tracer particle motion (0.013 m/s) shows that sand tracer is remobilized during 10 % of the time for the one year-observation period. On period P1, the sand tracer is remobilized during 9 % of the time, while during P2 the particle threshold is only exceeded 3 % of the time. On the two last periods the sediment remobilization becomes more frequent displaying a frequency of occurrence of 23% during P3 period and 17% during P4 (Figure 4.35).

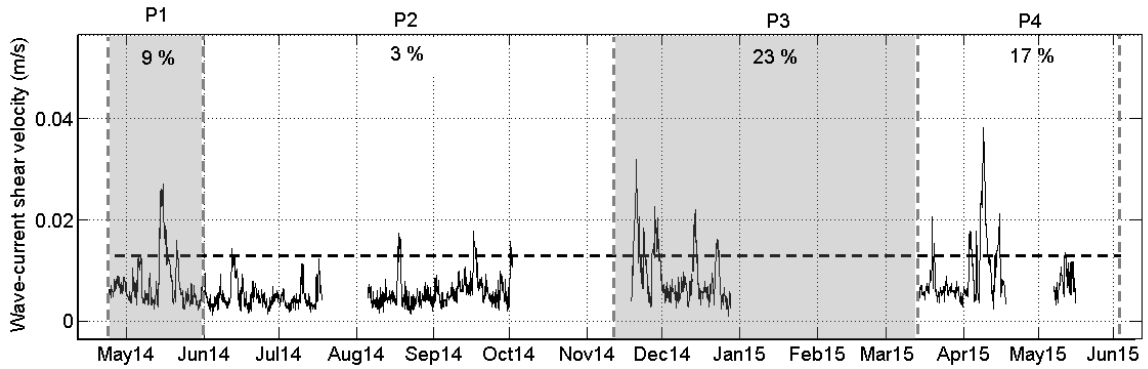

Figure 4.35 Time-series of maximum wave-current induced shear velocity (u_*) time-series. Tracer critical shear velocity (u_{*cr} – dashed line) and the percentage of time that traced sediment is remobilized under the combined action of waves and currents for each period of observation (P1 to P4).

Bottom boundary layer modelling shows that for the simulation period currents alone were never able to remobilize tracer particles and the mean wave-current shear stress only remobilizes sand tracers on P4 period during 1.78% of the time, which represents 0.28% of the entire observational period (Table 4.4). On the other hand, waves alone are able to remobilize tracers much more frequently: during almost 17% of the time during winter

months (P3) and less than 2% of the time on summer/autumn months (P2). For the entire observational period, waves put tracers available for transport during more than 8% of the time. Finally, the combined action of waves and currents enhance tracer remobilization in about 30%, being this enhancement greater during summer/autumn (P2) and less significant during spring (P1 and P4). Thus, maximum wave-current induced shear velocity remobilize sand tracer during 2.66 % of the time on P2 observational period and more than 22% during winter months (P3).

Table 4.4 Tracer remobilization at 14 m water depth.

Period of observation	Frequency of remobilization (% of time)			
	Current		Wave	
	Alone	Wave-current mean	Alone	Wave-current maximum
P1	0	0	8.09	9.03
P2	0	0	1.69	2.66
P3	0	0	16.98	22.64
P4	0	1.78	14.90	17.19
Entire	0	0.28	8.26	10.32

4.4.4.1.2 Sand fractions

The frequency of sediment remobilization seaward the closure depth for 5 sand fractions (very fine to very coarse) at 10, 14 , 20 and 32 m water depths are presented on Tables 4.5 to 4.8. For the one-year bottom boundary layer modelling, results also show that currents alone are never able to remobilize any fraction of sand at any simulated depth. On the other hand, waves alone are able to entrain very coarse sand even at 32 m depth, but only during 0.05 % of the time.

Results show a clear increase of sediment remobilization with decreasing depth, where maximum wave-current induced shear velocity entrain coarse sand during almost 15% of the time at 10 m depth (Table 4.5), while at 32 m water depth this occurs only during 0.37% of the time (Table 4.8). Very fine sand in turn, under the combined action of waves and currents, can be remobilized during over 15% of the time at 10 m depth and during less than 1% of the time at 32 m depth. At intermediate depths, very fine sand is entrained during about 8% (14 m depth) and less than 5 % of the time (20 m depth). An example of the sediment remobilization behaviour over one year is given in Figure 4.36 for coarse sand at 14 m depth.

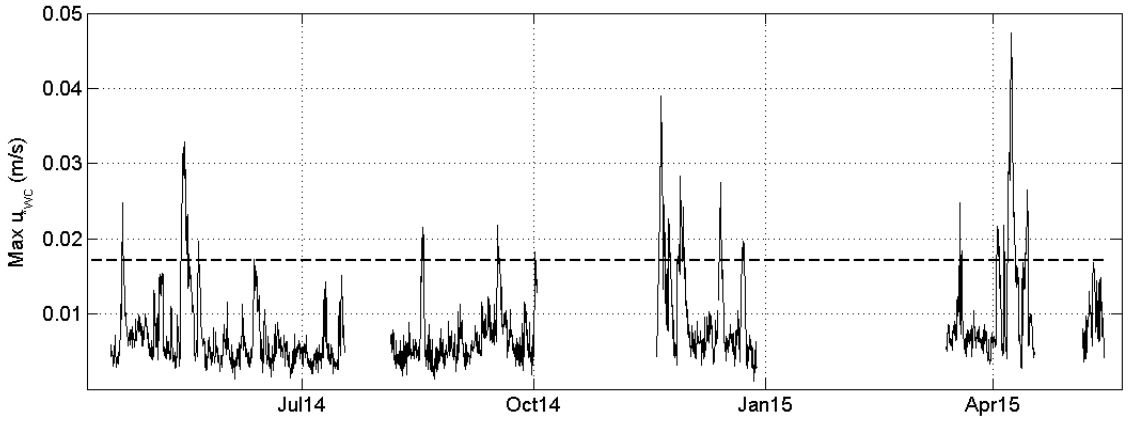

Figure 4.36 Maximum shear velocity for the combined action of waves and currents at 14 m water depth. Dashed line represents the critical shear stress for coarse sand.

A particularity is observed on results regarding wave-alone and maximum wave-current induced sediment remobilization for the different sand fractions. At first, a clear increase on sediment remobilization with decreasing grain size is observed from very coarse to medium sand. Still, this pattern changes and frequency of remobilization decreases from medium to very fine sand at all simulated depths (Tables 4.5 to 4.8).

Table 4.5 Remobilization frequency for different sand fractions at 10 m depth under the action of current- and wave-alone and mean and maximum wave-current bed shear stress.

Grain size		Frequency of remobilization (% of time)			
Sand class	ϕ scale	Current alone	Wave-current mean	Wave alone	Wave-current maximum
Very coarse	-0.5	0	0	6.57	6.94
Coarse	0.5	0	0.21	13.56	14.68
Medium	1.5	0	0.32	15.48	16.55
Fine	2.5	0	0.48	15.00	16.44
Very fine	3.5	0	0.80	13.51	15.37

Table 4.6 Remobilization frequency for different sand fractions at 14 m depth under the action of current- and wave-alone and mean and maximum wave-current bed shear stress.

Grain size		Frequency of remobilization (% of time)			
Sand class	ϕ scale	Current alone	Wave-current mean	Wave alone	Wave-current maximum
Very coarse	-0.5	0	0	2.72	3.20
Coarse	0.5	0	0.05	6.09	6.99
Medium	1.5	0	0.27	8.22	10.09
Fine	2.5	0	0.32	7.26	9.40
Very fine	3.5	0	0.43	5.98	8.33

Table 4.7 Remobilization frequency for different sand fractions at 20 m depth under the action of current- and wave-alone and mean and maximum wave-current bed shear stress.

Grain size		Frequency of remobilization (% of time)			
Sand class	ϕ scale	Current alone	Wave-current mean	Wave alone	Wave-current maximum
Very coarse	-0.5	0	0	1.01	1.33
Coarse	0.5	0	0	2.67	3.42
Medium	1.5	0	0.21	3.42	4.96
Fine	2.5	0	0.27	3.15	4.80
Very fine	3.5	0	0.27	2.67	4.54

Table 4.8 Remobilization frequency for different sand fractions at 32 m depth under the action of current- and wave-alone and mean and maximum wave-current bed shear stress.

Grain size		Frequency of remobilization (% of time)			
Sand class	ϕ scale	Current alone	Wave-current mean	Wave alone	Wave-current maximum
Very coarse	-0.5	0	0	0.05	0.05
Coarse	0.5	0	0	0.21	0.37
Medium	1.5	0	0.05	0.32	0.69
Fine	2.5	0	0.05	0.27	0.80
Very fine	3.5	0	0.11	0.21	0.80

According to bottom shear velocity calculations the active layer thickness (δ_{mix} in Equation 4.1) was estimated in 0.03 m which roughly matches qualitative observation of ripple height made by divers in the scope of SHORE project.

4.4.4.2 Bedforms

The wave-generated bedforms predicted by the model (Equations 3.22 and 3.21 in Chapter 3) are described in terms of wavelength (λ) and height (η). Calculations were made for the same water depths and grain size classes analysed in the last section.

Figure 4.37 shows the time-averaged wavelength which variation according to sediment median grain size are very similar at water depths 10 m, 14 m and 20 m. At these depths, λ ranges essentially between 0.1 and 0.3 m with a clear increase with grain-size. On the other hand, at 32 m depth the bedform wavelength are much smaller (less than 0.1 m) and increases with grain-size only from very fine to medium sand. From medium to coarse sand the time-average wavelength halved and slighly increase for very coarse sand. This apparently unusual result is due to the fact that both coarse and very coarse sand are remobilized by a single extreme wave event (Table 4.8), which means that before it the wavelength at 32 m depth was probably zero. Thus, although the bedforms generated have wavelenghts of 0.31 m and 0.26 m for very coarse and coarse sand, respectively, the time-average values are much smaller. The same behaviour is observed for the time-averaged bedform height that ranges between 0.015 and 0.04 m for 10 m, 14 m and 20 m water depths and always less than 0.01 m at 32 m water depth (Figure 4.38).

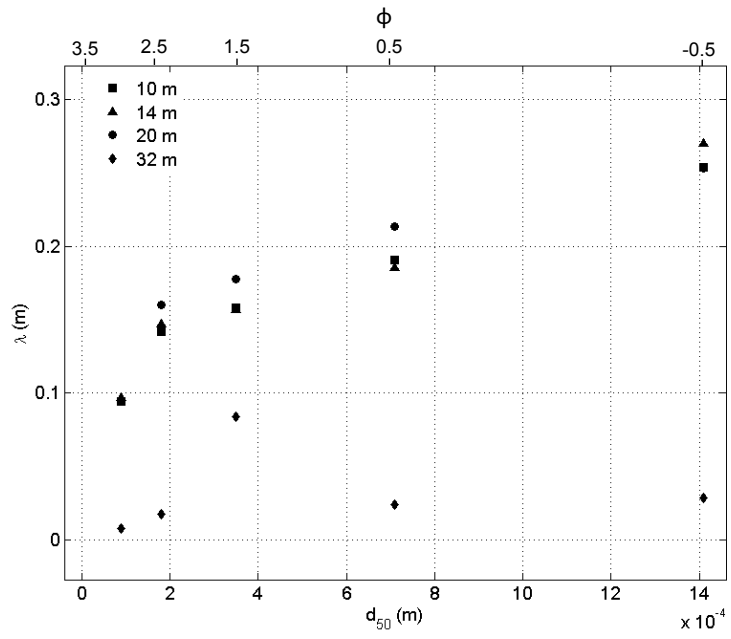

Figure 4.37 Variation of the predicted time-averaged bedform wavelength (λ) according to water depth and sediment median grain size.

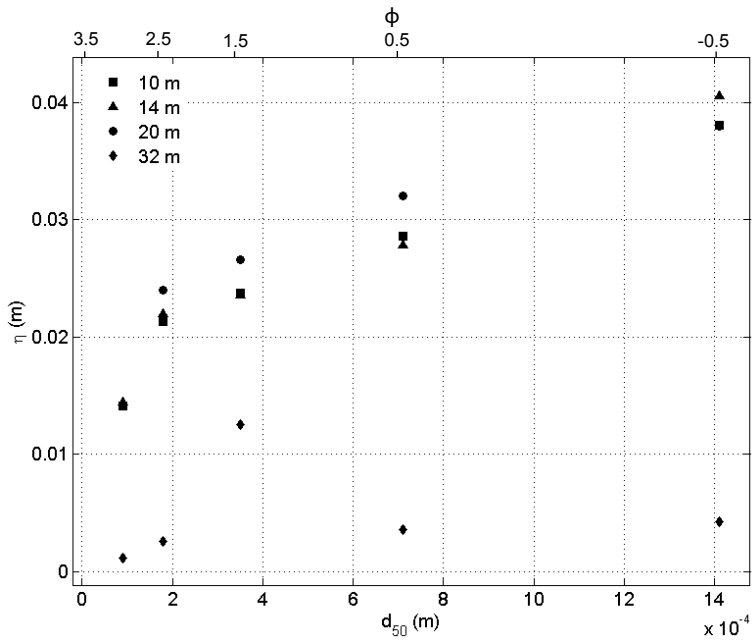

Figure 4.38 Variation of the predicted time-averaged bedform wave height (η) according to water depth and sediment median grain size.

The time evolution of the bedform geometry at 14 m depth is described on Figures 4.39 (λ) and 4.40 (η) for the 5 sand classes. The bedform wavelength ranges essentially between 0.1 m and 0.8 m, being λ higher than 0.2 m only for coarse and very coarse sand. Values regarding bedform height are mainly within 0.02 and 0.1 m, being higher than 0.03 m only for coarse and very coarse sand.

Figures 4.39 and 4.40 also show a clear increase of both λ and η with the median grain size. However, while the bedform geometry for very coarse to fine sand behaves nearly synchronized, for very fine sand bedform's size decreases during peaks of λ and η of other sand classes, evidencing a washout of the bedform during more energetic events.

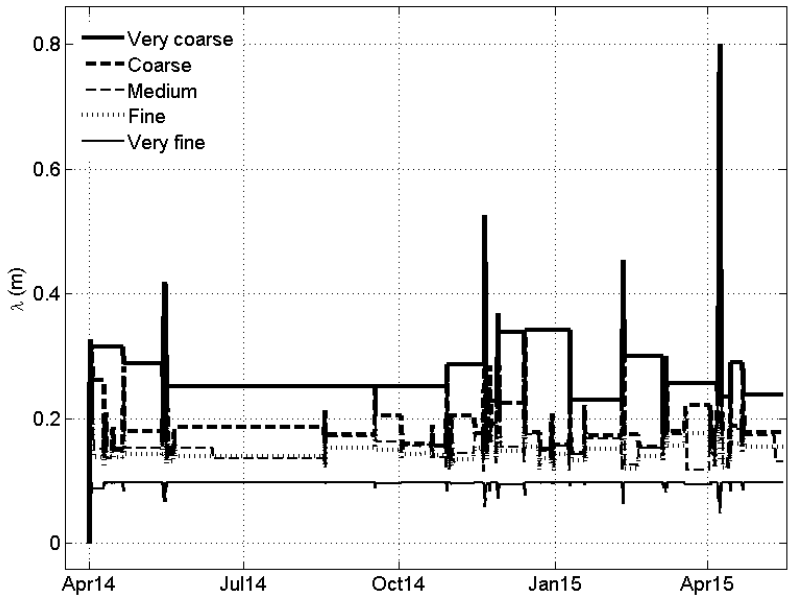

Figure 4.39 Time evolution of predicted bedform wavelenght (λ) for 5 sand classes at 14 m water depth.

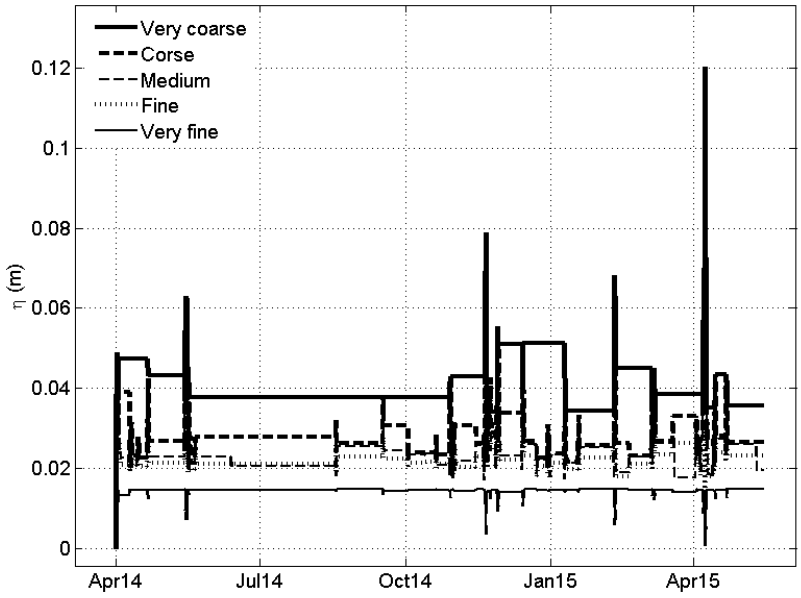

Figure 4.40 Time evolution of predicted bedform height (η) for 5 sand classes at 14 m water depth.

4.4.4.3 Sediment transport

The evaluation of the sediment transport seaward the depth of closure is described in terms of suspended load and bedload which calculations were made for the same water depths and sand classes analysed in the last sections. Attention must be given to the fact that sediment transport is only computed for the period where both wave and currents are simultaneously available.

4.4.4.3.1 Suspended load

The frequency of sediment suspension , i.e., the percentage of time the maximum bed shear stress (skin friction) is higher than the sediment particle fall velocity, is presented in Table 4.9. According to the model prediction, during the observation period, coarse and very coarse sand never get into suspension at any simulation depth while medium sand becomes part of the suspended sediment very rarely only at 10 m water depth (0.05% of time). Fine sand in turn get into suspension at 10, 14 and 20 m water depths with frequencies of occurrence of 4.69, 1.97 and 0.56 %, respectively. Finally, very fine sand is resuspended

at all depths with frequency of ocurrence ranging from about 14% (32 m depth) up to 53% (10 m depth).

Table 4.9 Frequency of sediment suspension (% of time) at each water depth.

Sand class	ϕ scale	Water depth (m)			
		10	14	20	32
Very coarse	-0.5	0	0	0	0
Coarse	0.5	0	0	0	0
Medium	1.5	0.05	0	0	0
Fine	2.5	4.69	1.97	0.59	0
Very fine	3.5	53.28	36.73	26.96	13.83

Results concerning the suspended load transport over time are illustrated for simulated depths of 14 m and 32 m in the alongshelf and cross-shelf directions (Figures 4.41 to 4.44). Negative values indicate a southwestward (alongshelf) and offshore (cross-shelf) sediment transport. At 14 m depth there is a clear dominance of a southwestward suspended transport for both fine and very fine sand with a magnitude up to 1.4×10^{-4} m^2/s (Figure 4.41). On the other hand, the cross-shelf transport have significant transport events at both onshore and offshore directions, being the major events offshore directed and reaching up to 2.5×10^{-5} m^2/s (Figure 4.42).

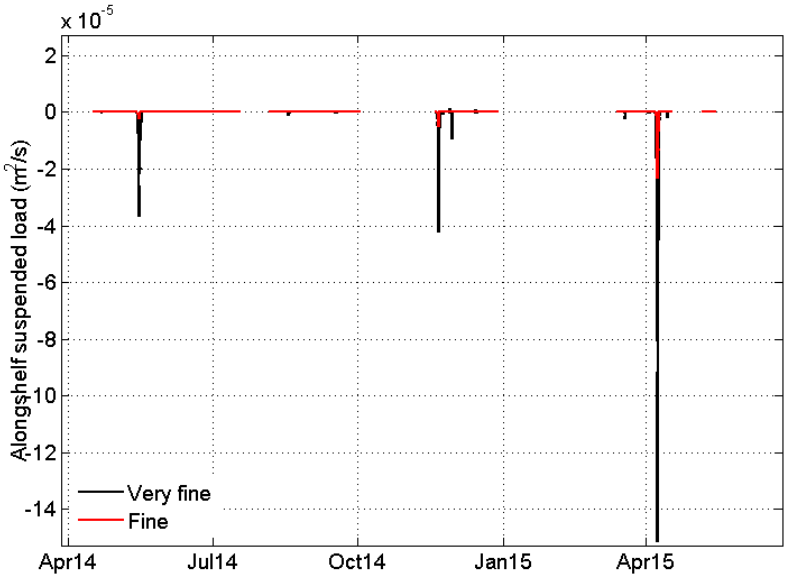

Figure 4.41 Alongshelf suspended load transport at 14 m water depth.

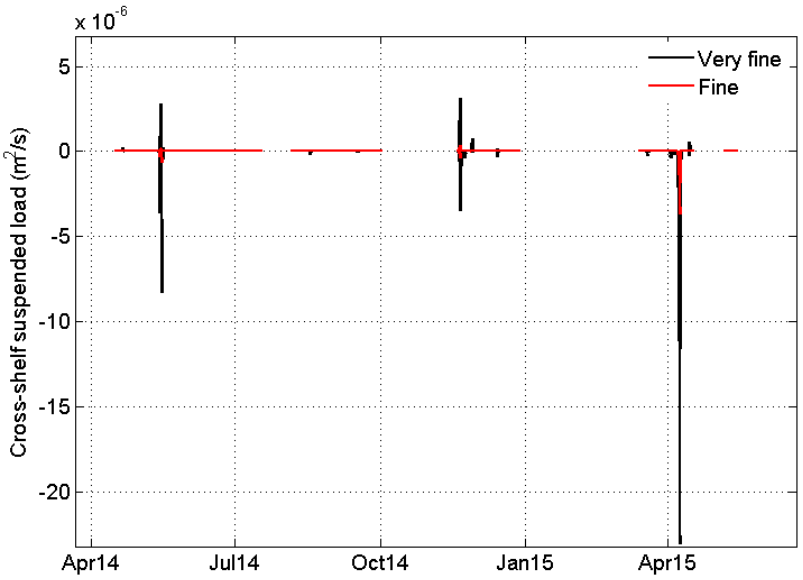

Figure 4.42 Cross-shelf suspended load transport at 14 m water depth.

At 32 m depth only very fine sand is resuspended. This occurs in a single event which induces a southwestward and offshore directed transport of about 2.8×10^{-5} m^2/s and 2.7×10^{-6} m^2/s, respectively (Figures 4.43 and 4.44).

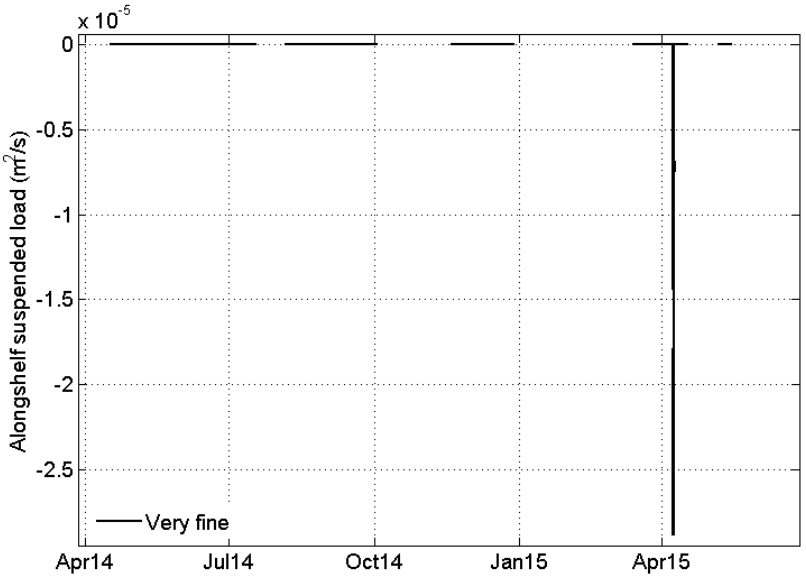

Figure 4.43 Alongshelf suspended load transport at 32 m water depth.

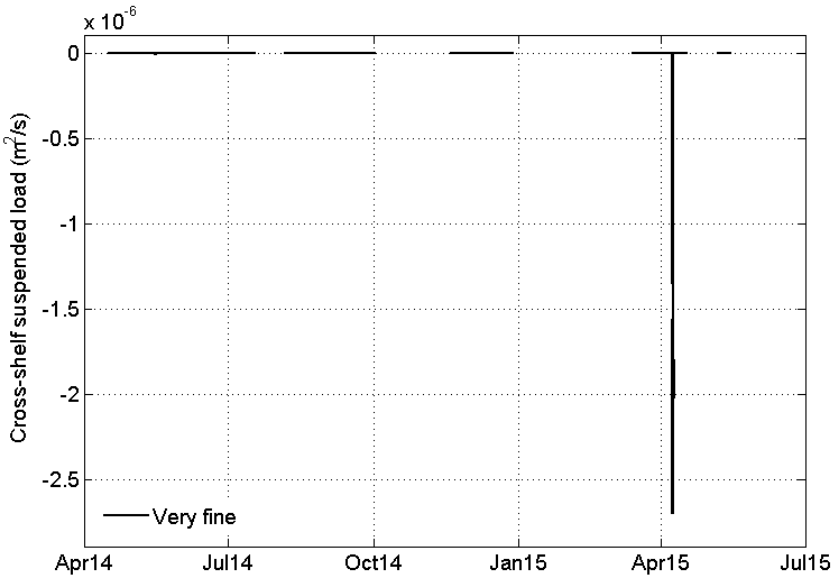

Figure 4.44 Cross-shelf suspended load transport at 32 m water depth.

A description of the potential annual suspended load transport rate for each sand fraction along the water depth is given for both alongshelf (Tables 4.10 and 4.11) and cross-shelf directions (Tables 4.12 and 4.13).

Results show that the alongshelf transport is systematically one order of magnitude higher than in the cross-shelf direction. The magnitude of the alongshelf suspended load transport vary from 0.37 m^2/year (medium sand) up to 24.48 m^2/year (very fine sand) at 10 m depth. Seaward this depth, fine and very fine sand are transported in suspension with magnitudes varying between 0.29 m^2/year and 10.23 m^2/year (Table 4.10).

Table 4.10 Magnitude of potential suspended load transport in the alongshelf direction (m^2/year).

Sand class	ϕ scale	Water depth (m)			
		10	14	20	32
Very coarse	-0.5	0	0	0	0
Coarse	0.5	0	0	0	0
Medium	1.5	0.37	0	0	0
Fine	2.5	3.06	1.12	0.29	0
Very fine	3.5	24.48	10.23	4.44	0.55

The magnitude of the alongshelf sediment transport described in Table 4.10 is almost entirely translated into a southwestward net transport. This parity increases with depth and also with sand size (Table 4.11).

Table 4.11 Potential net suspended load transport in alongshelf direction (m^2/year). Negative values represent a southwestward transport.

Sand class	ϕ scale	Water depth (m)			
		10	14	20	32
Very coarse	-0.5	0	0	0	0
Coarse	0.5	0	0	0	0
Medium	1.5	-0.37	0	0	0
Fine	2.5	-3.01	-1.11	-0.29	0
Very fine	3.5	-23.24	-10.16	-4.43	-0.55

The magnitude of the potential annual suspended load transport rate in the cross-shelf direction varies between 0.03 m^2/year (medium sand) and 3.55 m^2/year (very fine sand) at 10 m depth. Rates decreases with depth, presenting values of 0.16 m^2/year and 0.04 m^2/year (fine sand) at 14 m and 20 m depth, respectively. Very fine sand in turn shows sediment transport rates of 1.45 m^2/year, 0.62 m^2/year and 0.07 m^2/year at water depths of 14 m, 20 m and 32 m, respectively (Table 4.12).

Table 4.12 Magnitude of potential suspended load transport in the cross-shelf direction (m^2/year).

Sand class	ϕ scale	Water depth (m)			
		10	14	20	32
Very coarse	-0.5	0	0	0	0
Coarse	0.5	0	0	0	0
Medium	1.5	0.03	0	0	0
Fine	2.5	0.47	0.16	0.04	0
Very fine	3.5	3.55	1.45	0.62	0.07

Results regarding the annual sediment transport rate as suspended load in the cross-shelf direction points to an offshore net transport at all simulated depths (Table 4.13). Similarities between the magnitude of transport and the net transport increases with depth and also with sand size.

Table 4.13 Potential net suspended load transport in cross-shelf direction (m^2/year). Negative values represent a southwestward transport.

Sand class	ϕ scale	Water depth (m)			
		10	14	20	32
Very coarse	-0.5	0	0	0	0
Coarse	0.5	0	0	0	0
Medium	1.5	-0.03	0	0	0
Fine	2.5	-0.31	-0.13	-0.04	0
Very fine	3.5	-2.27	-1.02	-0.53	-0.07

4.4.4.3.2 Bed load

The bedload transport rates over time are illustrated for simulated depths of 14 m and 32 m in the alongshelf and cross-shelf directions (Figures 4.45 to 4.48). As well as in the suspended load transport, the alongshelf component has bedload transport rates one order of magnitude higher than the cross-shelf component. Also, transport rates tend to increase with sediment grain size. This apparently anomalous behaviour is easily explained by the strong dependence relationship between the sediment transport rate and the sediment particle volume (see Equations 3.25 to 3.28 in Chapter 3).

At 14 m depth the alongshelf bedload transport is predominantly southwestward with rates up to 5.0×10^{-6} m^2/s for very fine sand and up to 5.0×10^{-5} m^2/s for very coarse sand. There are few events of transport northeastward which transport rates are much lower than 5.0×10^{-6} m^2/s even for coarse sand (Figure 4.45). The cross-shelf bedload transport is mostly offshore directed but with significant onshore-directed transport events (Figure 4.46). Offshore sediment transport rates can exceed 1.0×10^{-5} m^2/s considering very coarse sand, while onshore transport do not reach 4.0×10^{-6} m^2/s for the same sand fraction.

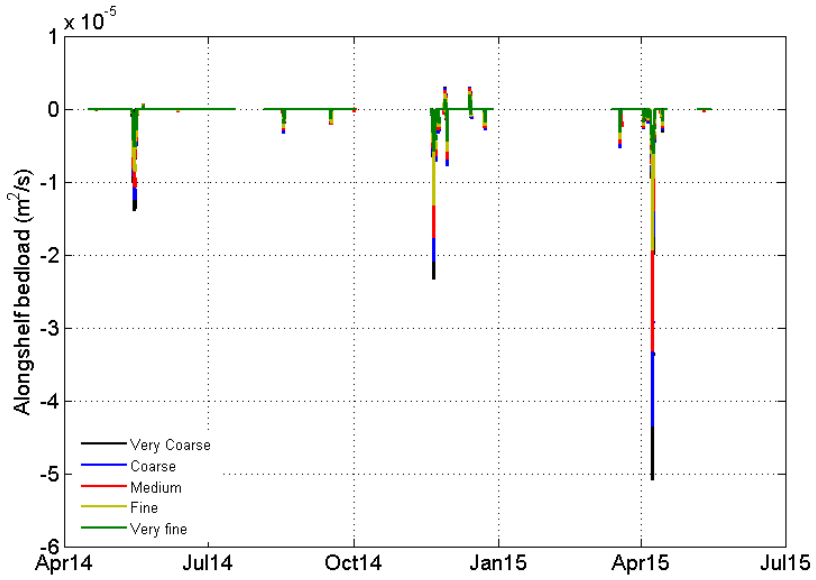

Figure 4.45 Alongshelf bedload transport at 14 m water depth.

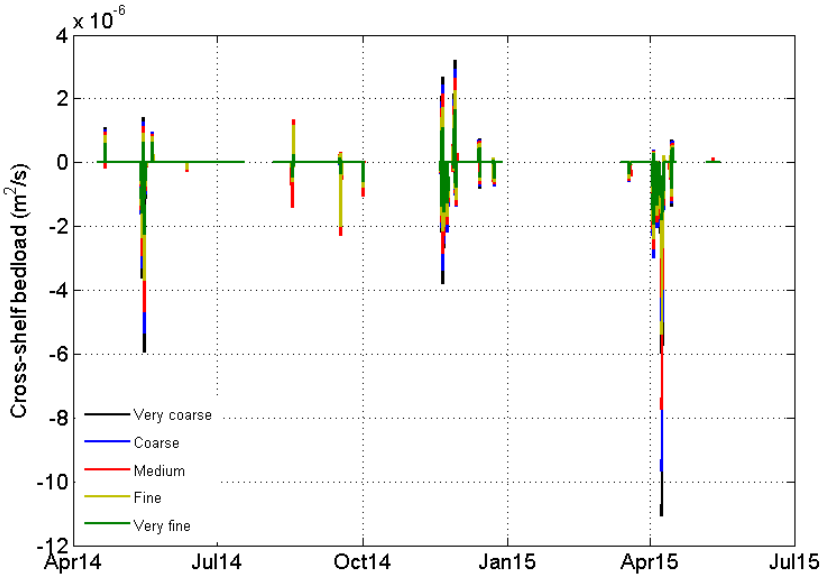

Figure 4.46 Cross-shelf bedload transport at 14 m water depth.

At 32 m depth alongshelf bedload transport is only southwestward and rates can reach about 5.0×10^{-6} m^2/s for very fine sand and more than 1.2×10^{-5} m^2/s for very coarse sand. Cross-shelf transport in turn is entirely offshore-directed with maximum sediment

transport rates of about 1.4×10^{-6} m^2/s and 2.4×10^{-6} m^2/s for very fine and very coarse sand, respectively.

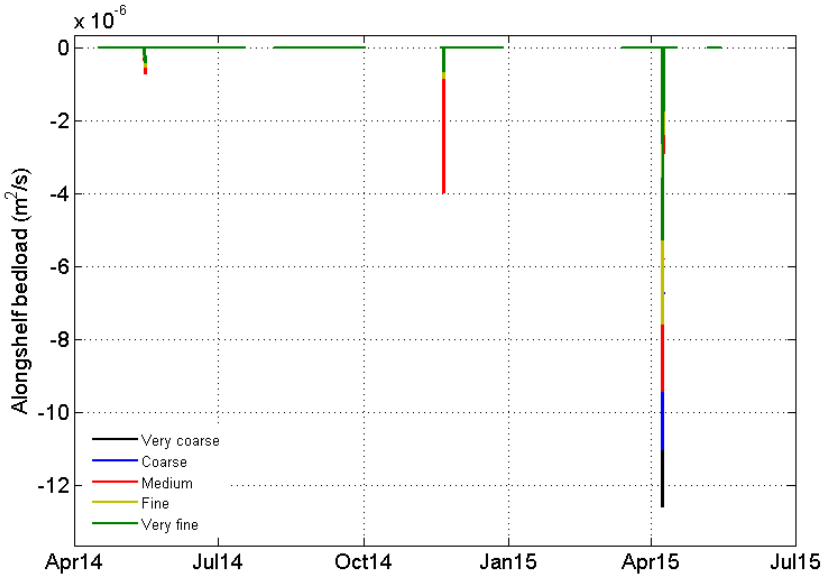

Figure 4.47 Alongshelf bedload transport at 32 m water depth.

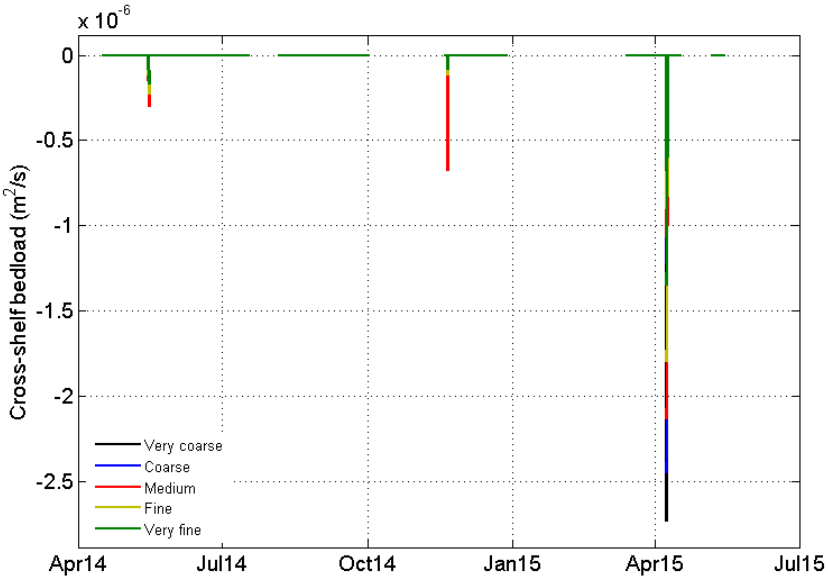

Figure 4.48 Cross-shelf bedload transport at 32 m water depth.

The annual bedload transport rate is presented for each sand fraction along the water depth in the alongshelf (Tables 4.14 and 4.15) and cross-shelf (Tables 4.16 and 4.17) directions.

The magnitude of the bedload transport increases with the sediment grain size from very fine to coarse sand and decreases from coarse to very coarse sand in both alongshelf (Table 4.14) and cross-shelf (4.16) directions. The same behaviour is observed for the net bedload transport in the cross-shelf direction (Tables 4.15 and 4.17).

The magnitude of the bedload transport in the alongshelf direction ranges from 0.14 (very coarse sand at 32 m depth) up to 12.07 m^2/year (coarse sand at 10 m depth). As well as for the suspended load, the magnitude of the alongshelf sediment transport (Table 4.14) is almost entirely translated into a southwestward net transport. This parity increases with depth and sediment grain size (Table 4.15). This behaviour is also observed for the bedload transport in the cross-shelf direction (Tables 4.16 and 4.17).

Table 4.14 Potential magnitude of bedload transport in the alongshelf direction (m^2/year).

Sand class	ϕ scale	Water depth (m)			
		10	14	20	32
Very coarse	-0.5	11.68	5.38	2.25	0.14
Coarse	0.5	12.07	6.11	2.79	0.35
Medium	1.5	10.46	5.61	2.65	0.38
Fine	2.5	7.84	4.32	2.09	0.29
Very fine	3.5	4.51	2.49	1.26	0.19

Table 4.15 Potential net bedload transport in the alongshelf direction in m^2/year. Negative values represent a southwestward transport.

Sand class	ϕ scale	Water depth (m)			
		10	14	20	32
Very coarse	-0.5	-10.80	-5.18	-2.16	-0.14
Coarse	0.5	-11.88	-5.83	-2.70	-0.35
Medium	1.5	-9.72	-5.29	-2.48	-0.38
Fine	2.5	-7.23	-4.10	-1.94	-0.28
Very fine	3.5	-4.10	-2.37	-1.18	-0.19

The magnitude of the annual bedload transport rate in the cross-shelf direction varies between 0.03 m^2/year (very coarse sand at 32 m depth) and 3.64 m^2/year (coarse sand at 10 m depth). Rates decreases with depth, presenting values, for example, from of 3.31 m^2/year down to 0.09 m^2/year for medium sand at 10 and 32 m depth, respectively. Net bedload transport rates increase with grain size from very fine to coarse sand, and decrease from coarse to very coarse sand (Table 4.16).

Table 4.16 Potential magnitude of bedload transport in the cross-shelf direction (m^2/year).

Sand class	ϕ scale	Water depth (m)			
		10	14	20	32
Very coarse	-0.5	2.99	1.23	0.49	0.03
Coarse	0.5	3.64	1.61	0.66	0.09
Medium	1.5	3.31	1.61	0.65	0.09
Fine	2.5	2.61	1.24	0.51	0.07
Very fine	3.5	1.63	0.74	0.31	0.05

Table 4.17 shows a net bedload transport offshore directed at all depth for all sand fractions. However, these results must be analysed with caution once the sediment transport model does not calculate wave streaming.

Table 4.17 Potential net bedload transport in the cross-shelf direction in m^2/year. Negative values represent an offshore transport.

Sand class	ϕ scale	Water depth (m)			
		10	14	20	32
Very coarse	-0.5	-2.05	-0.86	-0.43	-0.03
Coarse	0.5	-2.27	-1.08	-0.45	-0.09
Medium	1.5	-2.05	-1.06	-0.44	-0.09
Fine	2.5	-1.58	-0.80	-0.33	-0.07
Very fine	3.5	-0.93	-0.46	-0.18	-0.05

4.5 Discussion

4.5.1 Sediment transport

4.5.1.1 Numerical model validation

Results from the sediment transport numerical model were validated against field measurement data obtained through the sand tracer experiment. Tracer displacement points to annual averaged transport rates of 0.61 m^2/year on the alongshelf (southwestward) and of 0.31 m^2/year on the cross-shelf (towards onshore) direction. For the same depth of the tracer experiment (14 m) and considering medium sand (1.5 ϕ), modelling results present a bedload net sediment transport of about 5 m^2/year southwestward while the cross-shelf transport is about 1m^2/year offshore directed. These rates refers only to the bedload mode of

transport, once modelling results suggest that medium and coarser sand are only transported as bedload at this depth. Results regarding the direction of the cross-shelf transport estimated by the numerical model must be analysed with caution as the modelling approach has no parametrizations for computing wave asymmetry and the streaming effect. According to several authors (Aagaard, 2014; Holmedal et al., 2015; Kranenburg et al., 2013), only oscillatory wave motions and potentially streaming in the wave boundary layer can accomplish the onshore transport, which means that the present model is unable to properly predict the direction of cross-shelf sediment transport. This explain the divergence on the direction of the cross-shelf net sediment transport between tracer and modelling results.

Numerical modelling validation shows an overestimation of the sediment transport rates by the numerical model with values 8 and 3 times higher in the alongshelf and cross-shelf directions, respectively. These quite acceptable differences show a good behaviour of the numerical model and can be explained by one or a combination of the following factors due to sediment grain size heterogeneity:

- Tracer particles entrapment: the sand tracer particles are considerable finer (d_{50} = 1.5 ϕ) than native sediment (d_{50} = 0.4ϕ). Such contrast can result in tracer particle entrapment by the coarser native sand, thus reducing tracer mobility and consequently the sediment transport. More details about this phenomena can be found in Wiberg and Dungan (1987).

- Isometric sediment assumption: modelling approach assumes an isometric sediment which can significantly influence the sediment transport rates estimations as reported by Taborda (1999) and illustrated on Figure 4.49.

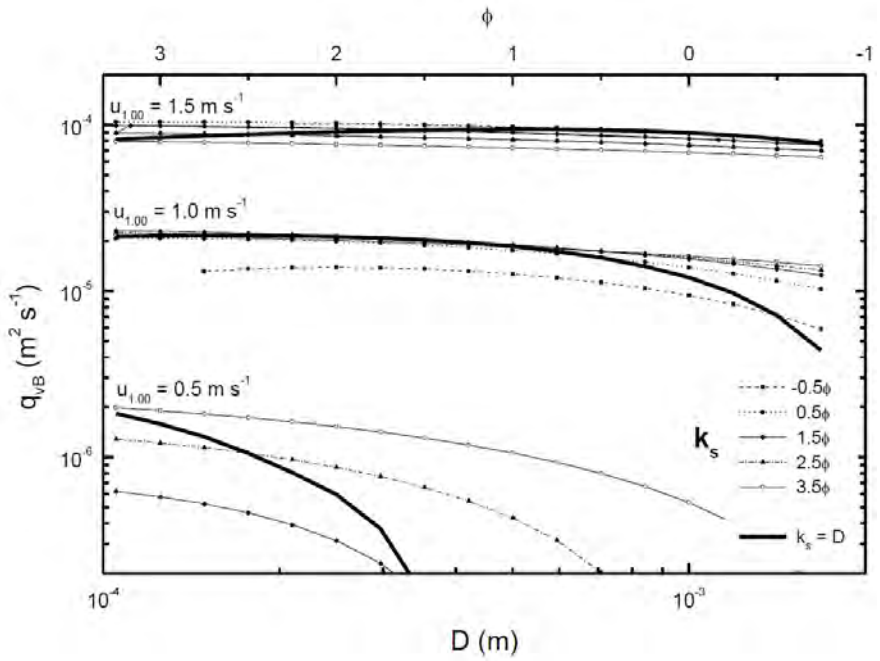

Figure 4.49 Bedload transport variation for a particle with a diameter D according to current velocity at 1 m from the bed ($u_{1.00}$) and to bottom roughness (ks). Extracted from Taborda (1999).

Very few works present quantitative estimates of sediment transport seaward the closure depth at a large temporal scale (monthly to yearly). Estimations from a numerical model described in van Rijn (1997), in the Northern Sea, revealed values between 0 and 15 m^2/year on the cross-shelf direction and between 15 and 60 m^2/year alongshelf-directed for an observation site at 20 m depth while Kleinhans and Grasmeijer (2006) have reported a net transport five times smaller for exactly the same conditions. Also, the empirical model developed by Patterson (2012) based on field data from Gold Coast, Australia, has estimated a cross-shore transport onshore-directed of about 13 m^2/year at 14 m depth. Despite the higher sediment transport rates in these case studies due to more energetic oceanographic conditions associated with smaller sediment grain sizes (fine sand), the order of magnitude is the same of the sediment transport data presented in this work.

4.5.1.2 Sediment transport dynamics

The numerical model approach was able to give a wider comprehension on the sedimentary dynamics offshore the closure depth. The behaviour regarding the two modes of sediment transport are herein analysed according to depth and sediment grain size as well as its link with the oceanographic forcing conditions.

Bottom boundary layer modelling results show that current-alone forcing is unable to remobilize any sand fraction at any simulated depth, being the waves the major driver of sediment remobilization. The relative importance of waves and currents on bottom dynamics varies with depth and it is marked by a clear decrease on the relative importance of waves with depth (Figure 4.50).

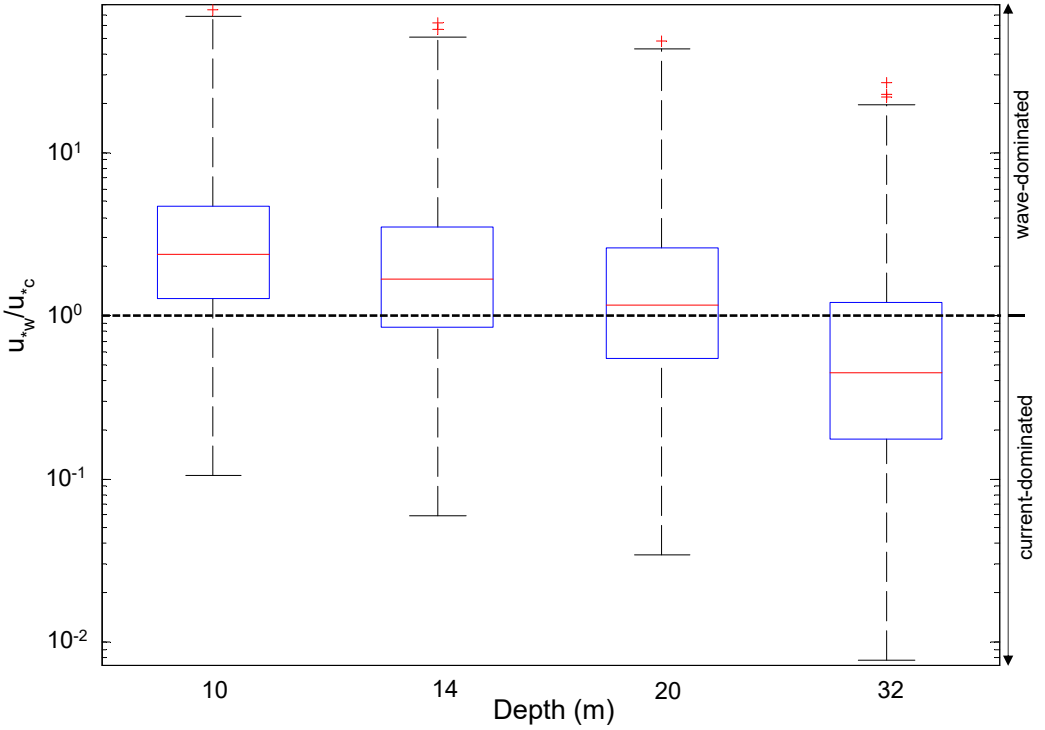

Figure 4.50 Ratio between wave (u_{*w}) and current (u_{*c}) induced shear velocities across the water depth.

Sediment transport modelling points to a dominance of the bedload transport at all depths when considering fine to very coarse sand. Very fine sand in turn is mostly transported as suspended load at all depths (Figure 4.51). A clear decrease on the suspended load transport with increasing particle diameter is obseved. On the other hand, the bedload transport increase with sediment grain size from very fine to coarse sand. This apparently anomalous behaviour was also observed by Taborda (1999) and it is explained by the dependence relationship between the bedload transport rate and the particle diameter (see Equations 3.25 to 3.28 in Chapter 3).

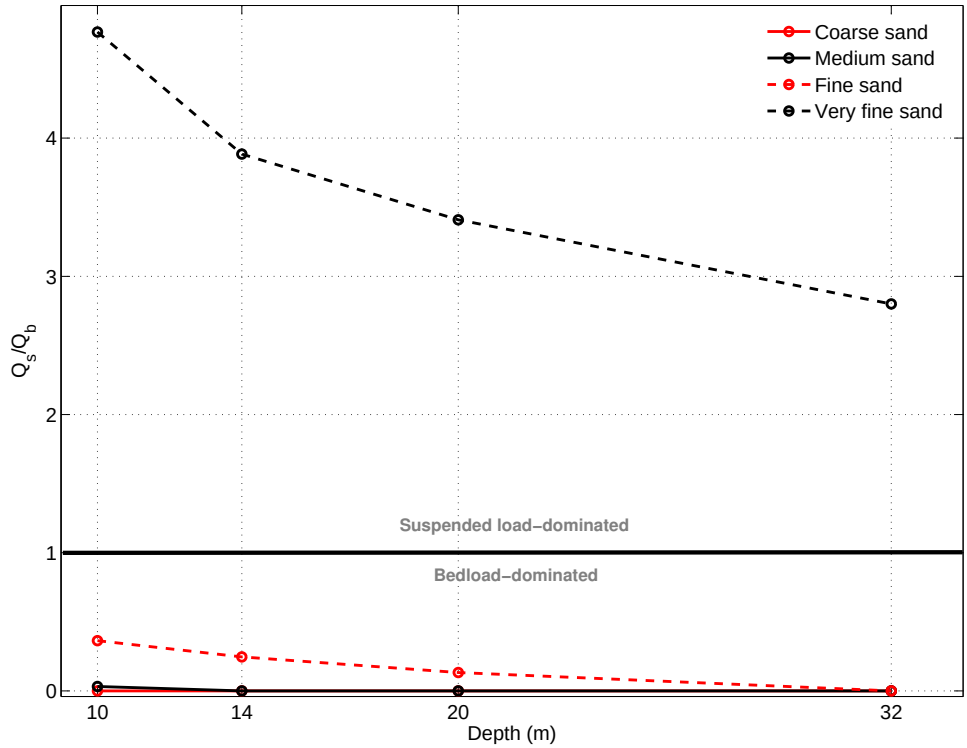

Figure 4.51 Ratio between potential magnitudes (yearly rates) of suspended (Q_s) and bedload (Q_b) according to depth for different sand fractions (coarse to very fine).

Sediment transport events occur mostly during high-energy wave events in relation to "levante" conditions which are characterized by waves coming from southeast and consequently inducing a southwestward flow. Bedload transport is mainly induced by incoming waves from south-southeast, being the most significant transport events under "levante" conditions. Suspended sediment transport in turn is less frequent and rarely promoted by waves from south, being the transport almost entirely induced under "levante" conditions (Figure 4.52).

A first look into the nearbed current pattern points to the predominance of a northeastward flow, a pattern that does not match the net sediment transport behaviour presented in this work. However, during sediment remobilization periods the current is dominated by a flow in the opposite direction and thus inducing a southwestward sediment transport (Figure 4.53).

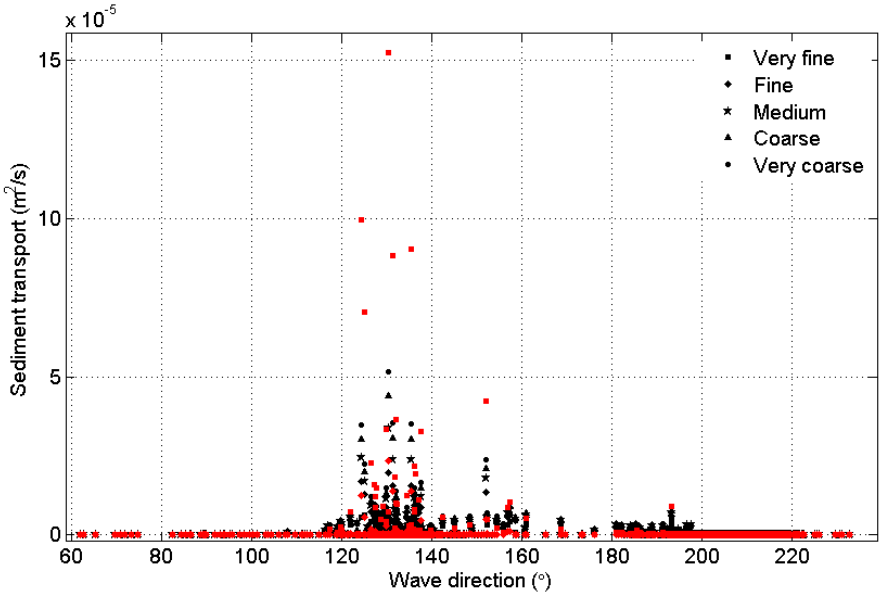

Figure 4.52 Variation of the sediment transport magnitude as bedload (black symbols) and suspended load (red symbold) according to the wave direction for each sand fraction (at 14 m depth).

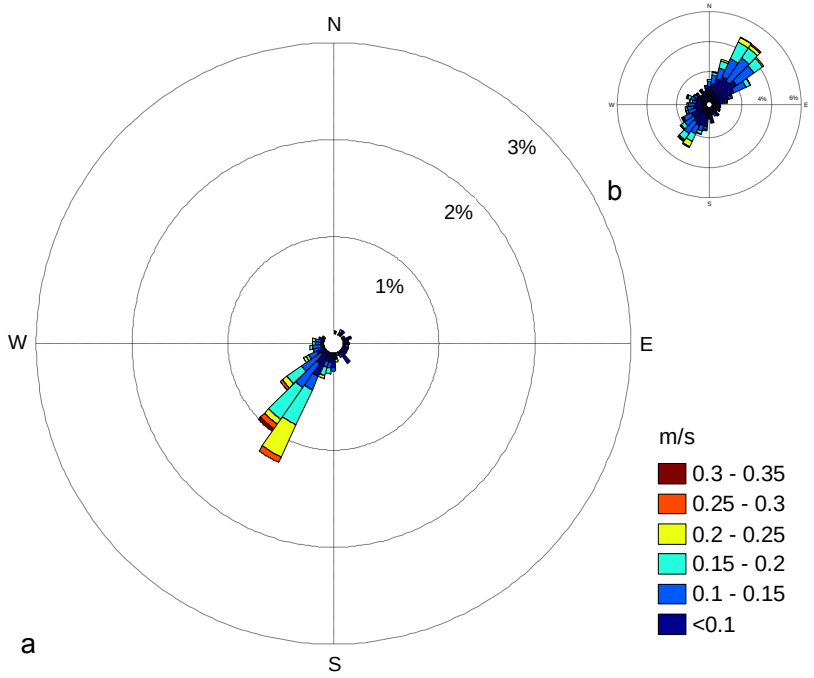

Figure 4.53 Nearbed current rose for the entire observational period (b) and only for the period considering above particle threshold conditions for medium sand (a). Graphic indicates where currents are flowing to (oceanographic convention).

Modelling results reinforces the predominance of the alongshelf sediment transport which is mainly dominated by a current-related component. Yet, observations regarding the last sand tracer survey (C4) during the spring of 2015 (P4 observation period) shows that a wave-related transport can occur during high energy wave events. In this particular case, after a major storm under "levante" conditions (Hs > 3 m) it was observed an onshore transport probably related to progressive wave streaming (Patterson, 2012). Sediment transport modelling approach was not able to simulate this onshore transport once the model has no parametrizations regarding wave asymmetry.

4.5.2 Conceptual sediment dynamic model

The analysis and interpretation of the sedimentary cover (Figures 4.54 and 4.55), bottom morphology (Figure 4.54) and bottom boundary layer dynamics shows that the continental shelf can be classified in 4 dynamically sectors described below. The water depth limits - referred to the mean sea level - are obviously approximated and boundaries should be considered gradual.

Sector A: from 0 to 6 m depth

The offshore limit of this zone is represented by the depth of closure. Bottom sediments are marked by the presence of well sorted fine to medium sand with no fragments of shells. Bottom morphology is relatively steep but no significant break in the slope is observed. The very frequent remobilization and sediment transport events are translated into significant morphological changes observed at annual time scale. There is a frequent exchange of sediment with the subaerial beach.

Sector B: from 6 to 10 m depth

This sector acts as a transition zone where bottom sediments are represented by medium to coarse sand moderately sorted (with no coat on sediment particles) which are frequently remobilized but rarely transported. Bottom morphology is flatter than sector A and a break in the slope can be observed around the offshore limit of this sector. Morphological variations are negligible and sediment is mainly transported as bedload in the alongshelf direction with a southwestward net transport. Also, high-energy wave events can episodically induce onshore transport.

Sector C: from 10 to 30 m depth

This zone is marked by the presence of coarse to very coarse sand with a reddish coat - suggesting a relict nature of the sedimentary deposit (Swift et al., 1971) - and containing fragments of shells. Bottom morphology become smoother with minor oscillations on the slope. Little remobilization is observed and sediment transport events basically occur during high energy wave events (mostly under "levante" conditions). As well as in sector B, this part of the continental shelf is dominated by the bedload mode of transport with a much lower net sediment transport and also dominated by a southwestward alongshelf component. Episodically, high energy wave events can also induce onshore sediment transport.

Sector D: offshore 30 m depth

Bottom sedimentary cover is marked by the dominance of muddy sediments (see Figures 4.23 and 4.27) which are under the action of milder nearbed hydrodynamic conditions, being sediment remobilization very rare (during between 0.05 and 0.8 % of the time depending on the grain size - see Table 4.8) and occurring only during high energy wave events when suspended load transport can also occur. In contrast to the other sectors, on this part of the continental shelf waves begin to have a secondary role and currents dominate the sedimentary dynamics (Figure 4.50).

The sediment dynamic model show that Sectors A to D have distinct characteristics regarding their sediment dynamic behaviour, thus representing different zones of the continental shelf. As such, the following boundaries are proposed on Table 4.18.

Table 4.18 Continental shelf classification according to the depth boundaries presented on the conceptual sediment dynamic model.

	Depth (m)	Continental shelf classification
Sector A	0 - 6	Upper inner shelf / Submarine beach
Sector B	6 - 10	Lower inner shelf
Sector C	10 - 30	Mid shelf
Sector D	> 30	Outer shelf

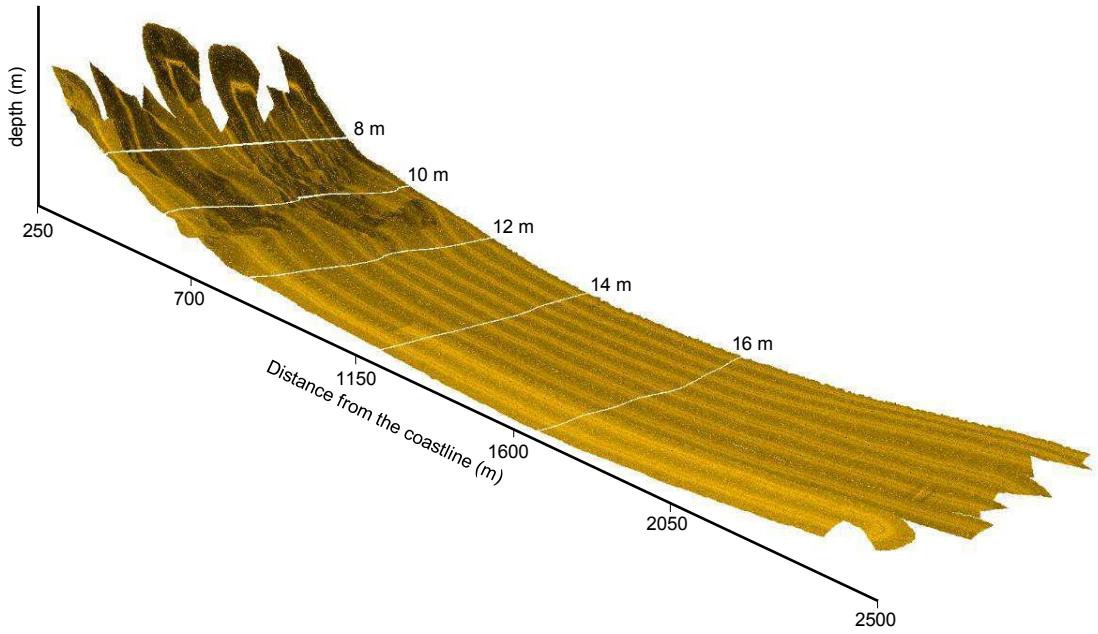

Figure 4.54 Merge between the side scan sonar survey and the bottom morphology.

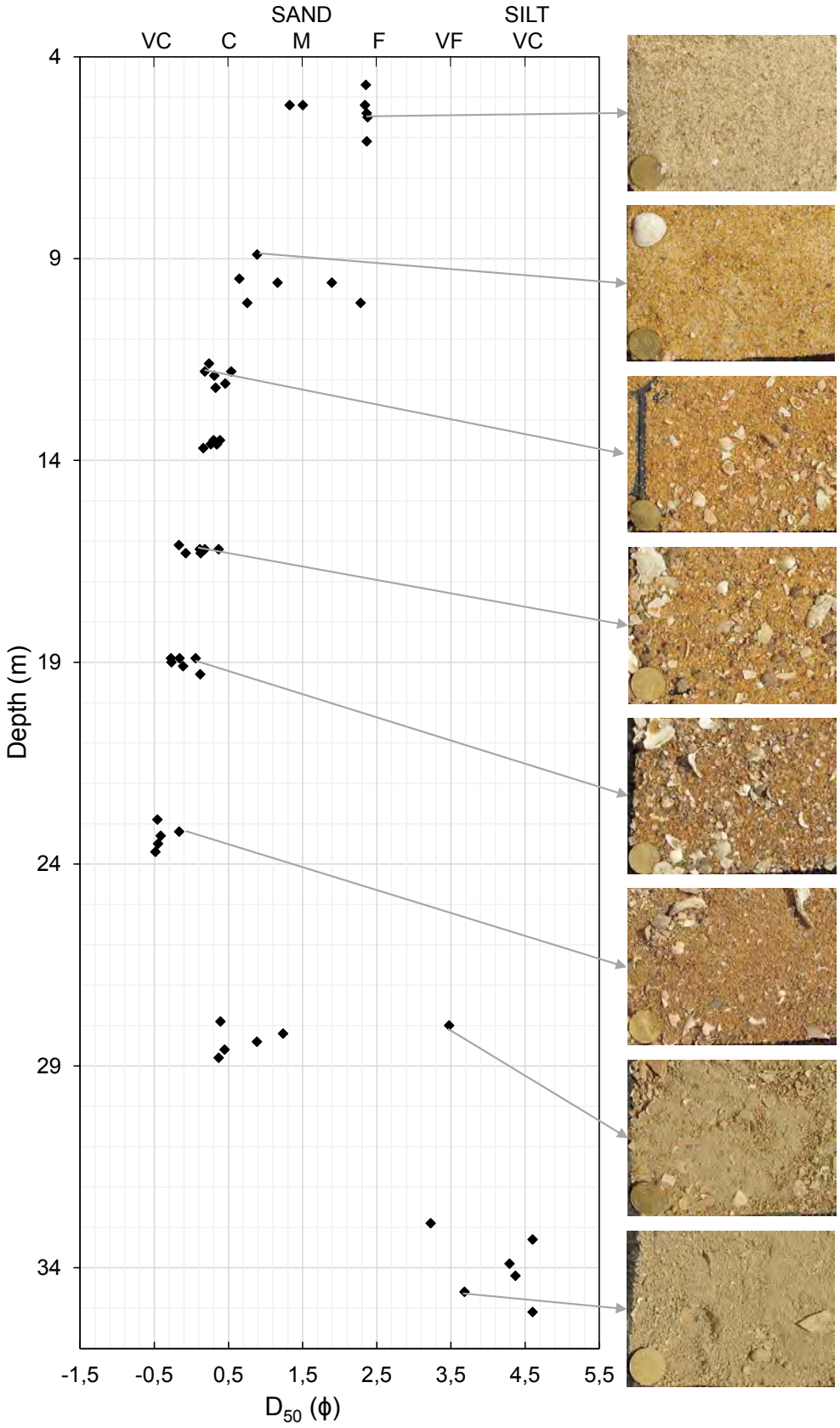

Figure 4.55 Continental shelf sediments: median grain size variation along depth.

4.6 Main achievements

The multiproxy approach carried out on this work was able to give valuable insights in what concerns the understanding of the sedimentary dynamics offshore the depth of closure. Main achievements relates to the quantification of the sedimentary processes and its relationship with the oceanographic forcing, thus representing a substantive advance in the state-of-the-art of the nearshore sedimentary dynamics.

Main achievements are summarized here:

1. Acquisitions of first direct estimates of the sediment transport seaward the depth of closure at seasonal time scale (sand tracer experiment).

2. Validation and implementation of a wave-current bottom boundary layer model.

3. Tracer sand experiment points to sediment transport rates of 0.61 m^2/yr on the along-shelf (southwestward) and 0.31 m^2/yr on the cross-shelf (towards onshore) direction.

4. Modeling results estimate the sediment transport rates in about 5.0 m^2/yr southwestward and 1.0 m^2/yr in the offshore direction, which revealed a superestimation of the numerical model.

5. Divergences on the direction of the cross-shelf transport are the result of the absence regarding calculations of wave-induced transport, being therefore a major limitation of the model that deserves further improvements.

6. Development of a conceptual sediment dynamic model for the nearshore where 4 dynamically distinct domains are identified: upper and lower inner shelf, mid shelf and outer shelf.

7. The recognition of the wave as the major driving the nearshore sedimentary dynamics.

Chapter 5

Sedimentary dynamics in a high-energy environment

5.1 Introduction

The importance of further understanding the nearshore sedimentary dynamics and the lack of reliable sediment transport data seaward the depth of closure (see Chapter 1) evidence the current need for evaluating the sedimentary dynamics in this area under different oceanographic conditions. While on Chapter 4 a moderate-energy environment is addressed, the present chapter focus on a high-energy coastal environment where the sedimentary dynamics is evaluated by using a similar approach carried out on Chapter 4, but without a tracer experiment. Thus, bottom boundary layer model results are herein also analysed under a multiproxy context where it is considered the sedimentary cover and the oceanographic forcing. The evaluation of the sedimentary dynamics in a high-energy environment is therefore carried our by accomplishing the following specific goals:

- Evaluate the dominant mode of transport as well as quantify sediment remobilization and transport according to depth and particle size.

- Analyse the relative importance of waves and currents on the sedimentary dynamics according to depth.

- Build a conceptual sediment dynamic model for a high-energy coastal environment.

5.2 Study area

The study area comprises the nearshore zone offshore Almagreiro beach and north of Peniche tombolo. This area is located at a NE-SW oriented coastal stretch of Portuguese west coast, being fully exposed to the NE Atlantic swell (Figure 5.1).

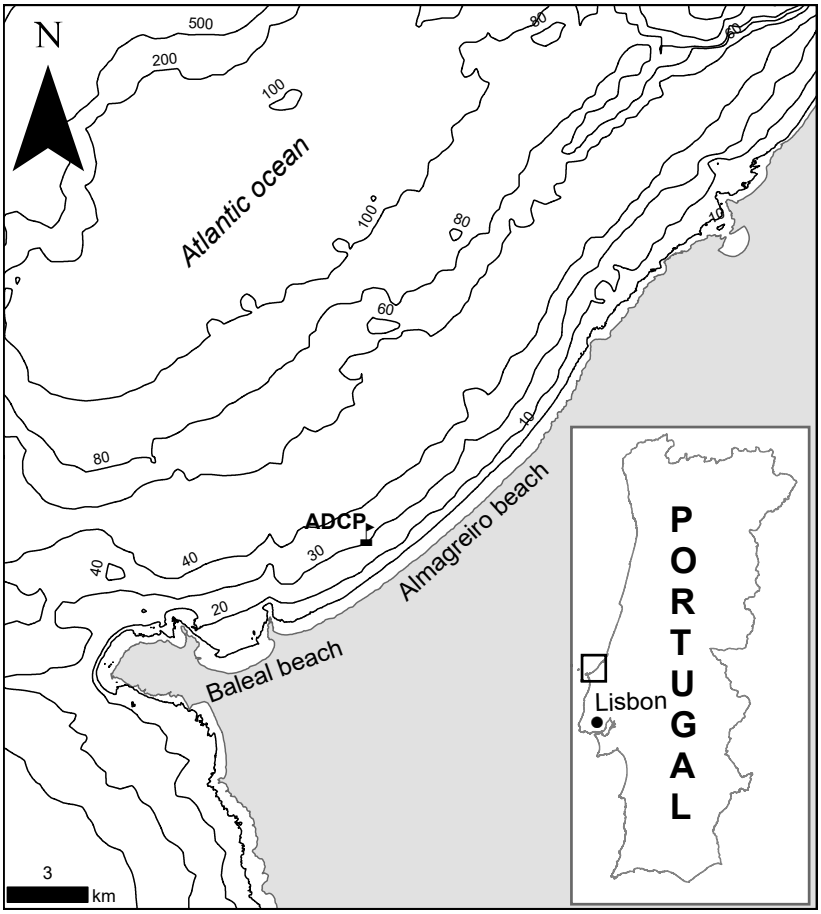

Figure 5.1 Study area, ADCP site and local bathymetry.

5.2.1 Oceanography

The study area is characterized by semi-diurnal tides propagating from S to N with amplitudes from 3 (spring tides) to 1 meter (neap tides). According to Rodrigues et al. (2012), the wind regime recorded at Cabo Carvoeiro (Peniche) weather station shows the dominance of northerly winds with frequency of occurrence of approximately 53% in summer (April to September) and 27% in winter (October to March).

According to data from the Figueira da Foz buoy (92 m depth) described on Costa et al. (2001), 40 % of signifcant wave height (H_s) data are within 1 and 2 m height, presenting

an yearly average H_s of 2.2 m. The peak period is mainly between 9 and 13 s (60% of observations) and present an average value of 11.4 s. The direction associated with the peak period is basically N-NW (90% of the observations) with no significant seasonal variation. Wave heights higher than 4.5 m for periods of time exceeding 12 hours are considered storm events at Portuguese west coast. According to Costa et al. (2001), it was registered an average of 3.4 stormy days during summer and 19.9 stormy days during winter with a predominance of NW coming direction.

During summer, northerly winds influences the coastal circulation by favoring upwelling conditions. Winter is frequently characterized by downwelling regime with a poleward flow of about 0.2 - 0.3 m/s in the water column (Relvas et al., 2007). Tide-induced currents have a greater frequency when compared to wind forcing currents and in general smaller magnitudes, so they are considered a secondary contribution to the mid shelf current. However, closer to the shore (nearshore), tide- and wind-induced currents can have magnitudes of same order (Rodrigues et al., 2012).

5.2.2 Morpho-sedimentary features

The mobile sedimentary cover between the shoreline and 30 m depth is composed by sediments represented by fine and medium sand with a general tendency of a seaward grain size decrease (Figure 5.2). Also, nearshore seabed surface till 30 m depth is characterized as mostly flat, with the exception of three major rocky outcrops that protrude from the smooth bottom and constrain the sedimentary deposits of this area (Figure 5.3). According to Rodrigues et al. (2012), bottom sediments are marked by medium sand (between 1 and 2 ϕ) down to about 16 m depth where Lapa et al. (2012) have defined to be the local depth of closure (DoC). This sediment is moderately well to well sorted with a poor content of calcium carbonate (< 1%). Seaward the DoC, bottom sediments are represented by moderately sorted fine sand down to about 30 m depth (Figure 5.3).

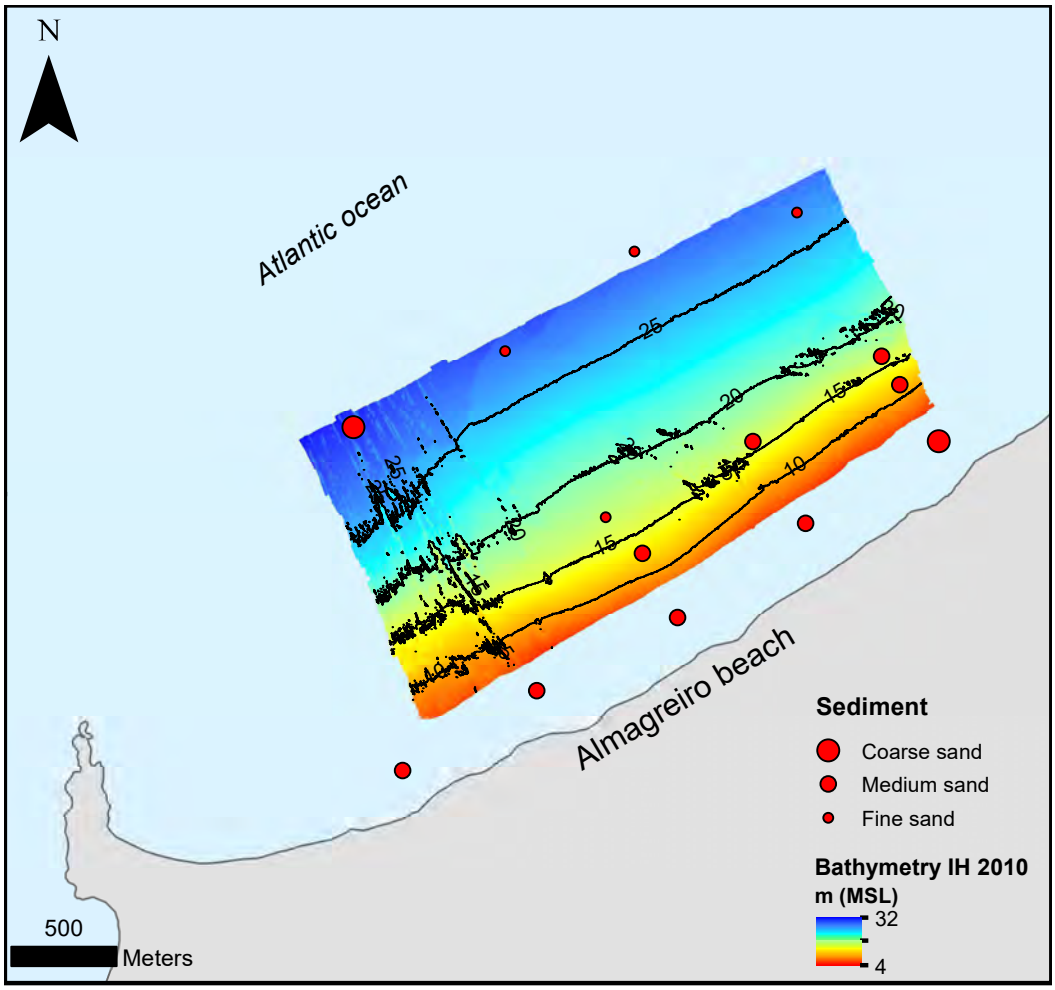

Figure 5.2 Surface sediments disctribution according to depth (Data acquired under the scope of SURGE project and kindly provided by the Hydrographic Institute).

According to IH (2010), seaward 30 m depth the sedimentary cover is composed by coarse sand till 40 m depth and very coarse sand down to about 80 m depth where it is observed an abrupt contact with muddy sediments (Figure 5.3).

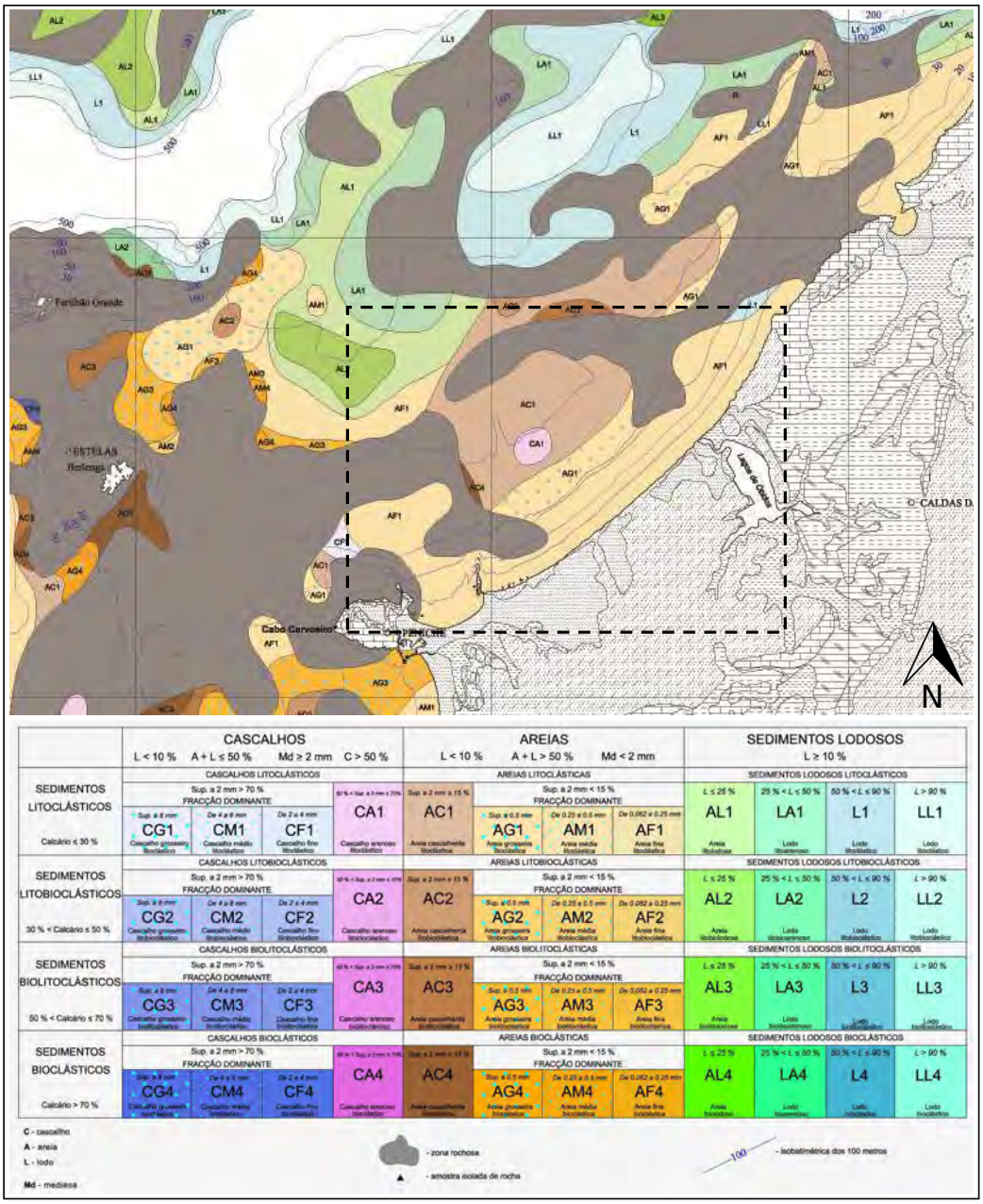

Figure 5.3 Surface sediments map from IH (2010). Water depth refers to ZH (Hydrographic zero) and dashed black polygon bounds the study area.

5.3 Materials and methods

5.3.1 Oceanographic monitoring

5.3.1.1 In situ measurement

Local oceanographic monitoring strategy was carried out by the Hydrographic Institute under the scope of SURGE[1] European project from October 2009 to October 2012. As described in Rodrigues et al. (2012), a 600 kHz RDI Workhorse Acoustic Doppler Current Profiler (ADCP), with a pressure gauge installed, was deployed in the study area offshore Almagreiro beach at about 30 m depth below MSL (Figure 5.1). The instrument was mounted facing upward in order to track the surface oscillation and the water column velocities. Current velocities along the water column were measured every 10 minutes within 1 m cells. Wave measurement was acquired in 17 minutes burst events with a 2 Hz sampling rate every 3 hours. The ADCP configuration parameters are listed on Table 5.1.

Table 5.1 Configuration of the 600 kHz ADCP.

		Waves				Currents	
No. of bins	Bin size (m)	Burst duration (min)	Sampling rate (Hz)	Burst interval (min)	Samples per wave burst	Averaging period (min)	Sampling rate (Hz)
35	1	17	2	180	1024	10	1/12

5.3.1.2 Wave modelling

Wave modelling was performed using SWAN 3rd generation model (Booij et al., 1999) where offshore wave regime recorded at MONICAN01 buoy (see http://monican.hidrografico.pt/), between April 2009 and June 2012, was propagated till the shore. The model simulation was performed under stationary mode over a 17 km x 12 km local grid nested into a 70 km x 84 km regional grid with cell sizes of 100 m and 500 m, respectively. Grid data is based on topographic data from ASTER GDEM 2 developed by the U.S. National Aeronautics and Space Administration (NASA) and Japan's Ministry of Economy, Trade and Industry (METI) available at http://asterweb.jpl.nasa.gov/; bathymetric data from GEBCO08 Grid (version 20091120) provided by General Bathymetric Chart of the Oceans (GEBCO) and available at http://www.gebco.net/; Vanney and Mougenot bathymetry (1981) available at http://geo.snirh.pt/snirlit/site/; and bathymetric models of Foz do Arelho provided by

[1]Simple Underwater Renewable Generation Energy (http://aw-energy.com/pt-pt/projetos/projeto-surge)

Portuguese Hydrographic Institute and available at http://www.hidrografico.pt. All elevation data were converted to the mean sea level datum, placed 2 m above hydrographic zero (ZH).

Wave-induced bottom dynamics was computed on a cross-shelf profile at 6 points at the following water depths: 10 m, 15 m, 20 m, 30 m, 40 m, 60 m and 80 m below mean sea level (MSL). Regional and local grids as well as simulation points of the wave modelling strategy are represented on Figure 5.4 while a bathymetric cross-shelf profile containing the simulation points is presented on Figure 5.5.

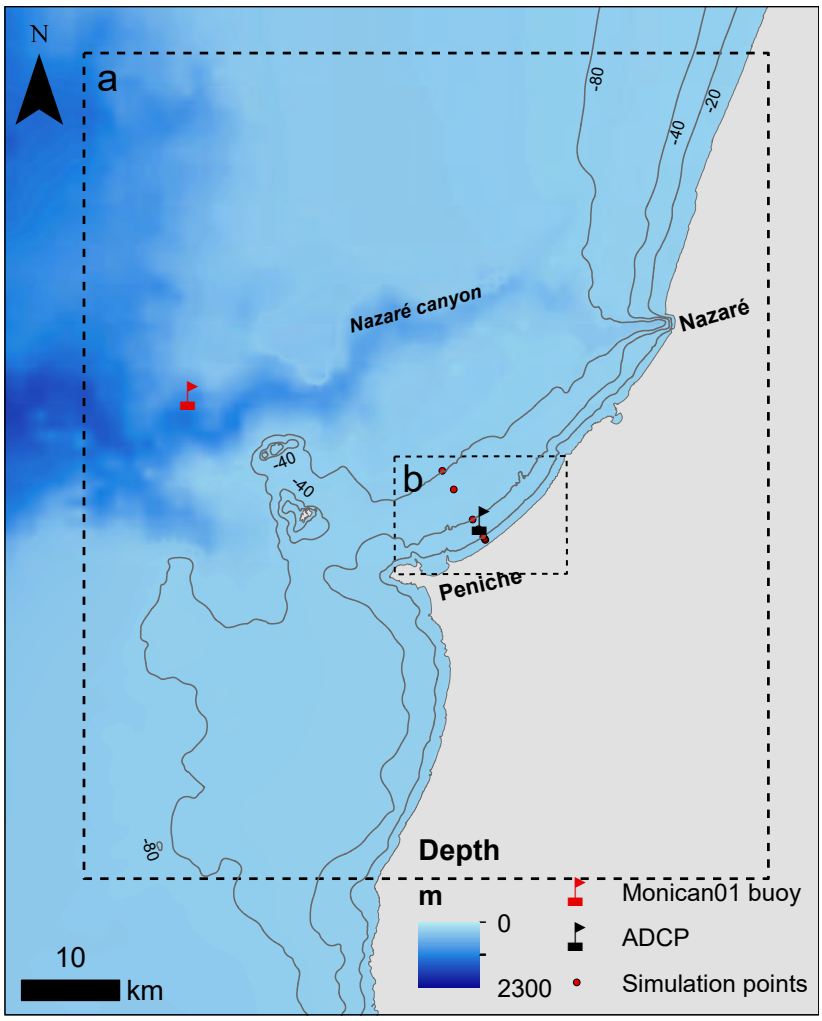

Figure 5.4 SWAN computational grids: a) regional domain (500 m resolution) and b) local domain (100 m resolution). Simulation points are located at 10 m, 15 m, 20 m, 30 m, 40 m, 60 m and 80 m below mean sea level.

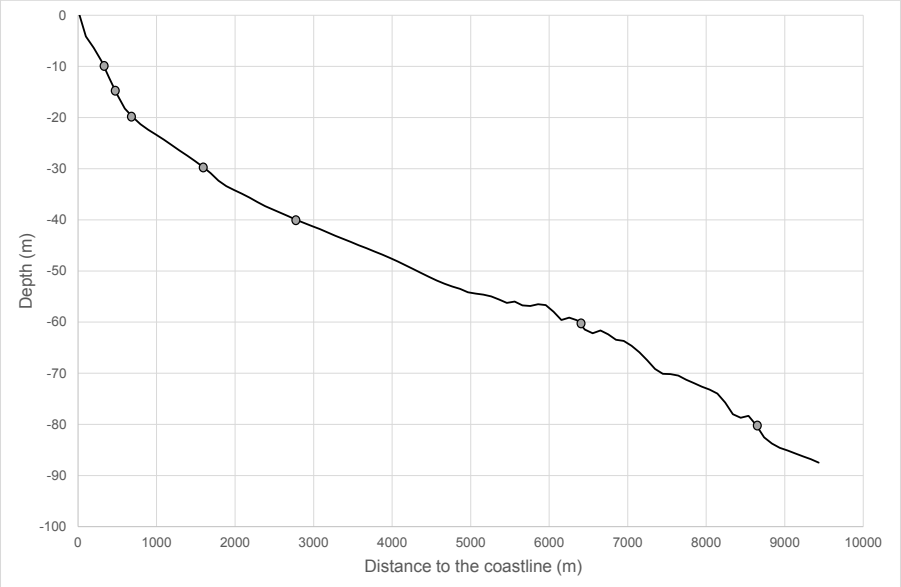

Figure 5.5 Bathymetric profile where grey circles represent simulation points of wave and bottom boundary layer modelling (referred to the MSL).

5.3.2 Wave modelling validation

The significant wave height and zero-crossing period calculated using SWAN propagation model were validated against in situ data measured by the ADCP placed offshore Almagreiro beach (Figure 5.6). Results show an excellent fit between observed and modeled significant wave height with a correlation (r) of 0.92 m. Wave period also present a good correlation (r = 0.76) where the best results are observed during more energetic periods (longer wave periods), when remobilization and transport are more pronounced. Validation statistics shows an excellent behaviour of the modelling strategy where correlation (r) values are very similar or better than those presented on the literature (e.g. Dykes et al., 2002; Hsu et al., 2002; Mazarakis et al., 2012).

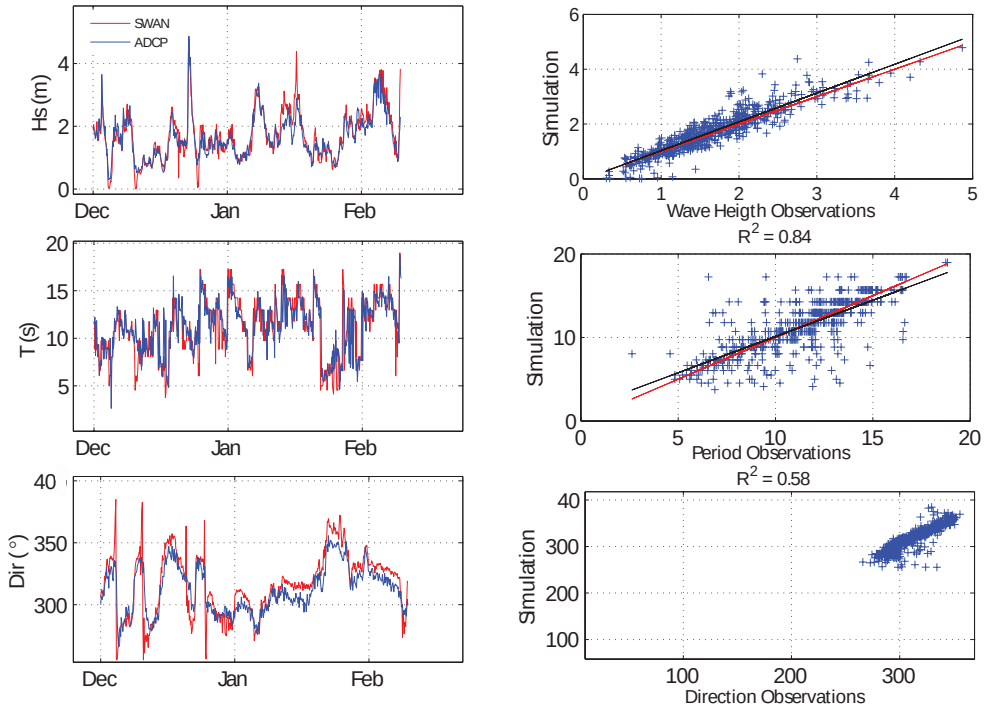

Figure 5.6 Validation results of the wave modelling strategy. Top: wave significant height; middle: wave mean period; bottom: wave mean direction.

5.3.3 Bottom boundary layer modelling

The sedimentary dynamics within the bottom boundary layer was evaluated through the application of the numerical model described in Chapter 3 which calculates sediment remobilization and transport. The model was supported by wave modelling data from SWAN propagation model and nearbed current data from the ADCP moored offshore Almagreiro beach, being the wave-current bottom induced dynamics only calculated when both wave and current data were available.

As on Chapter 4, for a wider comprehension of the nearshore sedimentary dynamics, the potential sediment remobilization and transport are computed for all sand fractions (very coarse to very fine sand) at different depths (10 m, 15 m, 20 m, 30 m, 40 m, 60 m and 80 m below MSL) where an uniform cross-shelf distribution of the current field was assumed. This assumption was supported on data supplied by the 3D global ocean model NEMO[1]

[1]Nucleous for European Modelling of the Ocean: an ocean modelling framework which is composed of 'engines' nested in an 'environment'. The 'engines' provide numerical solutions of ocean, sea-ice, tracers and biochemistry equations and their related physics (Madec, 2012). More information in http://www.nemo-ocean.eu/.

(available at http://marine.copernicus.eu/) that show a small variability of current intensity (<30%) across the cross-shelf profile.

5.4 Results

5.4.1 Oceanographic forcing

5.4.1.1 Currents

Nearbed currents measured offshore Almagreiro beach (ADCP - Figure 5.1) flow more frequently southwestward (≈ 37% of the time) when are observed the strongest magnitudes with an average value of 0.028 m/s. Northeastward currents in turn are observed during about 26% of the time and present an average magnitude of 0.017 m/s. Less frequent currents are those southeast directed (observed during about 14% of the time) with an average intensity of 0.007 m/s, while northwestward currents occur during 22% of the time and present the same average magnitude of northeastward currents (Figure 5.7).

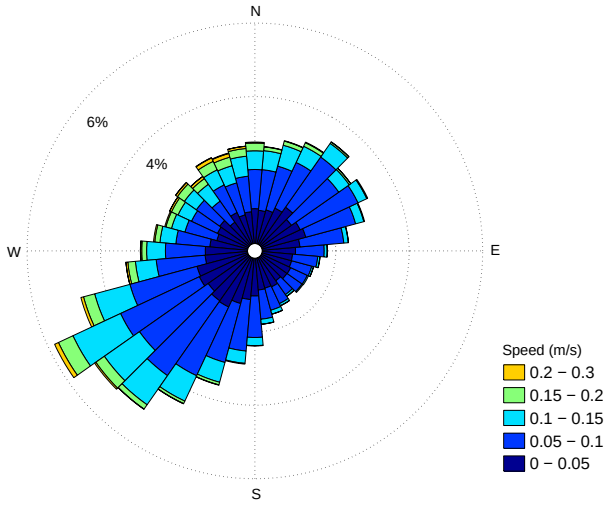

Figure 5.7 Current rose plot. This graph shows the directions in which currents flow to (oceanographic convention).

Nearbed currents are slightly dominated by its alongshelf component which present an average speed of 0.05 m/s while cross-shelf currents present an average speed of 0.04 m/s. Maximum alongshelf magnitudes are of about 0.28 m/s and a similar value is found on the cross-shelf component (0.27 m/s).

Neither the alongshelf nor the cross-shelf current present a clearly dominant direction as southwestward currents are observed during 51 % of the time while onshore currents are observed during about 52% of the time. For the southwestward and northeastward currents the average magnitude are similar, being both of about 0.05 m/s. Also, the onshore and offshore currents have magnitudes of about 0.04 m/s (Figures 5.7 and 5.8). Also, current orientation parallel to the shoreline denotes a bathymetric adjustment.

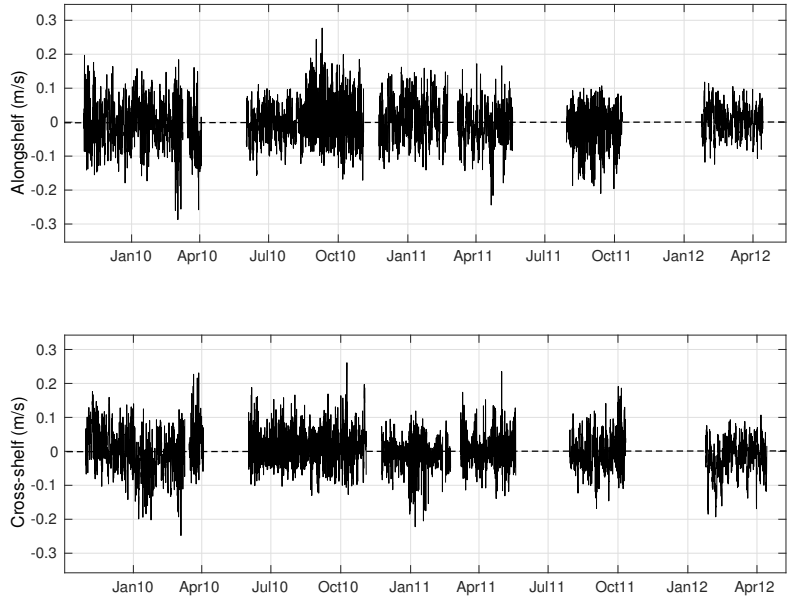

Figure 5.8 Time-series of alongshelf (top) and cross-shelf (bottom) current components from ADCP observations (30 m depth). Negative values correspond to southwestward (alongshelf) and offshore (cross-shelf) flows.

5.4.1.2 Waves

Wave data recorded by the ADCP (see deployment site on Figure 5.1) show a significant wave height (H_s) varying essentially between 1 and 3 m with a standard deviation of 0.87 m and an average value of 1.7 m. The peak period (T_p) ranges mainly between 5 and 20 s presenting an average of 10.6 s. Waves come essentially from northwest being both wave mean direction and wave mean power direction of 325° (Figures 5.9 and 5.10). Wave data registered during the observation period denotes a representative wave regime where statistics are similar to those described by Costa et al. (2001) for the Portugal west coast.

During the observation period it was observed 24 storm events (H_s> 4.5 m during at least 12 hours - Figure 5.10). All storms take place between October and April which are patently the most energetic months as shown in Figure 5.11.

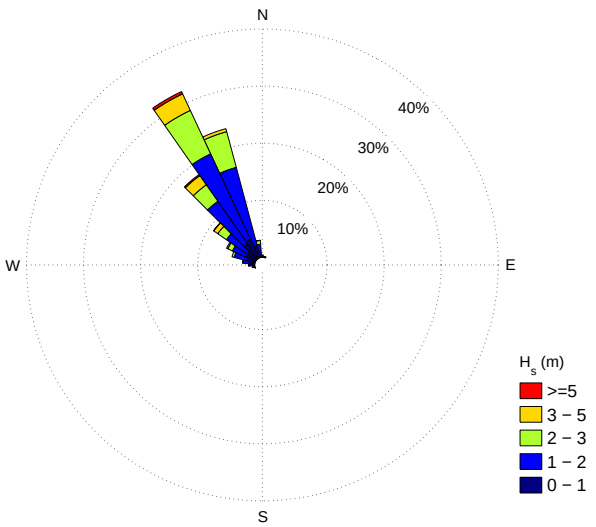

Figure 5.9 Wave rose plot (meteorological convention).

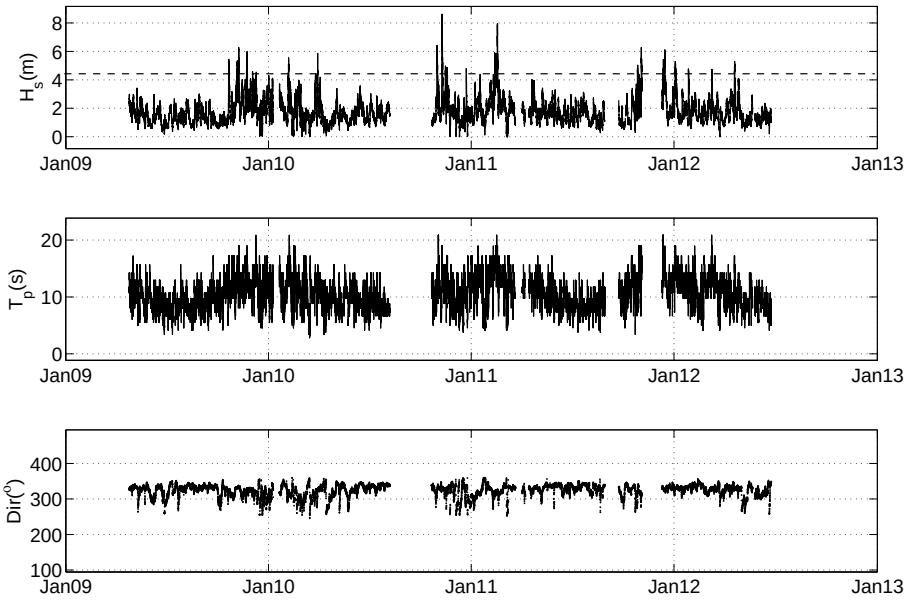

Figure 5.10 Wave regime at 30 m depth. Dashed line at upper graph: storm threshold conditions.

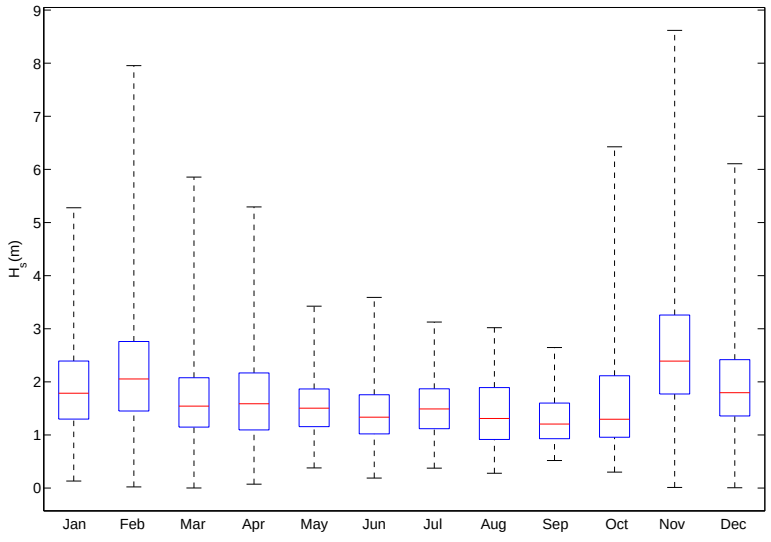

Figure 5.11 Monthly boxplot of the significant wave height (H_s) at ADCP deployment site (30 m depth).

5.4.2 Bottom boundary layer dynamics

Results from three-year bottom boundary layer modelling using ADCP measurements at 30 m depth revealed a clear dominance of wave-alone bottom shear stress. While current-alone induced shear velocities never exceed 1.0 $\times 10^{-2}$ m/s and present an average of 2.3 $\times 10^{-3}$ m/s, the wave-alone shear velocity can reach almost 5.0 $\times 10^{-2}$ m/s, with an average of 1.34 $\times 10^{-2}$ m/s (Figure 5.12). Boundary layer modelling was computed using the median grain size of the in situ sediment (0.18 mm - fine sand).

The maximum combined wave-current shear velocity ranges between 3.0 $\times 10^{-3}$ m/s and 5.4 $\times 10^{-2}$ m/s, with an average of 1.4 $\times 10^{-2}$ m/s. These values are similar to those computed using wave-alone approach, being those obtained through the current-alone approach much lower. Mean combined wave-current shear velocity varies from 1.5 $\times 10^{-4}$ to 1.5 $\times 10^{-2}$ m/s with an average of 4.1 $\times 10^{-3}$ m/s, values that are similar to the current-alone shear velocities.

Figure 5.14 shows that the maximum bed shear velocity in wave-current conditions is very often one order of magnitude greater than current-alone shear velocity, being frequently even 50 times greater. Also, the mean shear velocity under the same conditions is frequently twice or more the value of the current-alone shear velocity (Figure 5.15).

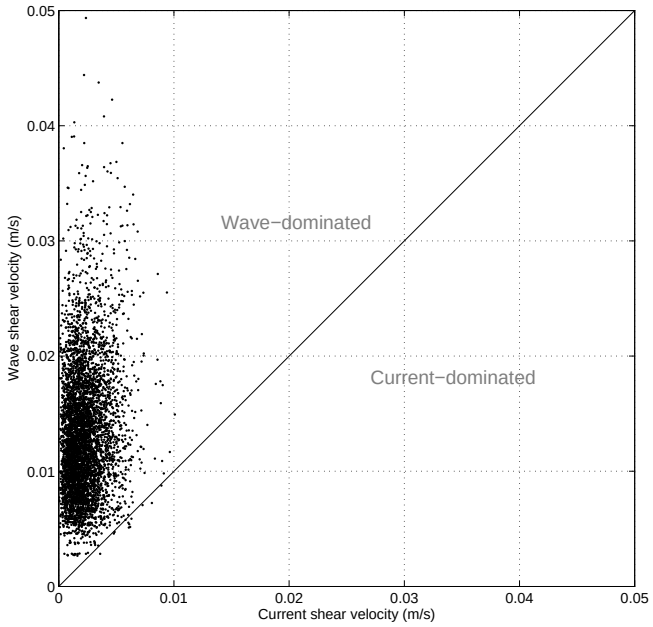

Figure 5.12 Wave-alone versus current-alone bed shear velocity at ADCP site (30 m depth).

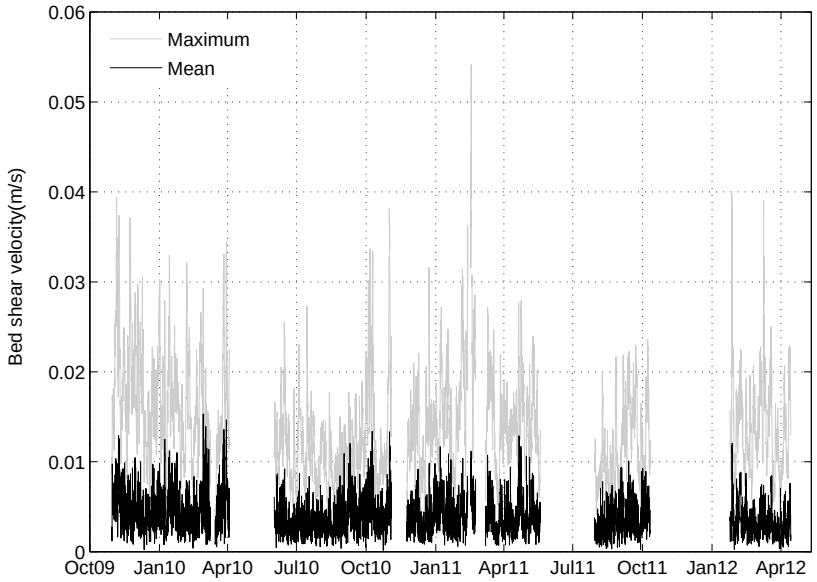

Figure 5.13 Time series of mean and maximum wave-current bed shear velocity for the observation period at ADCP site (30 m depth).

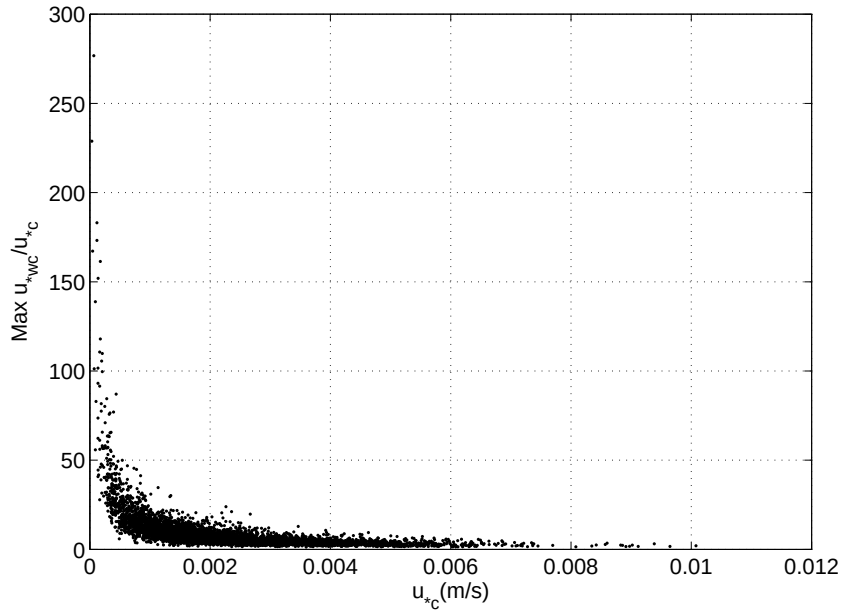

Figure 5.14 Relation between maximum bed shear velocity under combined wave-current conditions (Max u_*wc) and current-alone bed shear velocity (u_*c) at ADCP site (30 m depth).

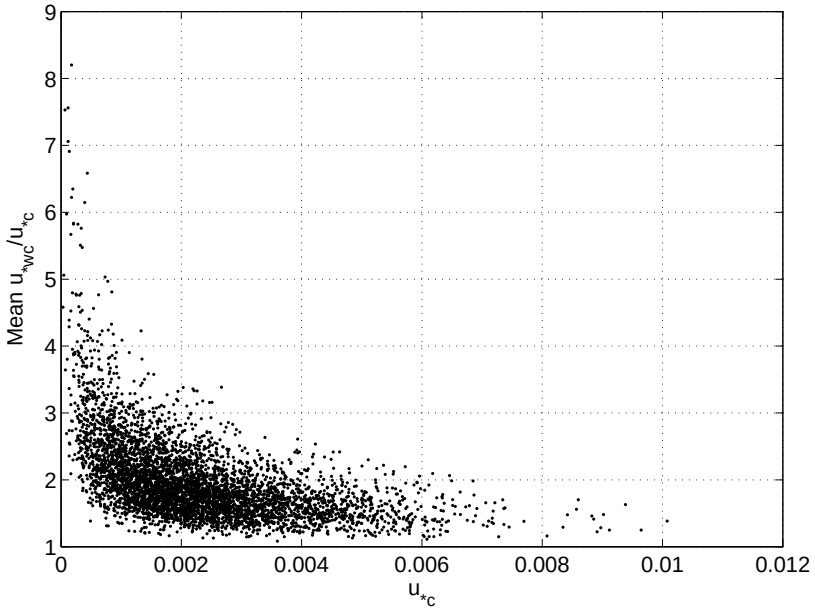

Figure 5.15 Relation between mean bed shear velocity under combined wave-current conditions (Mean u_*wc) and current-alone bed shear velocity (u_*c) at ADCP deployment site (30 m depth).

5.4.2.1 Sediment entrainment

The comparison between maximum wave-current shear velocity and the threshold of motion for the in situ sediment, estimated in 1.2×10^{-2} m/s for fine sand (0.18 mm), shows that bottom sediment is remobilized during about 50 % of the time (Figure 5.16).

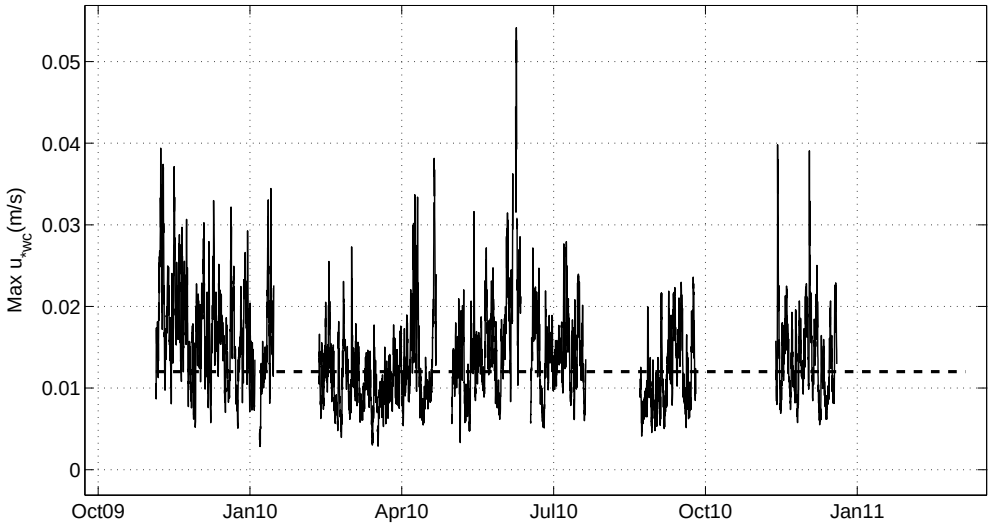

Figure 5.16 Maximum wave-current induced shear velocity (Max u_{*wc}). Dashed line: in situ particle threshold velocity (1.2×10^{-2} m/s) at ADCP site considering fine sand (0.18 mm).

The frequency of sediment remobilization over all the simulation depths are presented on Tables 5.2 to 5.8. Bottom boundary layer modelling shows that currents alone are never able to remobilize any fraction of sand, while waves alone are able to remobilize even very coarse sand at 80 m depth, but only during 0.61% of the time.

There is a clear decrease on sediment remobilization with increasing depth. While medium sand is remobilized during more than 95% of the time at 10 m depth, this frequency does not reach 5% at 80 m for the same sand class. Very coarse sand in turn is remobilized during about 85 % of the time at the shallower simulation point. This frequency of occurrence decrease to 0.69% at the deeper observation point.

The frequency of remobilization clearly increase with decreasing grain size from very coarse to medium sand. However, from medium to very fine sand there is no clear link between remobilization frequency and grain size with depth.

Table 5.2 Frequency of remobilization for sand fractions at 10 m depth under the action current- and wave-alone and mean and maximum wave-current bed shear velocity.

Grain size		Frequency of remobilization (% of time)			
Sand class	ϕ scale	Current alone	Wave-current mean	Wave alone	Wave-current maximum
Very coarse	-0.5	0	0	84.50	85.19
Coarse	0.5	0	0.51	94.04	94.40
Medium	1.5	0	2.51	95.35	95.88
Fine	2.5	0	4.10	94.89	95.63
Very fine	3.5	0	5.08	94.73	95.35

Table 5.3 Frequency of remobilization for sand fractions at 15 m depth under the action current- and wave-alone and mean and maximum wave-current bed shear velocity.

Grain size		Frequency of remobilization (% of time)			
Sand class	ϕ scale	Current alone	Wave-current mean	Wave alone	Wave-current maximum
Very coarse	-0.5	0	0	67.27	68.52
Coarse	0.5	0	0.15	84.66	85.66
Medium	1.5	0	1.30	88.90	90.28
Fine	2.5	0	2.22	87.39	89.34
Very fine	3.5	0	2.81	87.73	89.44

Table 5.4 Frequency of remobilization for sand fractions at 20 m depth under the action current- and wave-alone and mean and maximum wave-current bed shear velocity.

Grain size		Frequency of remobilization (% of time)			
Sand class	ϕ scale	Current alone	Wave-current mean	Wave alone	Wave-current maximum
Very coarse	-0.5	0	0	52.24	53.49
Coarse	0.5	0	0.05	72.67	74.10
Medium	1.5	0	0.74	78.67	80.95
Fine	2.5	0	1.35	76.32	78.83
Very fine	3.5	0	1.8	77.83	80.29

Table 5.5 Frequency of remobilization for sand fractions at 30 m depth under the action current- and wave-alone and mean and maximum wave-current bed shear velocity.

Grain size		Frequency of remobilization (% of time)			
Sand class	ϕ scale	Current alone	Wave-current mean	Wave alone	Wave-current maximum
Very coarse	-0.5	0	0	20.05	21.38
Coarse	0.5	0	0	40.55	43.52
Medium	1.5	0	0.15	48.96	52.26
Fine	2.5	0	0.43	45.99	50.17
Very fine	3.5	0	0.66	49.88	53.16

Table 5.6 Frequency of remobilization for sand fractions at 40 m depth under the action current- and wave-alone and mean and maximum wave-current bed shear velocity.

Grain size		Frequency of remobilization (% of time)			
Sand class	ϕ scale	Current alone	Wave-current mean	Wave alone	Wave-current maximum
Very coarse	-0.5	0	0	10.23	11.38
Coarse	0.5	0	0	24.80	27.38
Medium	1.5	0	0.05	32.60	36.10
Fine	2.5	0	0.18	29.48	34.11
Very fine	3.5	0	0.41	34.39	38.25

Table 5.7 Frequency of remobilization for sand fractions at 60 m depth under the action current- and wave-alone and mean and maximum wave-current bed shear velocity.

Grain size		Frequency of remobilization (% of time)			
Sand class	ϕ scale	Current alone	Wave-current mean	Wave alone	Wave-current maximum
Very coarse	-0.5	0	0	2.30	2.53
Coarse	0.5	0	0	6.34	7.88
Medium	1.5	0	0	9.90	12.48
Fine	2.5	0	0.08	8.36	11.92
Very fine	3.5	0	0.08	11.90	14.56

Table 5.8 Frequency of remobilization for sand fractions at 80 m depth under the action current- and wave-alone and mean and maximum wave-current bed shear velocity.

Grain size		Frequency of remobilization (% of time)			
Sand class	ϕ scale	Current alone	Wave-current mean	Wave alone	Wave-current maximum
Very coarse	-0.5	0	0	0.61	0.69
Coarse	0.5	0	0	2.38	2.79
Medium	1.5	0	0	3.30	4.22
Fine	2.5	0	0	2.92	3.92
Very fine	3.5	0	0.05	4.07	5.94

5.4.2.2 Bedforms

The wave-generated bedforms predicted by the model (Equations 3.22 and 3.21 in Chapter 3) are described in terms of wavelength (λ) and height (η) for the same water depths and classes addressed in the last section. Figures 5.17 and 5.18 show the time-averaged bedform wavelength and height, respectively. Both parameters have a similar behaviour and show a clear increase with sediment grain size.

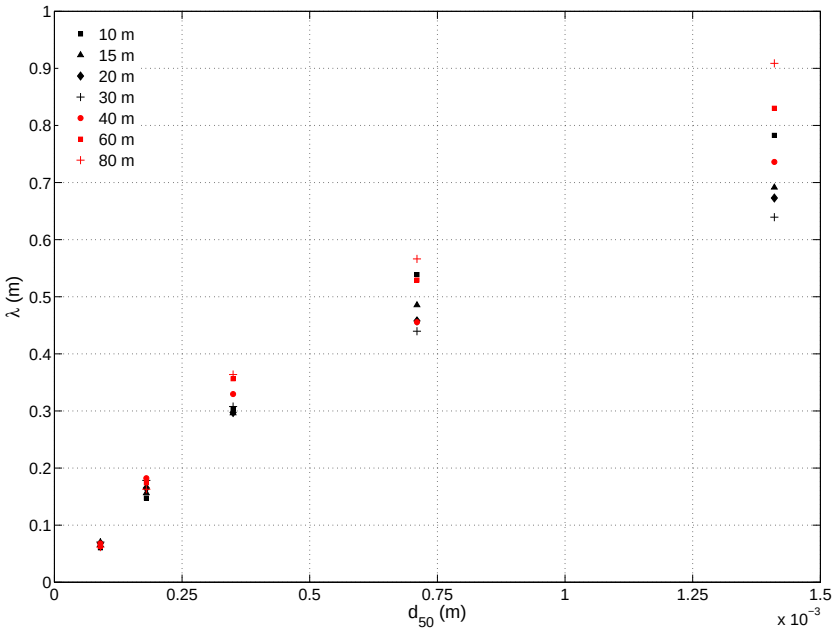

Figure 5.17 Variation of the predicted time-averaged bedform wavelength (λ) according to water depth and sediment median grain size (d_{50}).

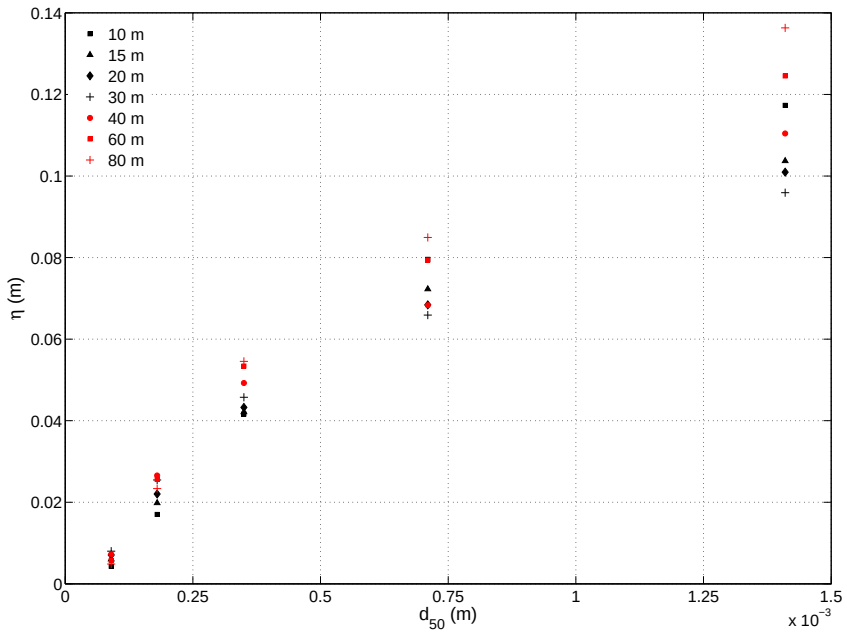

Figure 5.18 Variation of the predicted time-averaged bedform height (η) according to water depth and sediment median grain size (d_{50}).

While bedform wavelength is smaller than 0.1 m for very fine sand at all depths, this parameter for very coarse sand can vary from about 0.6 and 0.9 m according to depth. Also, the bedform height for the finest grain size is lower than 0.01 for all water depths and ranges essentially between 0.1 and 0.14 m for very coarse sand (Figures 5.17 and 5.18).

The expected time evolution, during the observation period, of the bedform geometry at 30 m depth is described on Figures 5.19 (λ) and 5.20 (η) for the 5 sand fractions (very fine to very coarse). The bedform wavelength ranges mainly between 0.1 and 0.8 m, being higher than 0.8 m only for very coarse sand. Values regarding the bedform height can be close to zero for very fine sand and higher than 0.16 m for very coarse sand.

While the time-evolution of medium to very coarse sand bedforms behave nearly synchronized, fine and very fine bedforms decrease during peaks of wavelength and heigh of the other sand classes (coarser). These results are probably related to washout events occurring during more energetic periods.

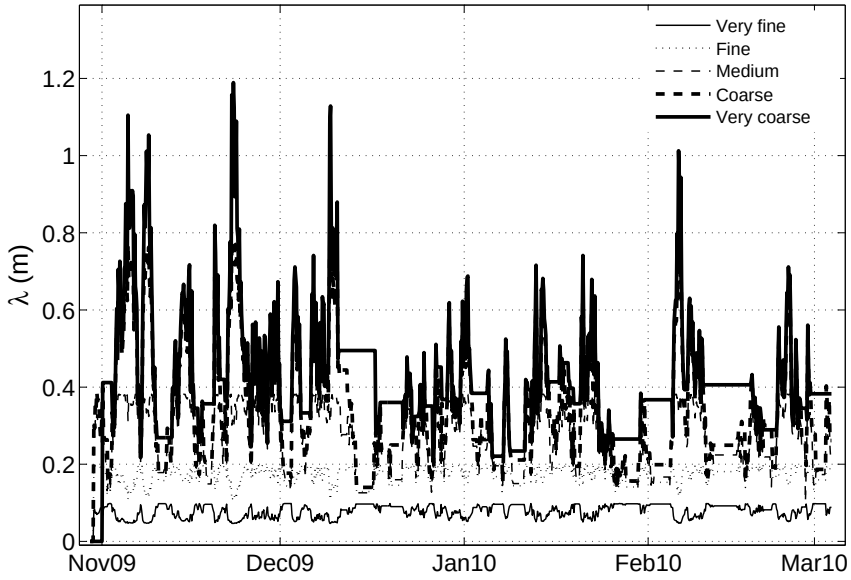

Figure 5.19 Time evolution of predicted bedform wavelength for the five sand fractions at 30 m depth.

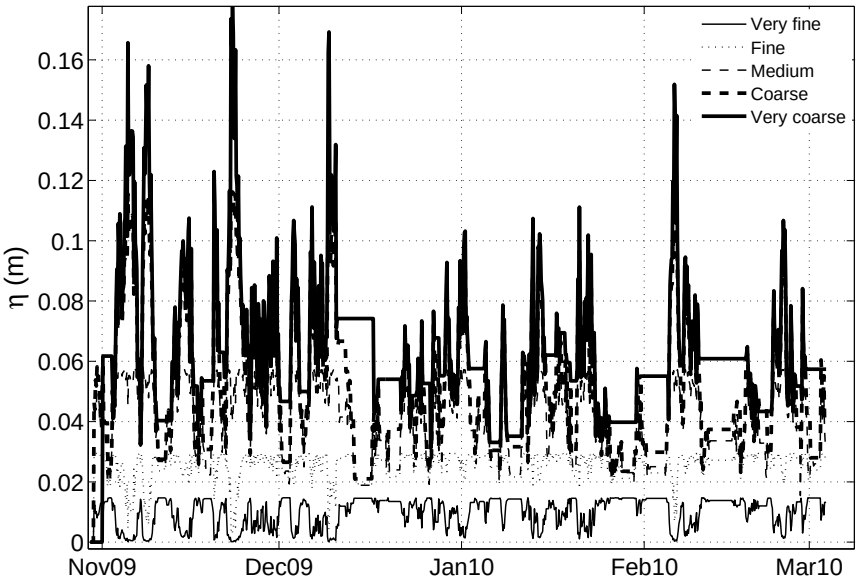

Figure 5.20 Time evolution of predicted bedform height for the five sand fractions at 30 m depth.

5.4.2.3 Sediment transport

The evaluation of the sediment transport along a transect from 10 m down to 80 m depth offshore Almagreiro beach is described in terms of suspended load and bedload. Attention must be given to the fact that sediment transport was only computed for the periods where both wave and current data were simultaneously available. Also, as referred on Chapter 4, results regarding the direction of the cross-shelf transport must be analysed with caution as the modelling approach has no parametrizations for computing wave asymmetry and streaming effect. According to several authors (Aagaard, 2014; Holmedal et al., 2015; Kranenburg et al., 2013), oscillatory wave motions and potentially streaming in the wave boundary layer can accomplish the onshore transport, which means that the present model is unable to properly predict the direction of cross-shelf sediment transport.

5.4.2.3.1 Suspended load

The frequency of sediment suspension, i.e., the percentage of time where the maximum bed shear velocity is higher than the sediment particle fall velocity, is presented in Table 5.9. According to numerical modelling estimations, very coarse sand never get into suspension at any simulation depth, while coarse sand becomes part of the suspended load only at 10 m depth. Medium sand in turn is suspended down to 30 m depth, while fine to very fine sand can be part of the suspended sediment at all simulation depths. However, while very fine sand is suspended during about 40% of the time at 80 m depth, fine sand is suspended only during 0.33% of the time at the same water depth. Obviously, the frequency of sediment suspension decrease with increasing depth for all sand fractions. Still, bottom wave-current conditions are able to put very fine sand into suspension more than 80% of the time down to 40 m depth.

Table 5.9 Frequency of sediment suspension (% of time) along the water depth.

Sand class	ϕ scale	Water depth (m)						
		10	15	20	30	40	60	80
Very coarse	-0.5	0	0	0	0	0	0	0
Coarse	0.5	0.05	0	0	0	0	0	0
Medium	1.5	7.87	2.17	0.84	0.05	0	0	0
Fine	2.5	75.81	56.05	40.14	13.78	6.55	1.61	0.33
Very fine	3.5	98.47	98.36	97.52	91.02	83.07	58.66	40.89

Results of the suspended load transport over time at 30 m depth are shown on Figures 5.21 and 5.22 in the alongshelf and cross-shelf directions, respectively. Very fine and fine sand are mostly transported southwestward and offshore. In the alongshelf direction transport rate magnitudes exceed 1.0×10^{-4} m^2/s for very fine sand and does not reach 2×10^{-5} m^2/s for fine sand. On the other hand, the most significant sediment transport event for medium sand is northeastward directed which does not reach 2×10^{-5} m^2/s.

Cross-shelf suspended load transport is mostly offshore directed with rates exceeding 1.2×10^{-4} m^2/s for very fine sand while for fine sand transport magnitudes barely reach 1.0×10^{-5} m^2/s (Figure 5.22).

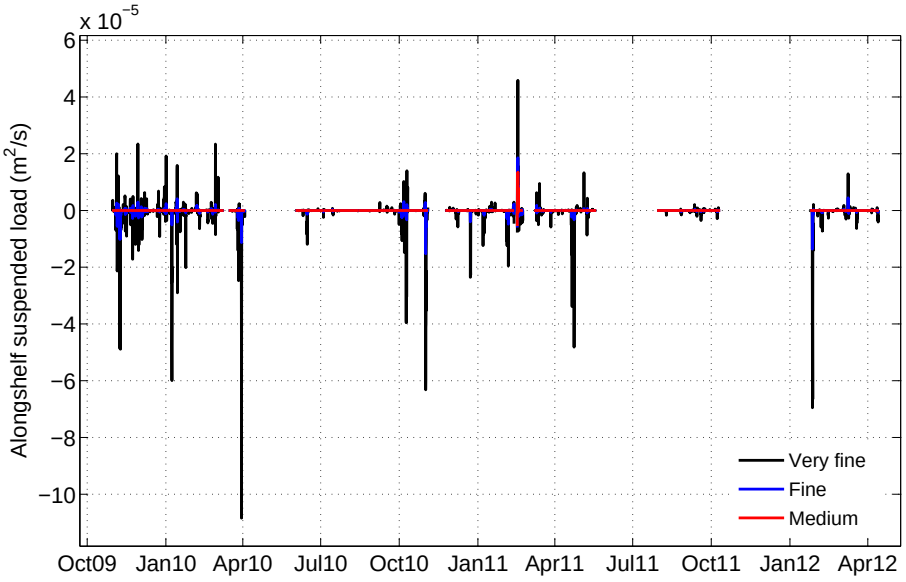

Figure 5.21 Potential alongshelf suspended load transport at 30 m depth. Negative values: southwestward.

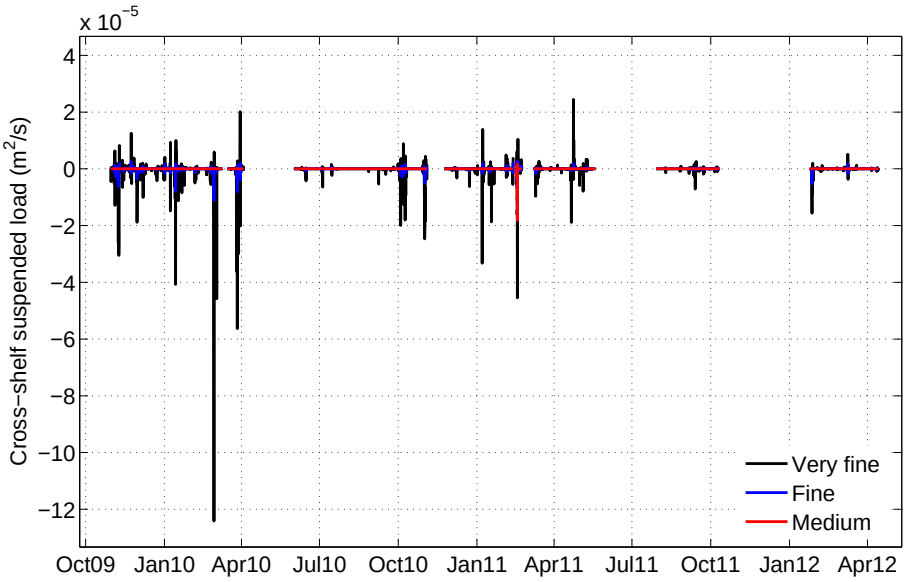

Figure 5.22 Potential cross-shelf suspended load transport at 30 m depth. Negative values: offshore.

The annual suspended load transport for each sand fraction along the water depth is presented for the alongshelf and cross-shelf directions where magnitudes (Tables 5.10 and 5.12) and net transport (Tables 5.11 and 5.13) are described. Results show that both net transport and magnitudes are almost always higher in the alongshelf direction. For example, at 30 m depth, the magnitude of the suspended load transport for fine sand are of about 0.78 m^2/year in the alongshelf direction and around 0.45 m^2/year in the cross-shelf direction. Net transport for the same conditions are of 0.37 m^2/year southwestward and 0.21 m^2/year offshore. An exception is observed for the transport as suspended load of medium sand at 30 m depth where the cross-shelf transport (0.02 m^2/year) is higher than the alongshelf one (0.01 m^2/year).

Very coarse sand are never transported into supension at any simulated depth, while very fine sand can be transported at all depths. Also, for both directions, suspended load transport decreases with depth and with increasing grain size.

The magnitude of the alongshelf suspended load transport vary between 0.01 m^2/year for medium sand at 30 m depth and 307 m^2/year for very fine sand at 10 m depth. Net transport estimations are within 0.1 m^2/year northeastward and 161 m^2/year southwestward for the same conditions, respectively.

Table 5.10 Magnitude of potential suspended load transport in the alongshelf direction (m^2/year).

Sand class	ϕ scale	Water depth (m)						
		10	15	20	30	40	60	80
Very coarse	-0.5	0	0	0	0	0	0	0
Coarse	0.5	0.63	0	0	0	0	0	0
Medium	1.5	9.60	2.03	0.58	0.01	0	0	0
Fine	2.5	26.16	9.54	4.28	0.78	0.27	0.03	0.004
Very fine	3.5	307.40	117.07	53.37	10.32	3.90	0.54	0.13

Table 5.11 Potential net suspended load transport in the alongshelf direction (m^2/year).

Sand class	ϕ scale	Water depth (m)						
		10	15	20	30	40	60	80
Very coarse	-0.5	0	0	0	0	0	0	0
Coarse	0.5	0.6	0	0	0	0	0	0
Medium	1.5	-4.7	-0.83	-0.12	0.01	0	0	0
Fine	2.5	-11.90	-4.13	-1.81	-0.37	-0.13	-0.02	-0.72e-3
Very fine	3.5	-161.32	-59.01	-25.76	-5.12	-1.89	-0.24	-0.07

Results regarding the annual sediment transport rate as suspended load in the cross-shelf direction has magnitudes up to about 165.13 m^2/year. Values of net cross-shelf transport in Table 5.13 show a clear dominance of offshore directed transport for all grain sizes at all depths, varying between 0.01 m^2/year for fine sand at 60 m depth up to 75.65 m^2/year for very fine sand at 10 m depth.

Table 5.12 Magnitude of potential suspended load transport in the cross-shelf direction (m^2/year).

Sand class	ϕ scale	Water depth (m).						
		10	15	20	30	40	60	80
Very coarse	-0.5	0	0	0	0	0	0	0
Coarse	0.5	0.79	0	0	0	0	0	0
Medium	1.5	5.25	1.15	0.36	0.02	0	0	0
Fine	2.5	14.93	5.63	2.58	0.45	0.15	0.02	0.002
Very fine	3.5	165.13	63.50	29.39	5.88	2.30	0.31	0.07

Table 5.13 Potential net suspended load transport in the cross-shelf direction (m^2/year).

Sand class	ϕ scale	Water depth (m)						
		10	15	20	30	40	60	80
Very coarse	-0.5	0	0	0	0	0	0	0
Coarse	0.5	-0.83	0	0	0	0	0	0
Medium	1.5	-2.42	-0.74	-0.27	-0.02	0	0	0
Fine	2.5	-6.12	-2.52	-1.16	-0.21	-0.09	-0.01	-0.002
Very fine	3.5	-75.65	-31.98	-15.56	-3.47	-1.32	-0.18	-0.04

5.4.2.3.2 Bed load

Estimated potential bedload net transport rates at 30 m depth time-series are presented on Figures 5.23 and 5.24, for alongshelf and cross-shelf directions, respectively. As in the suspended load transport, the alongshelf component has higher bedload transport rates but on the same order of magnitude of the cross-shelf component. Also, transport rates tend to increase with sediment grain size. This apparently anomalous behaviour, also observed on modelling results on Chapter 4, is explained by the strong dependence relationship between the sediment volumetric transport rate and the sediment particle volume (see Equations 3.25 to 3.28 in Chapter 3).

The alongshelf bedload transport is mostly southwestward, however significant sediment transport events are also observed in the northeast direction for all sand grain sizes and could exceed 3.0×10^{-5} m^2/s (coarse sand) at 30 m depth (Figure 5.23). Cross-shelf transport in

turn is predominantly offshore and can also have rates higher than 3.0 $\times 10^{-5}$ m^2/s in this direction, while onshore transport rates are lower, exceeding 1.0 $\times 10^{-5}$ m^2/s only once.

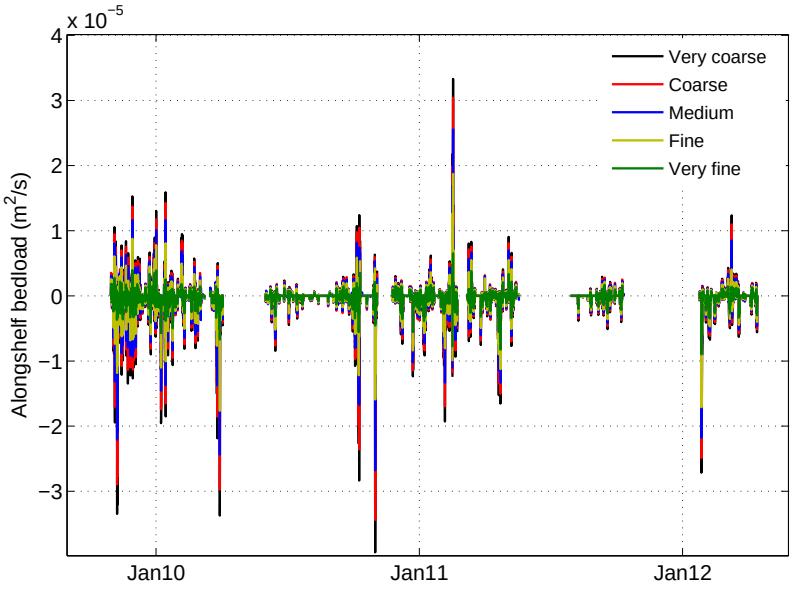

Figure 5.23 Potential alongshelf bedload transport at ADCP mooring site (30 m depth). Negative values represent a southwestward transport.

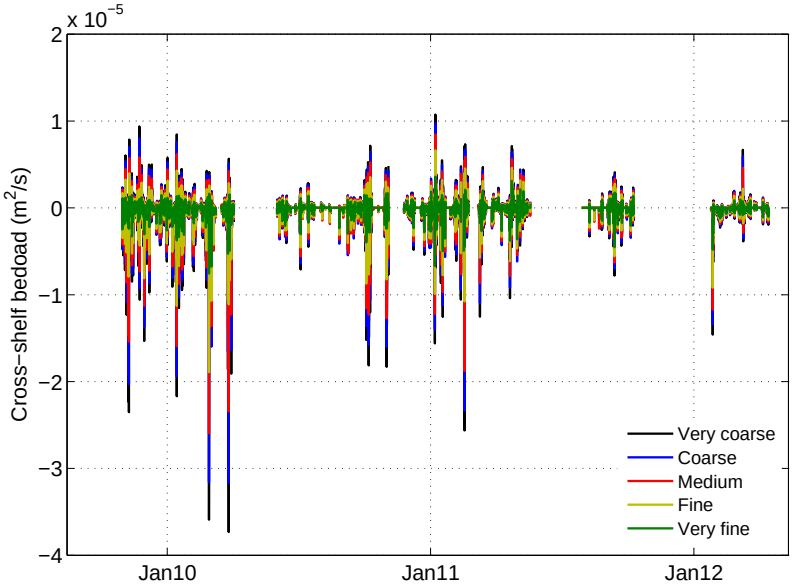

Figure 5.24 Potential cross-shelf bedload transport at ADCP mooring site (30 m depth). Negative values represent an offshore transport.

The annual bedload transport rate is presented for each sand fraction along the water depth in the alongshelf (Tables 5.14 and 5.15) and cross-shelf (Tables 5.16 and 5.17) directions. The magnitude of the bedload transport increases with the sediment grain size at water depths of 10 m, 15 m and 20 m. At greater depths, bedload transport decreases from coarse to very coarse sand. This behaviour is observed in the alongshelf and cross-shelf directions for both transport magnitude (Tables 5.14 and 5.16) and net transport (Tables 5.17 and 5.15).

Magnitude of the potential bedload transport in the alongshelf direction ranges from 0.77 m^2/year (very fine at 80 m depth) up to 286.78 m^2/year (very coarse at 10 m depth), while net transport rates are southwestward within 0.21 m^2/year (very coarse sand at 80 m depth) and 130.45 m^2/year (very coarse sand at 10 m depth).

Table 5.14 Magnitude of potential bedload transport in the alongshelf direction (m^2/year).

Sand class	ϕ scale	Water depth (m)						
		10	15	20	30	40	60	80
Very coarse	-0.5	286.78	173.02	115.15	41.49	21.35	4.39	0.94
Coarse	0.5	219.38	143.24	101.70	45.42	26.66	7.12	2.33
Medium	1.5	127.35	92.91	70.74	35.87	22.76	7.15	2.41
Fine	2.5	62.66	47.91	38.26	20.99	13.54	4.16	1.40
Very fine	3.5	35.49	24.62	18.62	9.95	6.63	2.35	0.77

Table 5.15 Potential net bedload transport in the alongshelf direction (m^2/year). Negative: southwestward.

Sand class	ϕ scale	Water depth (m)						
		10	15	20	30	40	60	80
Very coarse	-0.5	-130.45	-80.44	-54.96	-21.83	-11.28	-1.94	-0.21
Coarse	0.5	-97.28	-64.53	-46.62	-21.92	-13.49	-3.71	-1.02
Medium	1.5	-52.66	-39.45	-31.06	-16.87	-11.20	-3.78	-1.23
Fine	2.5	-25.05	-19.27	-16.03	-9.51	-6.62	-2.37	-0.71
Very fine	3.5	-14.95	-10.23	-7.89	-4.38	-3.13	-1.13	-0.42

The magnitude of annual cross-shelf sediment transport rates vary between 0.44 (very fine sand at 80 m depth) and 184.48 m^2/year (very coarse sand at 10 m depth), while net transport for the same conditions is between 0.26 and 77.57 m^2/year, respectively. All simulations result into an offshore net transport (Tables 5.16 and 5.17).

Table 5.16 Magnitude of potential bedload transport in the cross-shelf direction (m^2/year).

Sand class	ϕ scale	Water depth (m)						
		10	15	20	30	40	60	80
Very coarse	-0.5	184.48	110.31	72.51	24.83	12.48	2.47	0.68
Coarse	0.5	143.07	92.75	65.43	28.39	16.26	4.20	1.35
Medium	1.5	85.07	61.51	46.40	22.66	14.28	4.14	1.36
Fine	2.5	42.24	32.07	25.49	13.43	8.52	2.44	0.77
Very fine	3.5	23.59	16.29	12.32	6.43	4.30	1.41	0.44

Table 5.17 Potential net bedload transport in the cross-shelf direction (m^2/year). Negative values: offshore.

Sand class	ϕ scale	Water depth (m)						
		10	15	20	30	40	60	80
Very coarse	-0.5	-77.57	-47.76	-32.17	-11.94	-6.69	-1.55	-0.39
Coarse	0.5	-57.62	-38.52	-27.65	-12.95	-7.55	-2.36	-0.82
Medium	1.5	-32.42	-23.95	-18.55	-9.79	-6.44	-2.15	-0.85
Fine	2.5	-16.24	-12.34	-9.90	-5.52	-3.65	-1.29	-0.47
Very fine	3.5	-9.48	-6.56	-5.00	-2.79	-1.87	-0.69	-0.26

5.5 Discussion

5.5.1 Sediment transport dynamics

Bottom boundary layer results show that current-alone forcing is never able to remobilize any sand fraction at any water depth (starting at 10 m depth), being the waves the only mechanism able to remobilize bottom sediments and made them available for transportation. The relative importance of waves and currents on this dynamics is marked by a clear decrease on the relative importance of waves with depth (Figure 5.25). However, even at 80 m depth waves still plays the major role on bottom sedimentary dynamics.

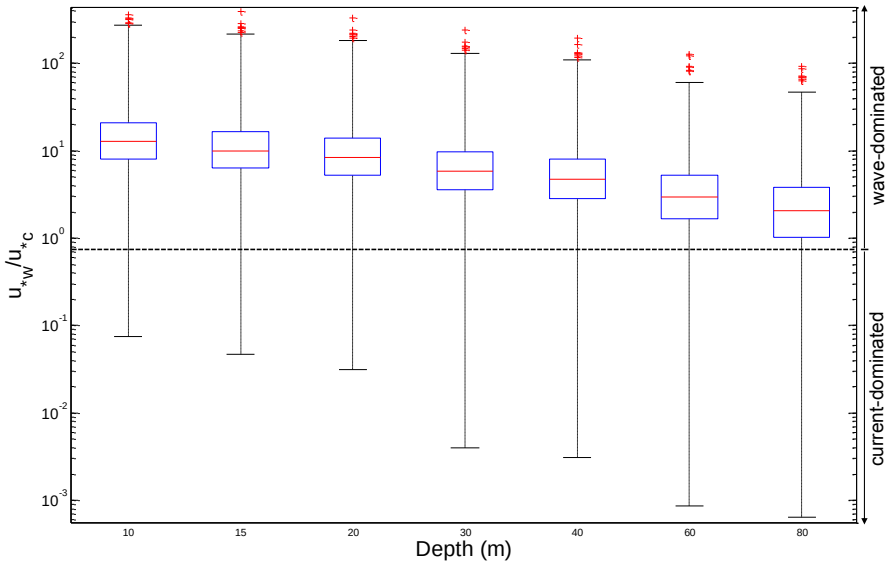

Figure 5.25 Ratio between wave (u_{*w}) and current (u_{*c}) induced bottom shear velocities along the water depth.

Sediment transport modelling results show that the bedload is the dominant mode of transport for almost all conditions while the suspended load transport only dominates for very fine sand at depths shallower than 30 m (Figure 5.26).

There is a clear decrease on the magnitude of suspended load transport with increasing particle diameter, while the bedload transport increase with sediment grain size from very fine to coarse sand at all depths. Seaward 20 m depth, the bedload transport decrease from coarse to very coarse sand. This apparently anomalous behaviour was also observed by Taborda (1999) and it is explained by the dependence relationship between the bedload transport rate and the particle diameter (see Equations 3.25 to 3.28 in Chapter 3).

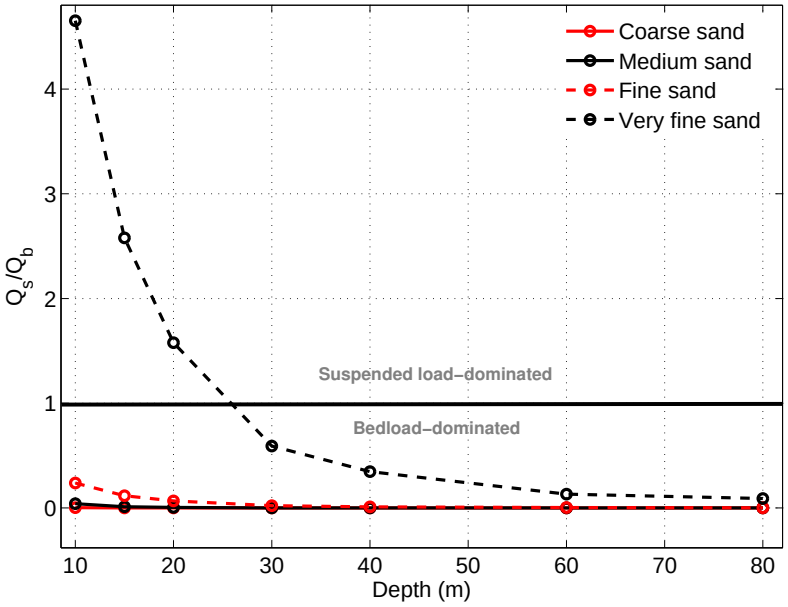

Figure 5.26 Ratio between potential magnitudes (yearly rates) of suspended (Q_s) and bedload (Q_b) according to depth for different sand fractions (coarse to very fine).

The relation between sedimentary dynamics and oceanographic forcing conditions are herein presented, under a probabilistic approach, for total sediment transport predictions (bedload and suspended load) made at 30 m depth considering fine sand. Under these conditions, nearbed current pattern that characterizes above particle threshold conditions is very similar to the current pattern observed during the entire monitoring period (Figure 5.27), having both a net southwestward.

Most favourable oceanographic conditions for sediment transport regarding wave and current directions are represented by waves coming from NW and by southwestward currents, while northwestward currents have a smaller contribution (Figure 5.28). Also, contributions (in parts per thousand) made by each combination of wave (represented by nearbed orbital velocities) and current (represented by the nearbed speed) are shown. It is seen that larger contributions are made by nearbed currents with speed lying between 0.05 and 0.15 m/s in combination with waves with nearbed orbital velocities u_w between 0.2 and 0.3 m/s (Figure 5.29).

Contributions made by specific wave conditions, represented by pairs of H_s and T_p, to the sediment transport are shown on Figure 5.30. In this graph, results show that larger contributions (>8 ppt) are made by waves in the range of $1.5<H_s<3.0$ m and Tp of around 12 s.

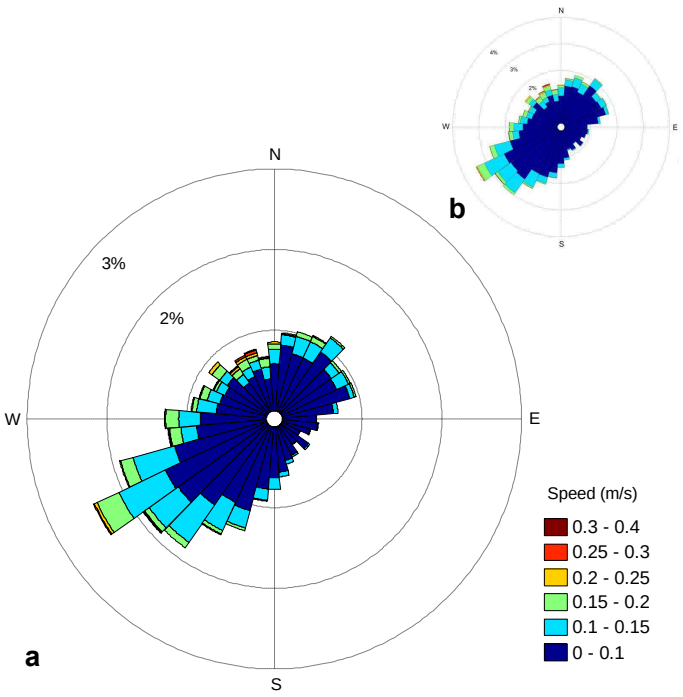

Figure 5.27 Nearbed current rose for the entire period of observation (b) and only for the period considering above particle threshold conditions (a) for fine sand.

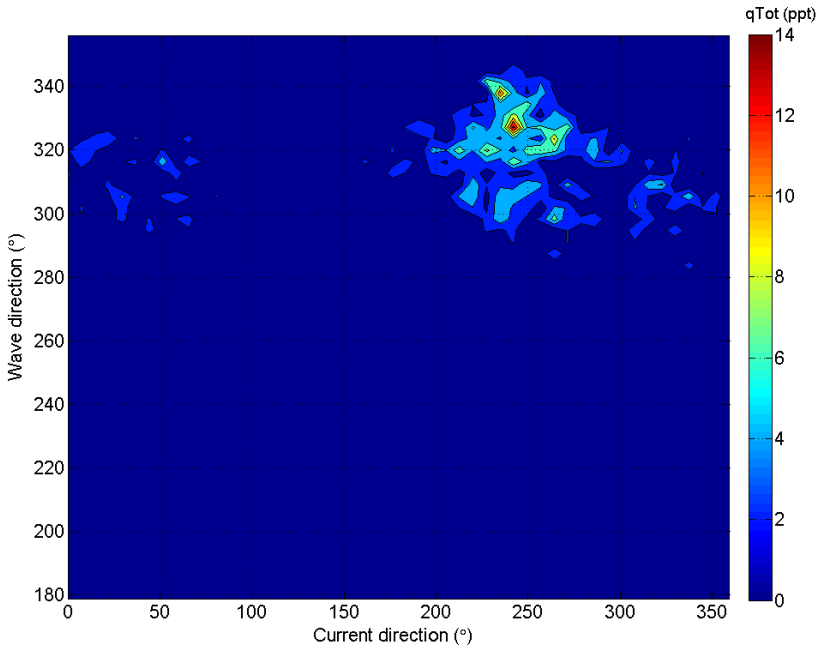

Figure 5.28 Contribution in part per thousand (ppt) made by wave and current direction combinations to the total sediment transport for fine sand at ADCP site (30 m depth).

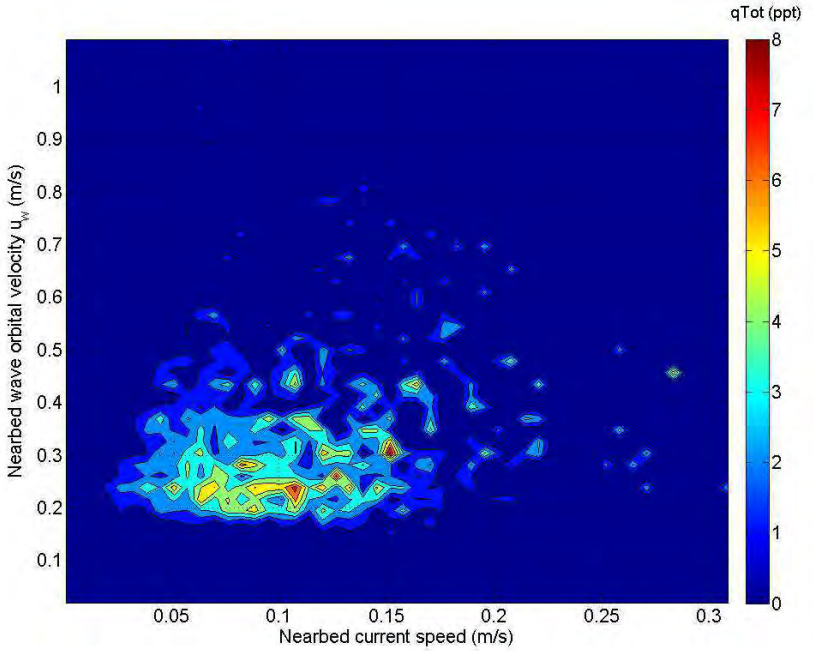

Figure 5.29 Contribution in part per thousand (ppt) made by wave nearbed orbital velocity and current speed combinations to the total sediment transport for fine sand at ADCP site (30 m depth).

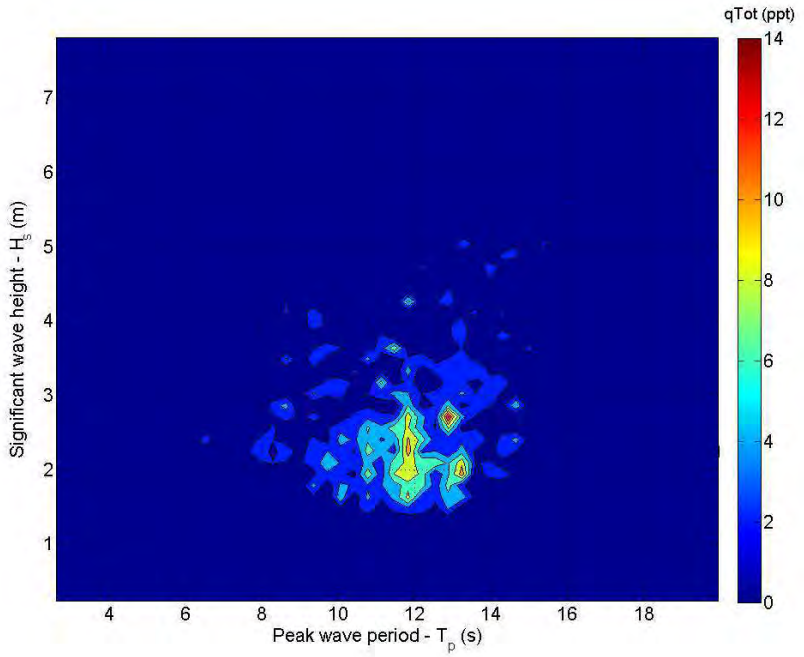

Figure 5.30 Contribution in part per thousand (ppt) made by wave significant height and peak period combinations to the total sediment transport for fine sand at ADCP site (30 m depth).

5.5.2 Conceptual sediment dynamic model

Based on the same approach carried out on Chapter 4, a conceptual sediment dynamic model is described in this section where the nearshore zone can be classified in four sector which depth boundaries are defined based on morphological and sedimentologcal criteria. The water depth limits are obviously approximated and boundaries should be considered gradual. Also, the analysis and interpretation of sedimentological data, oceanographic forcing and bottom boundary layer dynamics allow an integrated analysis of the sedimentary dynamics within each sector.

Sector A: from 0 to 15 m depth

This area lies between the low water level and the depth of closure where sediments are represented by medium sand with low content of calcium carbonate (<1%). Bottom dynamics is marked by very frequent sediment remobilization and sediment transport events that translate into measurable morphological changes. Suspended load dominates only for very fine sand, but can occur even for the coarse fraction. Local conditions enable a nearly permanent suspension of fine sand, while medium sand rarely gets into suspension (<8% of the time). Sediment transport is thus dominated by the bedload mode where the alongshelf transport, with a southwestward net , is approximattely twice the magnitude of the cross-shelf component, marked by a potential offshore net transport.

Sector B: from 15 to 30 m depth

Sea bottom is covered by littoral deposits represented by fine sand that gradually turn into coarser sand (offshore limit). Bottom morphology is marked by a break in the slope at approximately 20 m depth where it is observed a transition to a smooth bottom. Sediment remobilization is still significant, but with a much lower frequency than in sector A. This zone is also dominated by the bedload mode of transport with a predominance of the alongshelf component with a net southwestward. Suspended load dominates only for very fine sand but can occur also for fine and medium sand. Wave-current bottom induced dynamics put very fine sand into suspension during more than 90% of the time, while medium sand become part of the suspended load during at maximum 8 days a year. Suspended load net transport is southwestward for fine and very fine sand, being medium sand transported northeastward.

Sector C: from 30 to 80 m depth

Bottom sediments at this sector are marked by coarse and very coarse sand which extend down to an abrupt contact with muddy sediments (offshore limit). Sediment remobilization

still frequent, specially for very fine to medium sand down to 40 m depth, seaward this depth remobilization events become more unusual. The bedload transport dominates for all sand fractions, but sediment suspension still occur for very fine and fine sand. Net transport is southwestward and offshore directed for both modes of transport with a predominance of the alongshelf component.

Sector D: offshore 80 m depth

Bottom sedimentary cover is marked by muddy sediments lying over a smooth bottom. Sea bottom are under the action of milder nearbed hydrodynamic conditions which are rarely able to remobilize sand fractions, being the suspended load the dominant mode of transport occurring during extreme wave events.

The sediment dynamic model show that Sectors A to D have distinct characteristics regarding the sedimentary dynamics, thus representing different zones of the continental shelf. As such, the boundaries proposed are presented on Table 5.18.

Table 5.18 Continental shelf classification according to depth boundaries presented on the conceptual sediment dynamic model.

	Depth (m)	Continental shelf classification
Sector A	0 - 15	Upper inner shelf | Submarine beach
Sector B	15 -30	Lower inner shelf
Sector C	30 - 80	Mid shelf
Sector D	>80	Outer shelf

5.6 Main achievements

The integrated analysis involving results from a sediment transport numerical model together with sedimentological and oceanographic data was able to allow a further understanding of the sedimentary dynamics seaward the depth of closure in a high-energy environment. The evaluation and quantification of the sediment transport as well as its relationship with bottom sediment distribution and oceanographic conditions carried out on this work represent a valuable contribution for the state of the art of the nearshore sedimentary dynamics. Some of the major contributions are summarized here:

1. Application of a validated wave-current bottom boundary layer model able to evaluate and quantify sediment remobilization, suspension and transport:

    • Bedload is the dominant mode of transport within the nearshore zone.

    • Suspended load only dominates when considering very fine sand at depths shallower than 30 m and at depths where muddy fractions start to dominate bottom sediments.

    • The sediment transport in the alongshelf direction is systematically higher than in the cross-shelf direction.

    • Net transport is essentially southwestward and offshore directed.

2. The recognition of the major drivers of the sedimentary dynamics and their relative importance according to depth:

    • Waves plays the major role on bottom sediment dynamics at least down to 80 m depth.

    • There is no change on nearbed current direction during sediment remobilization periods.

3. Development of a conceptual sediment dynamic model for the nearshore environment in a high-energy environment dominated by waves:

    • The nearshore zone can be divided into 4 dynamically distinct areas according to depth: upper and lower inner shelf, mid sheld and outer shelf.

Chapter 6

Nearshore zonation and conceptual model

The sedimentary dynamics within the nearshore zone has been evaluated over two target areas energetically distinct: the high-energy (HE) Portuguese west coast totally exposed to the Atlantic swell and the relative sheltered moderate-energy (ME) Portuguese south coast. The multiproxy approach carried out on these two case studies enabled the interpretation of the sedimentary dynamics integrated with both oceanographic forcing and sedimentological data. Besides the obvious distinction between the study areas, it is seen patterns regarding the across-shelf sediment dynamic processes which led to the definition of limits bounding domains behaving dynamically similarly on both study areas. This zonation identified 4 dynamically distinct domains: upper and lower inner shelf, mid shelf and outer shelf. Their boundary depths are well represented on bottom sediments (6.1 Nearshore sedimentological zonation), being the prediction of these limits also performed through theoretical calculations based on wave conditions (6.2 Nearshore oceanographic zonation).

The integrated analysis of the results also allowed the development of a conceptual sediment dynamic model for a wave-dominated nearshore zone with low sediment supply. In this model the sedimentary dynamics within each nearshore domain is described and supported with data acquired in the scope of this work and complemented with external data.

6.1 Nearshore sedimentological zonation

In situ data revealed a coincident sedimentological sequence across both continental shelves approached in this work, despite their energetically distinct character. The delineation of the sedimentary deposits revealed that the high-energy environment presents the limits between these deposits at depths nearly three times greater than on the moderate-energy environment.

The inner shelf, characterized by littoral deposits composed mainly by fine to medium sand, has its seaward limit at approximately 10 m depth on the ME environment while this limit reaches about 30 m depth on the HE one. On both study areas a seaward fining trend is observed, being however more evident on the high energy environment. This domain is subdivided into an upper and a lower part which boundary between them is represented by the morphological depth of closure (DoC). The DoC at the ME environment is estimated to be at about 6 m depth (López-Doriga et al., 2015), while at the HE one is at about 15 m depth (Lapa et al., 2012).

The coarse sands of the mid shelf, which origin is likely to be associated with an old beach system leaved during last transgression ("relict" sands) as described in McManus (1975), are well marked on both continental shelves, being located within 10 and 30 m depth on the south coast (ME), while this coarse belt is observed between 30 and 80 m depth at the west coast (HE).

The abrupt contact between the mid shelf sands and sediments with a significant amount of mud characterizing the outer shelf (mudline) is found to be around 30 m depth on the moderate-energy environment, whereas this boundary is placed at about 80 m depth on the high-energy environment. Results are comparable to the ones from the review work of Immenhauser (2009) where the mudline depth for ME environments lies between 11 and 30 m and under HE conditions between 40 and 60 m depth.

The sedimentological zonation for both study areas can be seen on Figures 6.1 and 6.2.

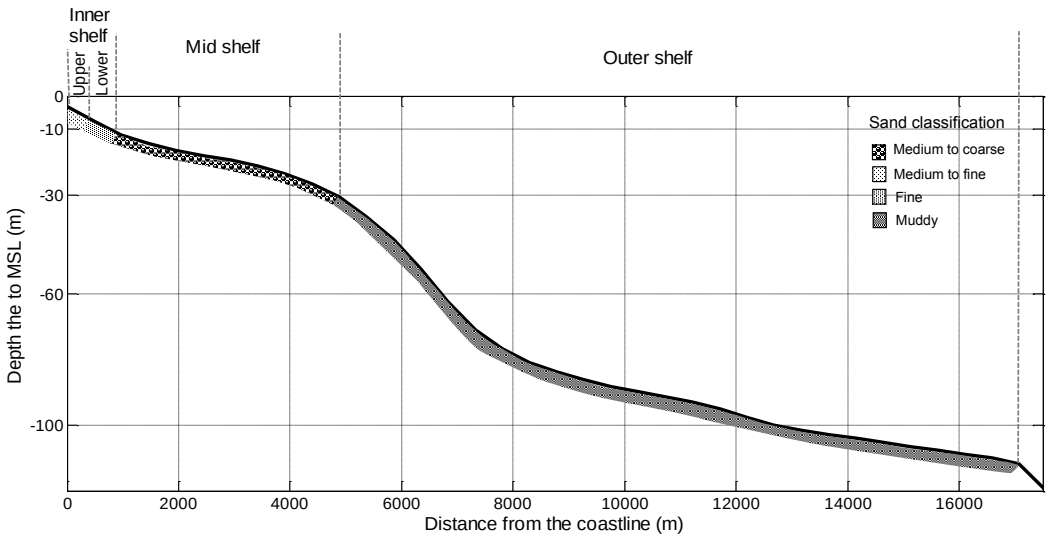

Figure 6.1 Nearshore sedimentological zonation at a moderate-energy environment across a continental shelf profile offshore Tavira barrier island, Portugal south coast.

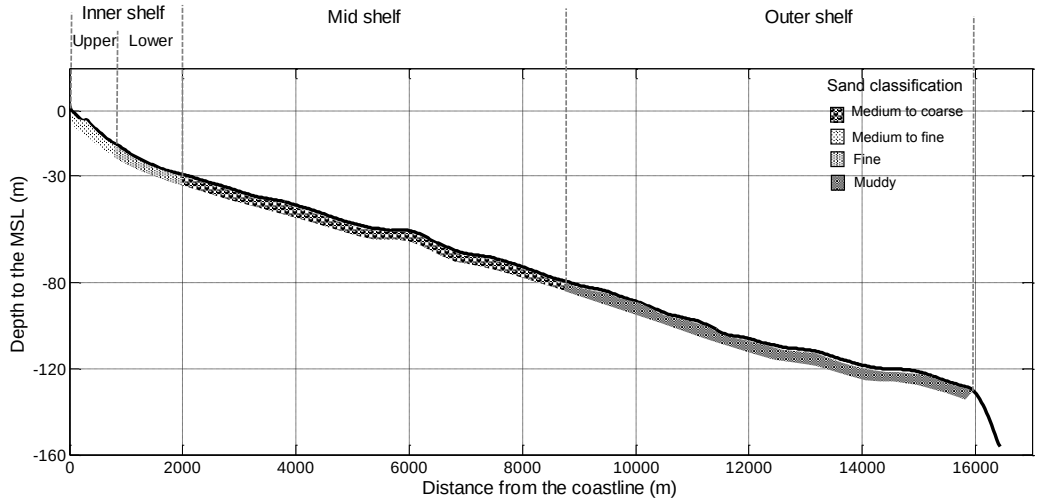

Figure 6.2 Nearshore sedimentological zonation at a high-energy envionment across a continental shelf profile offshore Almagreira beach, Portugal west coast.

6.2 Nearshore oceanographic zonation

The nearshore zone has specific behaviours depending on the processes acting across it. The positions of the boundaries within the nearshore zone (described in the previous section) vary from one area to another mainly due to the wave conditions. As the reaction of sediment grains to hydrodynamic processes results in reworking and redistribution of sediments, the

coupling between hydrodynamic regime and regional sediment textural patterns can also be established (Cowell et al., 1999). This assumption put in evidence that nearshore zonation can be based on hydrodynamic processes, similarly to the pioneer work of Hallermeier (1981) which gave rise to many others such as Birkemeier (1985) and Kashlan et al. (2017) on the US coast and Teixeira and Macedo (2001) on southern Portugal.

The boundary between the upper and lower inner shelf is herein considered the morphological depth of closure (DoC). The zonation proposed by Hallermeier (1981) defined this depth as the inner DoC, that represents the seaward boundary of a domain with intense bed activity caused by extreme near-breaking waves and breaker-related currents. The estimation of this depth can therefore rest upon the simplified formulation of Hallermeier (1981) based on the offshore wave climate:

$$h_c = 2\bar{H}_s + 11\sigma_{H_s} \tag{6.1}$$

where $\overline{H_s}$ is the mean annual significant wave height and σ_{H_s} the standard deviation of H_s.

The application of Equation 6.1 to the offshore data of Faro and Monican02 wave buoys, both made available by the Hydrographic Institute, results into very acceptable values for both study areas, being 7 m and 17 m depth, for the ME and HE environments, respectively. These depth values are 1 to 2 m deeper than the respective boundaries delineated according to the DoC estimation based on profile bathymetric measurements reported on the last section.

Efforts have already been made in order to find a relationship between wave-bottom induced forces and sediment distribution for deeper areas. Hallermeier (1981) also proposed a formulation for estimating the seaward limit of a domain where waves "*have neither strong nor negligible effects on the sand bed*", referred by this author as the outer DoC[1] that can be considered equivalent to the limit between inner and mid shelf in this work. Hallermeier's approximation is well disseminated among scientific community. In the work of Hilton and Hesp (1996), for example, the outer DoC estimation coincidentally corresponds to the juncture between the inner shelf fine sands and the mid shelf coarser sands. However, the dependence of this depth estimation on the in situ sediment grain size introduces a considerable degree of arbitrariness, specially on continental shelves presenting grain size discontinuities (normally represented by relict sand deposits), which is the case of the Portuguese continental shelf. The inconsistency of this dependence is clearly observed when applying Hallermeier's formulation to the present study. For the moderate-energy environment, for example, this depth estimation can be of 10, 15 or 20 m depth, if considering fine, medium or coarse sand, respectively. According to the formulation condition (sample

[1] $h_i = \bar{H}_s - 0.3\sigma\bar{T}_s(\frac{g}{5000D})^{0.5}$, where $\bar{H}_s$ and $\bar{T}_s$ are mean annual significant wave parameters, g is the gravity acceleration and D the median grain size determined from a sand sample from a water depth $h \approx 1.5h_c$.

from $h \approx 1.5h_c$), medium sand should be considered, thus 15 m would be the boundary depth (instead of 10 m depth presented according to the sedimentological zonation). On the high-energy environment, using the same approximation, the estimation of the inner shelf seaward limit ranges from 30 to 60 m depth (from coarse to fine sand), being the last value the depth correspondent to in the situ sediment grain size observations, equivalent to twice the boundary depth estimated by sedimentological zonation (30 m). The lack of consistency of existing formulations coupled with evidences of a direct relationship between regional sediment distribution and the nearbed wave-induced forces (Dunbar and Barrett, 2005; George and Hill, 2008) encouraged this work on estimating the boundaries within the continental shelf domains seaward the DoC based exclusively on offshore wave data.

A first empirical approximation for estimating the boundary between inner and mid shelf domains, considering H_s and the wavelength (L) associated to the 10^{th} percentile of the offshore peak period (assuming $L = \frac{gT^2}{2\pi}$), is herein proposed:

$$h_{in} = 2\sqrt{\bar{H}_s \frac{gT_{p,0.1}^2}{2\pi}} \tag{6.2}$$

where $T_{p,0.1}$ is the 10^{th} percentile of the offshore peak period.

The Equation 6.2 put in evidence a good correlation between the 10^{th} percentile of the offshore T_p and the boundary depth h_{in}. The depths estimated by the application of Equation 6.2 to the study areas are of 11 and 28 m below mean sea level for the ME and HE nearshore environments, respectively. Despite the relatively short-term wave data (about 3 years for both cases), results show an excellent agreement with sedimentological zonation boundaries where the seaward limits of the inner shelf are estimated to be around 10 and 30 m depth, for the ME and HE environments, respectively.

The mid shelf offshore boundary marks the beginning of muddy sediment deposition, being this limit also known as the mudline (Selley, 2000; Stanley et al., 1983; Yan et al., 2015). In hydrodynamic terms, it is the depth from which bottom wave-induced forces are no longer able to keep muddy particles under suspension. As such, Stanley et al. (1983) argued that the mudline depth on a given margin depends primarily on the energy levels of the physical forcing, with deeper mudlines occurring in more energetic environments. Similarly to the work of Dunbar and Barrett (2005), the estimation of the mudline depth is herein presented in relation to wave-induced forces, but to be easier to compute is represented in terms of nearbed wave orbital velocity (critical value for very fine sands) instead of shear stress values.

First, using wave linear theory, the orbital velocity at the bottom can be estimated by:

$$u_w = \frac{\pi H}{T \sinh(kh)} \tag{6.3}$$

where $k = \frac{2\pi}{L}$, being L the wavelength.

To solve this equation in order to a depth h, deep water approximation to the sinh(kh) and thus $L = \frac{gT^2}{2\pi}$ was assumed, becoming:

$$h = \frac{gHT}{4\pi u_w} \tag{6.4}$$

To figure out what the percentile of wave conditions that should be used, it was assumed that the solution should simultaneously satisfy the threshold velocity at the bottom and present a depth ratio solution of 3:1 for the HE and ME environments as observed in the field. This reasoning resulted in the following expression:

$$h_{mid} = \frac{gH_{s,0.75}T_{p,0.75}}{4\pi u_{w,cr}k} \tag{6.5}$$

where $T_{p,0.75}$ and $H_{s,0.75}$ is the 75^{th} percentile of the offshore peak period and significant wave height, respectively; $u_{w,cr}$ is the threshold wave orbital velocity for very fine sands (0.2 m/s) and k is an empirical constant equal to 1.55 used to match computed values to the ones observed in the field.

The application of this formula results in h_{mid} estimations of 29 and 87 m depth, for the ME and HE nearshore environments, respectively. Results agree with the sedimentological zonation described in the previous section, which are of about 30 and 80 m depth, for the same environments, respectively.

All parameters needed for estimating the boundaries within both nearshore environments are presented on Table 6.1.

Table 6.1 Wave parameters used on boundary depth estimations in Equations 6.1 6.2 and 6.5 for the moderate-energy (ME) and high-energy (HE) environments.

	$\bar{H}_s$	σ_{H_s}	$T_{p,0.1}$	$H_{s,0.75}$	$T_{p,0.75}$
ME	0.92	1.14	4.5	1.12	10.5
HE	2.28	0.53	7.5	2.8	12.5

The empirical formulations herein presented represent a first attempt for coupling the offshore wave regime with the regional sediment distribution pattern based on wave-alone

characteristics. These results can be seen as a steep forward on the assessment of the magnitude-frequency relationships involving the forcing mechanisms and the nearshore morphodynamic behaviour. However, the empirical character of this study obviously points to the necessity of further validation rather based on distinct wave-energy conditions and sediment supply conditions.

6.3 Conceptual sediment dynamic model

The analysis and interpretation of numerical modelling results and observed data led the development of a conceptual sediment dynamic model for a wave-dominated nearshore zone under low sediment supply conditions. The proposed model is based on the similarities regarding sediment distribution and wave-induced bottom dynamics observed on energetically distinct nearshore environments.

The cross-shelf sediment distribution pattern on the nearshore zone can be seen as a result from the balance between the onshore and offshore transport processes and the current sediment supply from continental sources. The onshore-offshore transport process are mainly controlled by wave-induced forces while the relevance of continental sources on the nearshore sediment distribution is clearly reported on the work of Rosa et al. (2013).

The response of sediment particles to hydrodynamic processes results in reworking and redistribution of sediments across the nearshore zone, which evidences a clear link between forcing agents and bottom sediment distribution.

As reported in many works, sediments tend to become finer in a seaward direction due to the decreasing wave bottom-induced forces with increasing depth (e.g. Gruber et al., 2004; Guillen et al., 1997; Liu and Zarillo, 1990). However, besides hydrodynamic forcing, nearshore deposits also depends on the sediment supply processes. In the case of the Portuguese coast, the relatively low sediment sediment supply in relation to the available wave energy is responsible for the interruption of this seaward fining sequence by a relatively coarse lag probably leaved during last transgression. This belt of coarser sediments out of equilibrium with the present hydrodynamic regime is usually referred in the literature as "relict" sands (Swift et al., 1971) and has been already reported on the Portuguese coast (Dias, 1987; Magalhães, 2001; Rodrigues et al., 1991).

Also, following the "equilibrium profile" concept (Brunn, 1962), the sediment tends to move across the shelf to a position in which is in equilibrium with the acting forces (dominated by waves). This equilibrium zone is generally defined for each grain size based on the part of the nearshore where the grain size fraction shows its peak of abundance. Obviously, the distribution of each grain size according to its "depth" of equilibrium is

representative of long-term dispersal patterns , which means that this depth is actually a depth range across the nearshore where a specific grain size dominates but also others sand sizes coexist.

The overall nearshore sediment dynamics is depicted in a conceptual model on Figure 6.3 and the dynamic processes within each domain are described on the next sections. Also, the overall data supporting the conceptual model are summarized on Tables 6.4.

6.3.1 The inner shelf

This is where land and sea meet and consequently where the sedimentary exchanges between the continental and oceanic domains take place. This domain is marked by littoral sediments in equilibrium with present hydrodynamic regime and composed by medium to fine sand where a seaward fining trend is observed. A clear distinction on the morphodynamic behaviour across the inner shelf allow the segmention of this zone into an upper and a lower domain, described below.

The **upper inner** shelf is composed by medium to fine sands which are under very frequent remobilization. According to modelling results, frequencies of occurrence are >15% and >90% in the ME and HE nearshore environments, respectively. Also, this domain is marked by intense sediment transport on both alongshelf and cross-shelf directions as well as a frequent sediment exchange with subaerial beach. This strong sedimentary activity is translated into measurable morphological changes (on the order of decimetre scale) which are observed down to the offshore boundary of this domain represented by the morphological DoC (Lapa et al., 2012; López-Doriga et al., 2015). Model results also points the bedload as the dominant mode of transport, which is likely to be the mechanism driving coarser sand onshore, while finer sand are essentially transported offshore as suspended load.

The **lower inner shelf** is marked essentially by fine sands where sediment remobilization is still frequent, occurring between 50 and 90% and between 10 and 15% of the time for the ME and HE environments, respectively. Oberle et al. (2014) simulations point that Northwest Iberian inner shelf (down to 30 m depth) are remobilized during about 80% of the time. This lower frequency can be attributed to the absence of the wave-current interactions on bottom stress estimation made in their work. This domain is marked by lower sediment transport rates where low cross-shelf and moderate alongshelf sediment transport is expected, both mainly transported as bedload. This relatively weaker sedimentary activity translates into moderate morphological changes on the bottom. Evidences of this behaviour are reported in Drago et al. (2015) through a sandpit experiment and also by Lapa et al. (2012) through seabed morphological monitoring.

The seaward fining trend across the inner shelf put in evidence the behaviour of this domain as a sedimentary unit. Therefore, its seaward boundary is classified as a sedimentological depth of closure due to a clear-marked interruption of this sequence by the mid shelf coarser sands.

6.3.2 The mid shelf

Despite the decrease on the wave-induced bottom dynamics, increasing sediment grain size is observed (medium to coarse sand), being therefore in situ sediments out of equilibrium with the present hydrodynamic conditions. These characteristics are compatible with the "relict" sands description which deposition conditions are usually associated to a lower sea level scenario (McManus, 1975). These sediments are still remobilized but with a much lower frequency (5-50% and 1-10% of the time for the ME and HE, respectively) than on the inner shelf, which contributes to the preservation of its original characteristics.

Sediment transport is considered low, being dominant in the alongshelf direction. However, tracer experiment results show that waves, especially in higher energetic conditions, can also advect sediment inducing an onshore sediment transport. The low transport rates observed in this domain, 0.61 m^3/m/yr on the alongshelf (southwestward) and 0.31 m^3/m/yr on the cross-shelf (towards onshore) direction, are translated into low morphological changes only observed on the scale of sand ripples and bioturbation. Numerical simulations performed on this work points to the existence of bedforms, which were also observed by divers in the scope of SHORE project, reinforcing the existence of significant sedimentary activity. Also, artificial disturbances performed on the seabed such as sandpits can enhance this sedimentary activity resulting in significant bottom morphological changes (e.g. Gonçalves et al., 2014). The frequent sediment remobilization induced by wave action can be associated to a high sediment diffusion within the mid shelf, while the very low magnitude of the current-related sediment transport is compatible with the relict nature of the sedimentary deposits. The seaward limit of this domain is marked by the abrupt contact with sediments with a significant amount of mud. This boundary marks the limit at where wave-induced forces starts to be able to remobilize bottom sediments. The description of this boundary totally matches the effective wave base concept.

6.3.3 The outer shelf

This domain is marked by muddy sediments composed mainly by silt and very fine sands lying over a smooth bottom where sediments are in equilibrium with the milder hydrodynamic conditions. The hydraulic behaviour of these small-sized sediments translates into easier

conditions for resuspension than for remobilization. Therefore, the sediment transport events, which only occur during extreme events, as reported by Oberle et al. (2014), are clearly dominated by the suspended load mode of transport. Waves can start to "feel" the bottom on this domain (wave base), but wave-induced forces are not able to remobilize sediments. Also, at the outer shelf is where current begin to play a major role on bottom-induced dynamics.

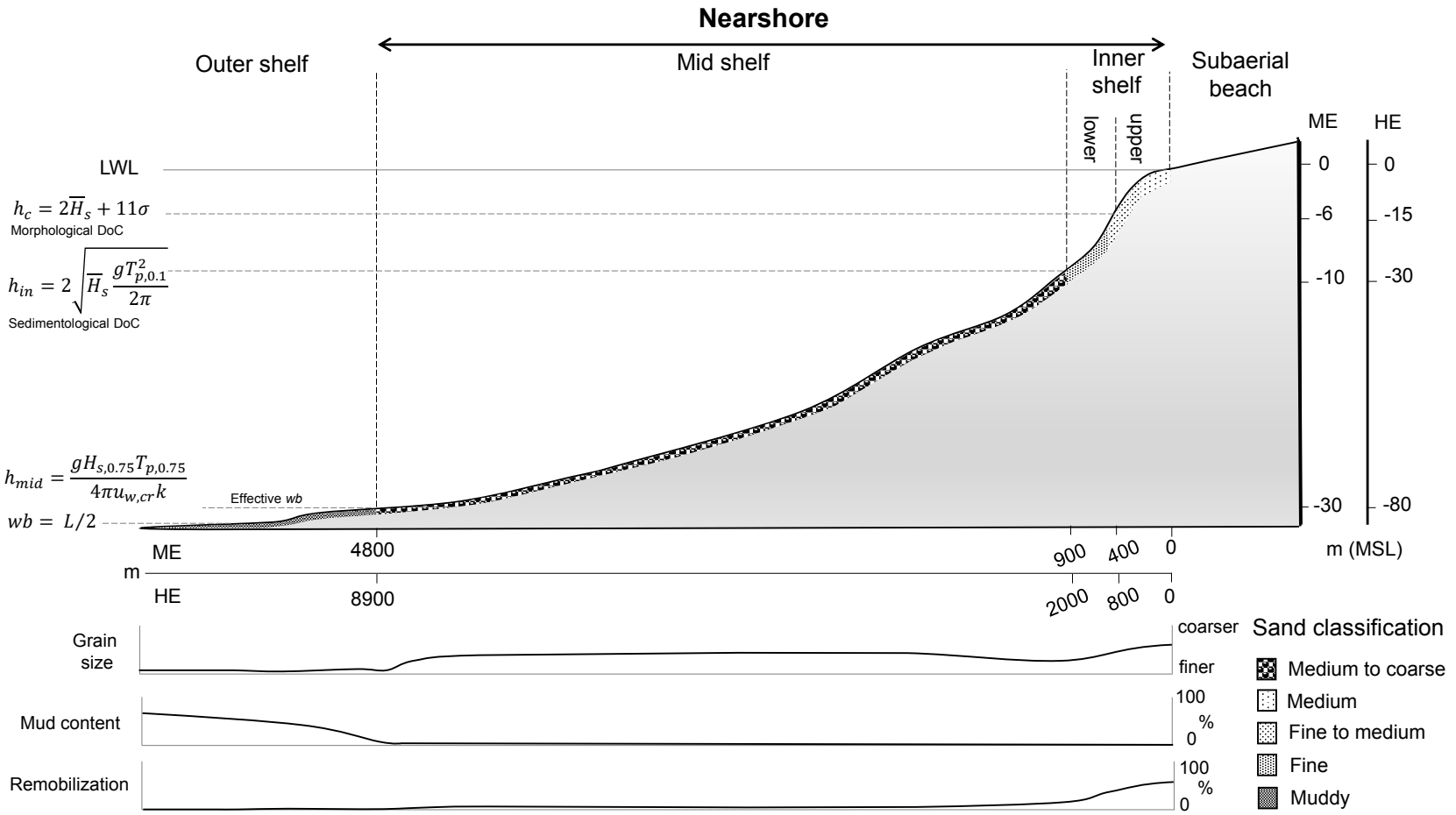

Figure 6.3 Conceptual nearshore sediment dynamic model and zonation considering a moderate-energy (ME) and a high-energy environment (HE). Boundary nomenclatures are based on the depth of closure (DoC) and wave base (wb) definitions.

			Inner shelf		Mid shelf	Outer shelf
			Upper	Lower		
Morphology	Changes		Large • > decimeters by DoC definition • Lapa et al.(2012) and López-Doriga et al. (2015)	Moderate • < decimeter by DoC definition (Nicholls et al, 1996). • sandpit evidences (Drago et al., 2015)	Low • microscale (ripples and bioturbation)	Very low • microscale (bioturbation)
			⚓ 💻	⚓ 💻	⚓📄 💻📄	⚓ 💻
Sediments	Texture		Medium to fine sand	Fine sand	Medium to coarse sand	Muddy sands
			⚓📄	⚓📄	⚓📄	⚓📄
	Remobilization % time	HE	> 90	50-90	5-50	<5
		ME	>15	10-15	1-10	<1
			💻📄	💻 💻📄	💻📄	💻📄
	Sand sediment transport	Cross- shelf	High	Low	Very low • tracer experiment	Negligible
			⚓ 💻📄	⚓ 💻📄	⚓📄 💻📄	💻📄
		Alongshelf	High	Moderate • sandpit (Drago et al., 2015)	Low • tracer experiment	Negligible
			⚓ 💻📄	⚓ 💻📄	⚓📄 💻📄	⚓💻
		Bedload to suspended load ratio	>1	>1	>1	<1
			💻📄	💻📄	💻📄	💻📄

⚓ external field data 💻 external modelling ⚓📄 | 💻📄 field data|modelling thesis output

Figure 6.4 Overall data supporting the conceptual sediment dynamic model. Remobilization and sediment transport data considers the sand fraction between fine and coarse sand.

Chapter 7

Conclusions and future research

The research conducted in this work improved the understanding of nearshore sedimentary dynamics in wave-dominated environments, and allowed a better understanding on the links between forcing mechanisms and induced sediment transport processes. Findings were supported by a successful coupling between numerical modelling and in situ data acquisition from two energetically contrasting nearshore zones. While some findings confirm existing models, others constitute a novel perspective to the understanding of the nearshore sedimentary dynamics.

Despite the energetically distinct character of the nearshore zones addressed in this work, similarities on their characteristics allowed the development of a general conceptual model for the sedimentary dynamics of wave-dominated continental shelves. The conceptual model constitutes a step forward in the harmonization of the sedimentological and oceanographic perspectives of the inner, medium and outer shelf domains.

The inner shelf domain – composed by littoral deposits with a seaward fining trend – is characterized by a "continuous" reworking of bottom sediments by the waves. Overall, the bedload transport mode is considered the mechanism driving coarser sands onshore, while the seaward transport of finer sands is made essentially as suspended load. This domain can be segmented in two sections: 1) the upper inner shelf, marked by intense sediment transport and frequent sediment exchange with subaerial beach (translated into measurable morphological changes) is limited offshore by the morphological depth of closure; and 2) the lower inner shelf, which extends down to the maximum depth where littoral deposits are observed lies, is characterized by finer sands frequently mobilized but only transported under high energy wave events.

At the mid shelf, while the bottom energy induced by the waves decreases, the grain size of bottom sediments increase, and consists of medium to coarse sands. This shows that sedimentation was performed under lower sea level conditions and sediments are known

as relict sediments. Sediment remobilization within this domain is significant, but net the sediment transport is very low and dominated by an alongshore component.

Finally, the abrupt contact with muddy sediments marks the begginnig of the outer shelf where sediments are in equilibrium with the milder hydrodynamic regime. In this domain, sediment resuspension is rare but occurs more easily than remobilization due to sediment particle hydraulic behaviour.

Overall, results showed that while the depth of closure constitutes a morphodynamic boundary, the sediment dynamics seaward this point is still active and characterized by very frequent remobilization with low net transport rates, specially on the lower inner shelf. On the mid shelf the sedimentary activity is considerable lower, becoming almost negligible on the outer shelf. This behavior has important implications in what concerns the management of shelf sediment resources.

Despite the valuable contribution to the understanding of nearshore sediment dynamics made by this work, further efforts should still be done regarding this theme. The incorporation of wave-related sediment transport due to wave streaming into numerical models as well as more sediment transport measurements are improvements to be prioritized in order to better estimate the magnitude of nearshore sedimentary activities. These improvements, associated with the predictive capacity of numerical models, can therefore constitute a powerful tool for the coastal management of natural resources, especially with regard to the current sea level rise scenario and the potential coastal sediment budget imbalances associated to it.

References

Aagaard, T. (2014). Sediment supply to beaches: cross-shore sand transport on the lower shoreface. *Journal of Geophysical Research: Earth Surface*, 119(1):913–926.

Aagaard, T., Black, K. P., and Greenwood, B. (2002). Cross-shore suspended sediment transport in the surf zone: a field-based parameterization. *Marine Geology*, 185:283–302.

Almeida, L. P., Ferreira, O., and Pacheco, A. (2010). Thresholds for morphological changes on an exposed sandy beach as a function of wave height. *Earth Surface Processes and Landforms*, 36(4):523–532.

Amoudry, L. O. and Souza, A. J. (2011). Deterministic coastal morphological and sediment transport modeling: a review and discussion. *Reviews of Geophysics*, 49:1–21.

Antunes, C. and Taborda, R. (2009). Sea Level at Cascais Tide Gauge : Data , Analysis and Results. *Journal of Coastal Research*, 2009(SI 56):218–222.

Ashton, A. D., Donnelly, J. P., and Evans, R. L. (2007). A discussion of the potential impacts of climate change on the shorelines of the Northeastern USA. *Mitigation and Adaptation Strategies for Global Change*, 13(7):719–743.

Backstrom, J., Jackson, D., Cooper, A., and Loureiro, C. (2015). Contrasting geomorphological storm response from two adjacent shorefaces. *Earth Surface Processes and Landforms*, 40(15):2112–2120.

Bagnold, R. (1966). An approach to the sediment transport problem from general physics. *Geological Survey Professional Paper*, 422-I.

Barnhardt, W., Andrews, B., and Butman, B. (2005). High-resolution geologic mapping of the inner continental shelf: Nahant to gloucester, massachusetts. Technical report, 2005-1293 U.S. Geological Survey.

Batten, B. K. (2003). *Morphologic Typologies and Sediment Budget for the Ocean Shoreline of Long Island, New York*. State University of New York at Stony Brook.

Beach, R. A. and Sternberg, R. W. (1996). Suspended-sediment transport in the surf zone: response to breaking waves. *Continental Shelf Research*, 16(15):1989 – 2003.

Becker, J. M., Firing, Y. L., Aucan, J., Holman, R., Merrifield, M., and Pawlak, G. (2007). Video-based observations of nearshore sand ripples and ripple migration. *Journal of Geophysical Research: Oceans*, 112(C1):1–14.

Bijker, E. (1967). *Some considerations about scales for coastal models with movable bed*. Publ. 50, Delft Hydraulics Lab.

Birkemeier, W. A. (1985). Field data on seaward limit of profile change. *Journal of Waterway, Port, Coastal and Ocean Engineering*, 111(3):598–602.

Black, K., Athey, S., Wilson, P., and Evans, D. (2007). The use of particle tracking in sediment transport studies: a review. In Balson, P. S. and Collins, M. B., editors, *Coastal and Shelf Sediment Transport*, pages 73–91. Geological Society of London, London, special publication, 274 edition.

Blondeaux, P. and Vittori, G. (2005). Flow and sediment transport induced by tide propagation : 2 . The wavy bottom case. *Journal of Geophysical Research*, 110(C08003):1–11.

Blott, S. J. and Pye, K. (2001). GRADISTAT: A grain size distribution and statistics package for the analysis of unconsolidated sediments. *Earth Surface Processes and Landforms*, 26:1237–1248.

Booij, N., Ris, R. C., and Holthuijsen, L. H. (1999). A third-generation wave model for coastal regions 1 . Model description and validation. *Journal of Geophysical Research*, 104:7649–7666.

Brown, J., Colling, A., Park, D., Phillips, J., Rothery, D., and Wright, J. (1994). Sediment movement by waves and currents. In Bearman, G., editor, *Waves, tides and shallow-water processes*, pages 72–92. Pergamon and The Open University, Oxford.

Brunn, P. (1962). Sea-level rise as a cause of shore erosion. *Journal of Waterways and Harbor Division*, 88:117–130.

Cacchione, D. and Drake, E. (1982). Measurements of Storm-Generated Bottom Stresses on the Continental Shelf. *Journal of Geophysical Research*, 87(C3):1952–1960.

Carlin, J., Dellapenna, T., Figlus, J., and Harter, C. (2015). Investigating morphological and stratigraphic changes to the submarine shoreface of a transgressive barrier island: Follets island, Northern Gulf of Mexico. In Wang, P., Rosati, J., and Cheng, J., editors, *Proceedings of Coastal Sediments*, pages 1–14.

Carter, L. and Carter, R. (1986). Holocene evolution of the nearshore sand wedge,south otago continental shelf, new zealand. *New Zealand Journal of Geology and Geophysics*, 29(4):413–424.

Carter, R. (1988). *Coastal Envirnoments: An Introduction to the Physical, Ecological and Cultural Systems of Coastlines*. Academic Press Limited, London.

Christoffersen, J. B. and Jonsson, I. (1985). Bed friction and dissipation in a combined current and wave motion. *Ocean Engineering*, 12(5):387–423.

Ciavola, P., Taborda, R., Ferreira, O., and Dias, J. A. (1997). Field measurements of longshore sand transport and control processes ona steep meso-tidal beach in Portugal. *Journal of Coastal Research*, 13(4):1119–1129.

Colebrook, C. and White, C. (1937). Experiments with fluid friction in roughened pipes. In *Proceedings of the Royal Society, Series A*, volume 161, pages 367–381.

Condie, S. a. and Sherwood, C. R. (2006). Sediment distribution and transport across the continental shelf and slope under idealized wind forcing. *Progress in Oceanography*, 70(2-4):255–270.

Costa, M., Silva, R., and Vitorino, J. (2001). Contribuição para o estudo do clima de agitação marítima na costa portuguesa. In *Proceedings of 2ª Jornadas Portuguesas de Engenharia Costeira e Portuária*, Sines.

Cowell, P. J., Hanslow, D. J., and Meleo, J. F. (1999). The shoreface. In Short, A. D., editor, *Handbook of Beach and Shoreface Morphodynamics*, pages 39–71. John Wiley and Sons, 2nd edition.

Crawford, A. M. and Hay, A. E. (2003). Wave orbital velocity skewness and linear transition ripple migration: Comparison with weakly nonlinear theory. *Journal of Geophysical Research*, 108(C3):3091.

Davidson-Arnott, R. (2011). Wave-dominated coasts. In Wolanski, E. and McLusky, D. S., editors, *Treatise on Estuarine and Coastal Science, Volume 3: Estuarine and Coastal Geology and Geomorphology*, pages 73—116. Elsevier.

Davies, A. G., Soulsby, R. L., and King, H. L. (1988). A numerical model of the combined wave and current bottoom boundary layer. *Journal of Geophysical Research*, 93(C1):491–508.

Davies, J. L. (1973). *Geographical Variation in Coastal Development*. Hafner Publishing Co., New York, 204p.

Davis, R. A. and Hayes, M. O. (1984). What is a wave-dominated coast? *Marine Geology*, 60:313–329.

de Vries, S., Schipper, M. A., and Stive, M. (2014). Measured gradients in alongshore sediment transport along the dutch coast. In *Proceedings of the International Conference on Coastal Engineering*, volume 1, pages 43–58.

Dias, J. (1987). *Dinâmica sedimentar e evolução recente da plataforma continental portuguesa setentrional*. Tese de Doutoramento, Universidade de Lisboa, Lisboa, 384p.

Drago, T., Taborda, R., Rosa, M., Bosnic, I., Garel, E., Teixeira, S., Cascalho, J., and Silva, A. (2015). Insights on shoreface sedimentary dynamics through the analysis of the evolution of a small sand pit offshore tavira – preliminary results. In *Resumenes sobre el VIII Simposio MIA15*, pages 615–618.

Drake, D. E. and Cacchione, D. A. (1989). Estimates of the suspended sediment reference concentration and resuspension coefficient from near-bottom observations on the California shelf. *Continental Shelf Research*, 9(1):51–64.

Drapeau, G. and Long, B. (1984). Measurements of bedload transport in the nearshore zone using radioisotopic sand tracers. *Coastal Engineering*, 85:1252–1264.

Duane, D. B. and James, W. (1980). Littoral Transport in the Surf Zone Elucidated by an Eulerian Sediment Tracer Experiment. *Journal of Sedimentary Petrology*, 50(3):929–942.

Duarte, J., Taborda, R., Ribeiro, M., Cascalho, J., Silva, A., and Bosnic, I. (2014). North beach (Nazaré) sand tracer experiment. In *EGU General Assembly Conference Abstracts*, volume 16 of *EGU General Assembly Conference Abstracts*, page 14268.

Dunbar, G. B. and Barrett, P. J. (2005). Estimating palaeobathymetry of wave-graded continental shelves from sediment texture. *Sedimentology*, 52:253–269.

Dykes, J. D., Hsu, Y. L., and Rogers, W. E. (2002). The development of an operational swan model for ngli. In *OCEANS '02 MTS/IEEE*, volume 2, pages 859–866.

Elko, N., Feddersen, F., Foster, D., Hapke, C., Mcninch, J., Mulligan, R., Ozkan-haller, H. T., Plant, N., and Raubenheimer, B. (2014). The future of nearshore processes. Technical report, The nearshore processes community.

Ferré, B., Sherwood, C. R., and Wiberg, P. L. (2010). Sediment transport on the Palos Verdes shelf, California. *Continental Shelf Research*, 30(7):761–780.

Flores, J. S. (2011). *Process-Based Modelling of the Brent Delta: Influence of paleobathymetry from the Oseberg Fm. pinch out on the wave dominated Brent Delta progradation. North Sea Norwegian Sector – Huldra Field.* Master thesis, TU Delft Section for Geotechnology, Delft, 107p.

Fredsøe, J. (1984). Turbulent boundary layer wave–current motion. *Journal of Hydraulic Engineering*, 110:1103–1120.

Garcia, M. and Parker, G. (1991). Entrainment of bed sediment into suspension. *Journal of Hydraulic Engineering*, 117(4):414–435.

Garel, E., Laiz, I., Drago, T., and Relvas, P. (2016). Characterisation of coastal countercurrents on the inner shelf of the Gulf of Cadiz. *Journal of Marine Systems*, 155:19–34.

George, D. A. and Hill, P. S. (2008). Wave climate, sediment supply and the depth of the sand–mud transition: A global survey. *Marine Geology*, 254(3):121 – 128.

Gonçalves, D., Pinheiro, L., Silva, P., Rosa, J., Rebêlo, L., Bertin, X., Braz Teixeira, S., and Esteves, R. (2014). Morphodynamic evolution of a sand extraction excavation offshore Vale do Lobo, Algarve, Portugal. *Coastal Engineering*, 88:75–87.

Goud, M. R. and Aubrey, D. G. (1985). Theoretical and observational estimates of nearshore bedload transport rates. *Marine Geology*, 64:91–111.

Gracia, V., Jimenez, J. A., Sanchez-arcilla, A., Guillen, J., and Palanques, A. (1998). Short-term relatively deep sedimentation on the Ebro delta coast. Opening the closure depth. In *Coastal Engineering Proceedings*, pages 2902–2912.

Grant, D. and Madsen, O. S. (1986). The continental shelf bottom boundary layer. *Annual Review of Fluid Mechanics*, 18:265–305.

Grant, W. and Madsen, O. (1979). Combined Wave and Current Interaction With a Rough Bottom. *Journal of Geophysical Research*, 84(C4):1797–1808.

Grasso, F., Michallet, H., and Barthélemy, E. (2011). Sediment transport associated with morphological beach changes forced by irregular asymmetric, skewed waves. *Journal of Geophysical Research*, 116(C3):C03020.

Gruber, N. L. S., Toldo, E. E., Barboza, E. G., and Nicolodi, J. L. (2004). A Shoreface Morphodynamic Zonation and the Equilibrium Profile Variability on the Northern Coastline of Rio Grande do Sul , Brazil. *Journal of Coastal Research*, (SI39):504–508.

Guillen, J., Palanques, A., and Ciencias, I. D. (1997). A shoreface zonation in the Ebro Delta based on grain size distribution. *Journal of Coastal Resarch*, 13(3):867–878.

Guisado, E., Malvárez, G. C., and Navas, F. (2013). Morphodynamic Environments of the Costa del Sol, Spain. *Journal of Coastal Research*, (SI 65):500–505.

Hallermeier, R. J. (1978). Uses for a calculated limit depth to beach erosion. *Coastal Engineering*, 88(1):1493–1512.

Hallermeier, R. J. (1981). A profile zonation for seasonal sand beaches from wave climate. *Coastal Engineering*, 4:253–277.

Harris, C. K. and Wiberg, P. L. (1997). Approaches to quantifying long-term continental shelf sediment transport with an example from the Northern California STRESS mid-shelf site. *Continental Shelf Research*, 17(11):1389–1418.

Hill, P. S., Nowell, A. R. M., and Jumars, P. A. (1988). Flume Evaluation of the Relationship Between Suspended Sediment Concentration and Excess Boundary Shear Stress. *Journal of Geophysical Research*, 93(12):499–509.

Hilton, M. J. and Hesp, P. (1996). Nearshore-surfzone system limits and the impacts of sand extraction. *Journal of Coastal Resarch*, 12(2):496–519.

Holmedal, L., Aagaard, T., Wang, H., and Myrhaug, D. (2015). Observed and modelled streaming in field measurements. In *Proceedings of Coastal Sediments*, pages 1–8, San Diego.

Hsu, Y. L., Rogers, W. E., and Dykes, J. D. (2002). WAM performance in the Gulf of Mexico with COAMPS wind. In *Proc. 7th Int. Workshop on Wave Hindcasting and Forecasting*, pages 151–159.

IH (2010). Sed4: Sedimentos superficiais da plataforma continental do cabo carvoeiro ao cabo da roca. In *Carta da Série Sedimentológica*, Instituto Hidrográfico, Lisboa.

Immenhauser, A. (2009). Estimating palaeo-water depth from the physical rock record. *Earth Science Reviews*, 96:107–139.

Inman, D. L. and Chamberlain, T. K. (1959). Tracing Beach Sand Movement with Irradiated Quartz. *Journal of Geophysical Research*, 64(1):41–47.

Kashlan, L., Brown, S., and Lillycrop, L. (2017). Charleston harbor, sc, regional sediment management study; beneficial use of dredged material through nearshore placement. Technical report, US Army Corps of Engineers.

King, C. A. M. (1951). Depth of disturbance of sand on sea beaches by waves. *Journal of Sedimentary Petrology*, 21(3):131–140.

Kleinhans, M. G. and Grasmeijer, B. T. (2006). Bed load transport on the shoreface by currents and waves. *Coastal Engineering*, 53:983–996.

Knaapen, M. A. F., van Bergen Henegouw, C. N., and Hu, Y. Y. (2005). Quantifying bedform migration using multi-beam sonar. *Geo-Marine Letters*, 25(5):306–314.

Komar, P. (1998). *Beach processes and sedimentation*. Prentice Hall, 2nd edition.

Komar, P. D. and Inman, D. L. (1970). Longshore Sand Transport on Beaches. *Journal of Geophysical Research*, 75(30):5914–5927.

Kranenburg, W. M., Ribberink, J. S., Schretlen, J. J. L. M., and Uittenbogaard, R. E. (2013). Sand transport beneath waves: The role of progressive wave streaming and other free surface effects. *Journal of Geophysical Research: Earth Surface*, 118(1):122–139.

Kraus, N. C., Isobe, M., Igarashi, H., Sasaki, T., and Horikawa, K. (1982). Field experiments on longshore sand transport in the surf zone. *Coastal Engineering*, pages 969–988.

Kraus, N. C., Larson, M., and Wise, R. (1998). Coastal Engineering Technical Note: Depth of closure in beach-fill design. Technical report, U.S. Army.

Lapa, N., Rodrigues, A., Taborda, R., Duarte, J., and Pinto, J. (2012). The sedimentary processes of the portuguese inner shelf off almagreiro beach (peniche). In *Actas das 2as Jornadas de Engenharia Hidrográfica*, pages 279–282.

Larson, M. and Kraus, N. (1995). Prediction of cross-shore sediment transport at different spatial and temporal scales. *Marine Geology*, 126:111–127.

Larson, M., Rosati, J., and Kraus, N. (2002). Overview of regional coastal processes and controls. Coastal and hydraulic engineering technical note, US Army Engineer Research and Development Center, Coastal and Hydraulics Laboratory.

Li, M. Z., Wright, L. D., and Amos, C. L. (1996). Predicting ripple roughness and sand resuspension under combined flows in a shoreface environment. *Marine Geology*, 130:139–161.

Liu, J. and Zarillo, G. (1990). Shoreface dynamics : Evidence from bathymetry and surficial sediments. *Marine Geology*, 94:37–53.

López-Doriga, U., Bouzas, A., and Ferreira, O. (2015). Depth of closure variability at tavira, south portugal. In *Proceedings of 3a Conferência sobre Morfodinâmica Estuarina e Costeira*, pages 14–15.

Madec, G. (2012). NEMO ocean engine. Note du Pôle de modélisation. *Institut Pierre-Simon Laplace (IPSL), France,*, 27:ISSN No 1288–1679.

Madsen, O. and Wood, W. (2002). Sediment transport outside the surfzone. In King, D., editor, *Coastal Engineering Manual, Part III, Coastal Sediment Processes*. U.S. Army Corps of Engineers, Washington, DC.

Madsen, O. S. (1987). Use of Tracers in Sediment Transport Studies. *Proceedings of Coastal Sediments*, 49(424-435).

Magalhães, F. (2001). *Os sedimentos da plataforma continental portuguesa: contrastes espaciais, perspectiva temporal, potencialidades económicas*. Tese de Doutoramento, Universidade de Lisboa, Lisboa, 287p.

Markert, E., Kröncke, I., and Kubicki, A. (2015). Small scale morphodynamics of shoreface-connected ridges and their impact on benthic macrofauna. *Journal of Sea Research*, 99:47 – 55.

Masselink, G., Austin, M. J., O'Hare, T. J., and Russell, P. E. (2007). Geometry and dynamics of wave ripples in the nearshore zone of a coarse sandy beach. *Journal of Geophysical Research: Oceans*, 112(C10):2156–2202.

Mazarakis, N., Kotroni, V., Lagouvardos, K., and Bertotti, L. (2012). High-resolution wave model validation over the Greek maritime areas. *Natural Hazards and Earth System Sciences*, 12:3433–3440.

McManus, D. (1975). Modem versus Relict Sediment on the Continental Shelf. *Geological Society of America Bulletin*, 86:1154–1161.

Meyer-Petter, E. and Muller, R. (1948). Formulas for bed-load transport. In *Proceedings of 2nd meet of the International Association for Hydraulic Structures Research*, pages 39–64, Stockholm.

Miller, M. C. and Komar, P. D. (1979). Measurements of Sand Spreading Rates under Near-Bottom Wave Orbital Motions. *The Journal of Geology*, 87(6):593–608.

Morang, A. and Birkemeier, W. A. (2005). Depth of closure on sandy coasts. In Schwartz, M. L., editor, *Encyclopedia of Coastal Science*, pages 374–376. Springer Netherlands, Dordrecht.

Myrhaugh, D. and Slaattelid, O. (1989). Combined wave and current boundary layer model for fixed rough seabeds. *Ocean Engineering*, 16(2):119–142.

Nicholls, R. J., Birkemeier, W. A., and Lee, G.-h. (1998). Evaluation of depth of closure using data from Duck, NC, USA. *Marine Geology*, 148:179–201.

Nicholls, R. J., Member, A. A., Birkemeier, W. A., Member, A., and Hallermeier, R. J. (1996). Application of the depth of closure concept. *Coastal Engineering*, 299:3874–3887.

Niedoroda, A., Swift, D., Hopkins, T., and Ma, C. (1984). Shoreface morphodynamics on wave-dominated coasts. *Marine Geology*, 60:331–354.

Niedoroda, A. W., Swift, D. J. P., and Hopkins, T. S. (1985). The shoreface. In Davis, R. A., editor, *Coastal Sedimentary Environments*, pages 533–624. Springer-Verlag, 2nd edition.

Nielsen, P. (1992). *Coastal Bottom Boundary Layers and Sediment Transport*, volume 4 of *Advanced Series on Ocean Engineering*. World Scientific Publishing, Singapore, 248p.

Nittrouer, C. A. and Wright, L. D. (1994). Transport of particles across the continental shelves. *Review of Geophysics*, 32(1):85–113.

Nugzar, M., Griffiths, C., Dyt, C., Robson, B., and Nichol, S. (2012). Coastal sediment-transport modelling and observational needs. In *Proceedings of Australian Coastal and Oceans Modelling and Observations Workshop (ACOMO)*, volume 4, Canberra.

Oberle, F., Storlazzi, C., and Hanebuth, T. J. J. (2014). Wave-driven sediment mobilization on a storm-controlled continental shelf (Northwest Iberia). *Journal of Marine Systems*, 139:362–372.

Ortiz, A. C. and Ashton, A. D. (2016). Exploring shoreface dynamics and a mechanistic explanation for a morphodynamic depth of closure. *Journal of Geophysical Research: Earth Surface*, 121(2):442–464.

Otvos, E. G. (1982). Low-energy coast. In Schwartz, M., editor, *Beaches and Coastal Geology*, pages 522–522. Springer US.

Patterson, D. C. (2012). Shoreward sand transport outside the surfzone, northern Gold Coast, Australia. In *Coastal Engineering Proceedings*, pages 1–15, Santander.

Relvas, P. and Barton, E. (2002). Mesoscale patterns in the Cape São Vicente (Iberian Peninsula) upwelling region. *Journal of Geophysical Research*, 107(C10):3164.

Relvas, P., Barton, E., Dubert, J., Oliveira, P. B., Peliz, A., da Silva, J., and Santos, a. M. P. (2007). Physical oceanography of the western iberia ecosystem: Latest views and challenges. *Progress in Oceanography*, 74(2-3):149–173.

Ribberink, J. S. (1998). Bed-load transport for steady flows and unsteady oscillatory flows. *Coastal Engineering*, 34:59–82.

Robertson, W., Zhang, K., Finkl, C. W., and Whitman, D. (2008). Hydrodynamic and geologic influence of event-dependent depth of closure along the South Florida Atlantic Coast. *Marine Geology*, 252:156–165.

Rodrigues, A., Lapa, N., and Pinto, J. (2012). Environmental characterization of almagreiro beach and adjacent inner shelf – surge (tf-gm-05/12). Technical report, Instituto Hidrográfico.

Rodrigues, A., Magalhães, F., and Dias, J. (1991). Evolution of the north portuguese coast in the last 18,000 years*. *Quaternary International*, 9:67–74.

Rosa, F., Rufino, M. M., Ferreira, O., Matias, A., Brito, A. C., and Gaspar, M. B. (2013). The influence of coastal processes on inner shelf sediment distribution : The Eastern Algarve Shelf (Southern Portugal). *Geologica Acta*, 11(1):59–74.

Rosati, J. D. (2005). Concepts in Sediment Budgets. *Journal of Coastal Research*, 212(1966):307–322.

Rosati, J. D., Dean, R. G., and Walton, T. L. (2013). The modified Bruun Rule extended for landward transport. *Marine Geology*, 340:71–81.

Roy, P., Cowell, P., Ferland, M., and Thom, B. (1994). Wave-dominated coasts. In Carter, R. and Woodroffe, C., editors, *Coastal evolution: Late quaternary shoreline evolution*, pages 121–186. Cambridge University Press.

Roy, P. S. and Stephens, A. W. (1980). Geological controls on process-response, S.E. Australia. *Coastal Engineering*, 57:913–933.

Rufino, M., Gaspar, M., Maynou, F., and Monteiro, C. (2008). Regional and temporal changes in bivalve diversity off the south coast of Portugal. *Estuarine, Coastal and Shelf Science*, 80(4):517–528.

Sánchez, R., Mason, E., Relvas, P., da Silva, J., and Peliz, A. (2006). On the inner-shelf circulation in the northern Gulf of Cádiz, southern Portuguese shelf. *Deep Sea Research Part II: Topical Studies in Oceanography*, 53(11-13):1198–1218.

Santos, A. I., Oliveira, A., Zacarias, N., Pinto, J. P., and Ribeiro, M. (2014). Suspended sediment transport patterns in the inner shelf - S. Pedro de Moel (Portugal). *Journal of Sea Research*, 93:47–56.

Schwab, W., Thielert, E. R., Allen, J. R., Fostert, D. S., Swift, B. A., and Denny, J. F. (2000). Influence of Inner-Continental Shelf Geologic Framework on the Evolution and Behavior of the Barrier-Island System Between Fire Island Inlet and Shinnecock Inlet, Long Island, New York. *Journal of Coastal Research*, 16(2):408–422.

Selley, R. (2000). *Applied Sedimentology*. Academic Press, 2nd edition, 523p.

Shields, A. (1936). *Application of similarity principles and turbulence research to bed-load movement (translation of original in German by W. P. Ott and J. C. van Uchelen, California Institute of Technology)*. Publ. 50, Delft Hydraulics Lab.

Short, A. (1999). *Handbook of beach and Shoreface Morphodynamics*. John Willey and Sons, 379p.

Silva, A., Taborda, R., Rodrigues, A., Duarte, J. a., and Cascalho, J. a. (2007). Longshore drift estimation using fluorescent tracers: New insights from an experiment at Comporta Beach, Portugal. *Marine Geology*, 240(1):137–150.

Smith, J. and McLean, S. (1977). Spatially Averaged Flow Over a Wavy Surface. *Journal of Geophysical Research*, 82(12):1735–1746.

Smyth, C. E. and Li, M. (2005). Wave-current bedform scales, orientation, and migration on Sable Island Bank. *Journal of Geophysical Research*, 110(C02023).

Soulsby, R. (1997). *Dynamics of marine sands: a manual for practical applications*. Thomas Telford, 248p.

Soulsby, R. and Smallman, J. (1986). A direct method of calculating bottom orbital velocity under waves. Technical report, SR 76, HR Wallingford, Wallingford, UK.

Soulsby, R. and Whitehouse, R. (2005a). Prediction of ripple properties in shelf seas. mark 1 predictor for time evolution. Technical report, HRWallingford, Wallingford, UK.

Soulsby, R. and Whitehouse, R. (2005b). Prediction of ripple properties in shelf seas. mark 2 predictor for time evolution. Technical report, HRWallingford, Wallingford, UK.

Soulsby, R., Whitehouse, R., and Marten, K. (2012). Prediction of time-evolving sand ripples in shelf seas. *Continental Shelf Research*, 38:47–62.

Soulsby, R. L. and Damgaard, J. S. (2005). Bedload sediment transport in coastal waters. *Coastal Engineering*, 52(8):673–689.

Soulsby, R. L., Hamm, L., Klopman, G., Myrhaug, D., and Simons, R. R. (1993). Wave-current interaction within and outside the bottom boundary layer. *Coastal Engineering*, 21:41–69.

Stanley, D. J., Addy, S., and Behrens, E. W. (1983). The mudline: variability of its position relative to the shelfbreak. *SEPM special publication*, 33:279–298.

Styles, R. and Glenn, S. (2005). Long-term sediment mobilization at a sandy inner shelf site, LEO-15. *Journal of Geophysical Research*, 110(C4):C04S90.

Sunamura, T. and Kraus, N. C. (1984). Prediction of average mixing depth of sediment in the surf zone. *Marine Geology*, 62:1–12.

Svendsen, I. A. (2006). *Introduction to nearshore hydrodynamics*, volume Vol. 24 of Advanced Series on Ocean Engineering. World Scientific.

Swift, D. J. P., Stanley, D. J., and Curray, J. R. (1971). Relict Sediments on Continental Shelves : A Reconsideration. *The Journal of Geology*, 79(3):322–346.

Taborda, R. (1999). *Modelação da dinâmica sedimentar na plataforma continental portuguesa*. Tese de doutoramento, Universidade de Lisboa, Lisboa, 367p.

Tanner, F. (1960). Florida coastal classification. *Gulf Coast Assoc. Geol. Socs. Trans*, 10:259–266.

Teixeira, S. and Macedo, F. (2001). Prospecção de manchas de empréstimo ao largo da albufeira, algarve. Technical report, Agência Portuguesa do Ambiente.

Thorne, P. D. and Hurther, D. (2014). An overview on the use of backscattered sound for measuring suspended particle size and concentration profiles in non-cohesive inorganic sediment transport studies. *Continental Shelf Research*, 73:97 – 118.

Thornton, E. (1972). Distribution of sediment transport across the surf zone. *Coastal Engineering Proceedings*, 1(13):1049–1068.

Unesco (1983). Algorithms for computation of fundamental properties of seawater. Technical report, Unesco technical papers in marine science 44, 53pp.

van Kesteren, W. and Bakker, W. (1984). Near bottom velocities in waves with a current; analytical and numerical computations. In *Proceedings of 19th Conference on Coastal Engineering*, pages 1161–1177, Houston, TX.

van Rijn, L. (1984). Sediment transport: part i: bed load transport; part ii: suspended load transport; part iii: bed forms and alluvial roughness. *Journal of Hydraulic Engineering*, 110:1733–1754.

van Rijn, L. and Walstra, D. (2004). Analysis and modelling of sand mining pits. Technical report, WL Delft Hydraulics, 34p.

van Rijn, L. C. (1997). Sediment transport and budget of the central coastal zone of Holland. *Coastal Engineering*, 32(1):61–90.

Vermeer, M. and Rahmstorf, S. (2009). Global sea level linked to global temperature. In *PNAS*, number 9, pages 1–6.

Vincent, E. and Green, O. (1990). Field measurements of the suspended sand concentration profiles and fluxes and of the resuspension coefficient over a rippled bed. *Journal of Geophysical Research*, 95(11):591–601.

Wang, P. (2005). Nearshore sediment transport measurement. In Schwartz, M. L., editor, *Encyclopedia of Coastal Science*, pages 698–701. Springer Netherlands, Dordrecht.

Wang, P., Kraus, N. C., and Davis, R. A. (1998). Total Longshore Sediment Transport rate in the Surf Zone: Field Measurements and Empirical Predictions. *Journal of Coastal Research*, 14(1):269–282.

White, T. E. (1998). Status of measurement techniques for coastal sediment transport. *Coastal Engineering*, 35:17–45.

Wiberg, P. and Dungan, S. (1987). Calculations of the Critical Shear Stress for Motion of Uniform and Heterogeneous Sediments. *Water Resources Research*, 23(8):1471–1480.

Williams, J. (2012). Recent advances in instrumentation used to study sediment transport. *Int. Assoc. Sedimentol. Spec. Publ.*, 44:173–196.

Wright, L., Boon, J., Kim, S., and List, J. (1991). Modes of cross-shore sediment transport on the shoreface of the middle atlantic bight. *Marine Geology*, 96:19–51.

Yan, W., jian Chen, Z., gen Deng, J., yan Zhu, H., cheng Deng, F., and li Liu, Z. (2015). Numerical method for subsea wellhead stability analysis in deepwater drilling. *Ocean Engineering*, 98:50 – 56.